

OPTIMAL DESIGN OF SPV SYSTEM AND APPLICATIONS

A Thesis Submitted to the
Delhi Technological University
For the Award of Doctor of Philosophy
In
Electrical Engineering

Submitted By:
ASTITVA KUMAR
(2K16/PhD/EE/12)



Under the Joint Supervision of
Prof. M. Rizwan **Prof. Uma Nangia**

DEPARTMENT OF ELECTRICAL ENGINEERING
DELHI TECHNOLOGICAL UNIVERSITY
(Formerly Delhi College of Engineering)
DELHI-110042, INDIA
2021

Table of Contents

DECLARATION.....	I
CERTIFICATE.....	II
ACKNOWLEDGEMENT.....	III
LIST OF FIGURES	V
LIST OF TABLES	IX
LIST OF SYMBOLS, ABBREVIATION AND NOMENCLATURE	XI
List of Symbols.....	xi
List of Abbreviations	xiv
ABSTRACT.....	XVII
CHAPTER 1	
INTRODUCTION.....	1
1.1 GENERAL	1
1.2 RENEWABLE ENERGY STATUS IN INDIA	3
1.3 RENEWABLE ENERGY INITIATIVES IN INDIA.....	5
1.4 BASICS OF SPV SYSTEM	7
1.5 DESIGNING OF SPV SYSTEM AND APPLICATION	8
1.5.1 Grid Connected SPV System	8
1.5.2 Standalone SPV System	9
1.5.3 Hybrid System.....	9
1.6 PROBLEM FORMULATION	10
1.7 OUTLINE OF THESIS	11

CHAPTER 2

LITERATURE REVIEW	14
2.1 INTRODUCTION.....	14
2.2 MATHEMATICAL MODELLING OF RES AND MICROGRID	14
2.3 OPTIMIZATION TECHNIQUES	16
2.4 SHORT TERM SOLAR POWER AND ENERGY FORECASTING	17
2.5 DESIGN AND SIZING OF HYBRID MICROGRID	21
2.6 POWER ENHANCEMENT IN SPV SYSTEM.....	24
2.6.1 Array Reconfiguration Method.....	24
2.6.2 Designing MPPT Controllers.....	28
2.7 KNOWLEDGE GAP ANALYSIS	30
2.8 PROBLEM FORMULATION	30

CHAPTER 3

MODELLING OF RENEWABLE ENERGY BASED MICROGRID

COMPONENTS.....	31
3.1 INTRODUCTION.....	31
3.2 RENEWABLE ENERGY SOURCES.....	31
3.2.1 Solar Photovoltaic System	32
3.2.2 Wind Energy Generation System.....	35
3.3 ENERGY STORAGE ELEMENTS.....	36
3.3.1 Battery Energy Storage System (BESS)	36
3.3.2 Energy Balance	37

3.3.3	Fuel Cell	38
3.4	INVERTER MODELLING.....	40
3.5	DC/DC CONVERTER.....	40
3.6	CONCLUSION	41

CHAPTER 4

STUDY AND ANALYSIS OF INTELLIGENT TECHNIQUES.....	42	
4.1	INTRODUCTION.....	42
4.2	BRIEF OVERVIEW.....	42
4.2.1	Design Variables	44
4.2.2	Constraints.....	45
4.2.3	Objective Function	45
4.2.4	Variable bounds.....	45
4.3	EVOLUTIONARY ALGORITHMS	45
4.3.1	Artificial Neural Networks (ANN)	46
4.3.2	Adaptive Neuro Fuzzy	48
4.4	POPULATION BASED OPTIMIZATION.....	50
4.4.1	Particle Swarm Optimization	50
4.3.2	Grey Wolf Optimizer	53
4.5	DEVELOPMENT OF MODIFIED GREY WOLF PARTICLE SWARM OPTIMIZATION	57
4.6	RESULTS AND DISCUSSION.....	59

4.7	CONCLUSION	62
-----	------------------	----

CHAPTER 5

GWO-ANN BASED APPROACH FOR SHORT TERM SPV POWER

FORECASTING	64
--------------------------	-----------

5.1	INTRODUCTION.....	64
-----	-------------------	----

5.2	IMPORTANCE OF SPV POWER FORECASTING.....	64
-----	--	----

5.3	LEARNING/TRAINING ALGORITHMS	66
-----	------------------------------------	----

5.4	SITE DETAILS AND DATA PROCESSING	67
-----	--	----

5.5	SOLAR ENERGY FORECASTING USING AEROSOL INDEX	70
-----	--	----

5.5.1	NARX ANN based Modelling for Solar Irradiance Forecasting	71
-------	--	----

5.5.2	Results and Discussion.....	73
-------	-----------------------------	----

5.6	GWO-ANN BASED SPV POWER FORECASTING	75
-----	---	----

5.6.1	Statistical Indicators	77
-------	------------------------------	----

5.7	PERFORMANCE EVALUATION OF GWO ANN BASED MODEL	78
-----	---	----

5.8	CONCLUSION	83
-----	------------------	----

CHAPTER 6

DESIGN AND ANALYSIS OF SPV BASED MICROGRID FOR A SELECTED

LOCATION.....	85
----------------------	-----------

6.1	INTRODUCTION.....	85
-----	-------------------	----

6.2	CONCEPT OF MICROGRID	86
-----	----------------------------	----

6.3	SELECTION OF GEOGRAPHICAL LOCATION/SITE.....	87
-----	--	----

6.4	SIZING OF RE COMPONENTS USING LP.....	90
6.4.1	Proposed Two Stage Linear Programming	90
6.4.2	Problem Formulation.....	91
6.4.3	Sizing of Battery Energy Storage System.....	93
6.4.4	Constraints.....	93
6.4.5	Results and Discussion.....	94
6.5	SIZING OF SPV BASED MICROGRID FOR SELECTED SITE IN DEREGULATED ENVIRONMENT.....	98
6.5.1	Problem Formulation.....	98
6.5.2	Load Management System Considering Load Flexibility.....	99
6.5.3	MGWPSO Sizing Algorithm for SPV based Microgrid	101
6.5.4	Results and Discussion.....	103
6.5.6	Performance Analysis of MGWPSO based SPV Microgrid.....	106
6.6	TECHNO-ECONOMIC IMPACT OF INTELLIGENT EMS IN HYBRID MICROGRID	112
6.6.1	Importance of Energy Management Strategy.....	112
6.6.2	Hybrid Intelligent Approach based EMS	114
6.6.3	Results and Discussion.....	115
6.7	CONCLUSION	119

CHAPTER 7

IMPROVING THE PERFORMANCE OF SPV SYSTEM USING ARRAY

RECONFIGURATION AND MPPT CONTROLLER..... 121

7.1	INTRODUCTION	121
7.2	IMPACT OF PARTIAL SHADING.....	122
7.3	CLOUD MOVEMENT AND MODELING OF SHADE.....	123
7.4	GWO BASED ARRAY RECONFIGURATION METHOD	126
7.4.1	Methodology	127
7.4.2	Results and Discussions	132
7.5	ANFIS BASED MPPT CONTROLLER FOR SPV SYSTEM.....	139
7.5.1	ANFIS model	140
7.5.2	Results and Discussion.....	144
7.6	CONCLUSION	150

CHAPTER 8

CONCLUSIONS AND FUTURE SCOPE OF WORK..... 152

8.1	CONCLUSIONS	152
8.2	FUTURE SCOPE	154

LIST OF PUBLICATIONS

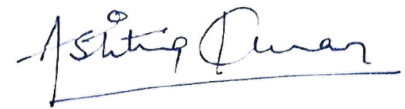
REFERENCES..... 157

DECLARATION

I, Astitva Kumar, a student of Ph.D. hereby declare that the thesis titled **Optimal Design of SPV System and Applications** which is submitted by me to the Department of Electrical Engineering, Delhi Technological University, Delhi in partial fulfillment of the requirement for the award of the degree of Doctor of Philosophy has not previously formed the basis for the award of any Degree, Diploma Associate ship, fellowship or other similar title or recognition.

Place: Delhi

Date: 13/10/2021



(ASTITVA KUMAR)

CERTIFICATE

On the basis of the declaration submitted by Mr. Astitva Kumar, student of Ph.D., We hereby certify that the thesis titled **Optimal Design of SPV System and Applications** which is submitted to the Department of Electrical Engineering, Delhi Technological University, Delhi in partial fulfillment of the requirement for the award of the degree of Doctor of Philosophy is an original contribution with existing knowledge and faithful record of research carried out by him under our guidance and supervision.

To the best of our knowledge this work has not been submitted in part or full for any Degree or Diploma to this University or elsewhere.

Date: 13/10/2021



(Prof. M. Rizwan)

Supervisor

Professor

Department of Electrical Engineering

Delhi Technological University

Delhi, India



(Prof. Uma Nangia)

Supervisor

Professor and Head

Department of Electrical Engineering

Delhi Technological University

Delhi, India

ACKNOWLEDGEMENT

First and foremost, I sincerely acknowledge my most sincere gratitude to my supervisors Prof. M. Rizwan and Prof. Uma Nangia for their valuable guidance, support, and motivation throughout this research work. They have been outstanding mentors and working with them has been a remarkable experience. The valuable hours of discussion that I had with them undoubtedly helped in supplementing my thoughts in the right direction for attaining the desired objectives. I consider it my proud privilege to have worked with them, ever ready to lend a helping hand. I am forever thankful to them for all their wise words and inspiring thoughts.

I am also thankful to all faculty members of the Department of Electrical Engineering, Delhi Technological University, Delhi, for their encouragement and moral support for the completion of this thesis.

I would like to extend my special thanks to SRC members mainly Prof. Majid Jamil, Professor, Department of Electrical Engineering, JMI Delhi who have given me valuable guidance and advice to improve the quality of my research work.

I extend my thanks to my friends and colleagues especially, Suryakant, Hemant, Ajishek, Bilal, Pallavi, Dr. Priyanka Chaudhary, Dr. Prakash Chittora, Dr. Imran Quadri, Saket, and Akash Seth for their constant motivation and for reminding me to complete my work at the earliest.

The assistance of the valuable staff in the Renewable Energy Research Facility of Delhi Technological University is gratefully acknowledged. I am especially thankful to Mr. Vickey Kumar Prasad, Mr. TPS Rana, and Mr. Ankit Kumar for their substantial assistance during my research.

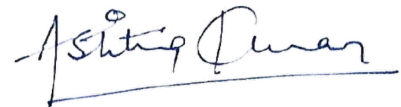
I want to take this opportunity to thank my mother, from the bottom of my heart for everything that she has done and continues to do for me. She never lost her faith in me and sacrificed a great lot in her life to help me come this far. Every bit of mine would always remain indebted to my loving father whose blessings have been and will always be an inseparable part of every stride of my life. I also want to thank my brothers, Devpravar, Akash, Vaibhav, and Nitish for being a constant source of support.

This acknowledgment would not be complete without mentioning my wife. She has been the steady wind under my wings. She is my core support system and words cannot articulate my admiration for her. She gave her unconditional support and continues to be a source of inspiration during my research.

I am wholly indebted to ALMIGHTY who is omnipotent and superpower of the universe.

Place: Delhi

Date: 13/10/2021

A handwritten signature in black ink, reading "Astitva Kumar". The signature is written in a cursive style with a horizontal line underneath.

(Astitva Kumar)

LIST OF FIGURES

Fig. 1.1 Worldwide RE capacity in GW during 2011-2020	2
Fig. 1.2 Global SPV capacity in GW during 2011-2020	2
Fig. 1.3 India's RE sources installed capacity	4
Fig. 1.4 India's SPV growth during 2011 – 2020	5
Fig. 1.5 Basic composition of an SPV system	7
Fig. 1.6 Grid-connected SPV system	8
Fig. 1.7 Standalone SPV system	9
Fig. 1.8 Hybrid system	10
Fig. 3.1. Single diode model of PV cell with R_s and R_p	32
Fig. 3.2. Power generation from SPV over a year	34
Fig. 3.3. Power generation from wind energy conversion system	35
Fig. 3.4. Equivalent circuit of a solid oxide fuel cell (SOFC)	39
Fig. 3.5. DC/DC boost converter	41
Fig. 4.1. Classification of optimization techniques	43
Fig. 4.2. A flowchart for the optimal design procedure	44
Fig. 4.3. Schematic diagram of ANN	46
Fig. 4.4. Two layer feedforward MLP neural network	46
Fig. 4.5. A first-order TSK model with two inputs	49
Fig. 4.6. A two inputs architecture of ANFIS model	49
Fig. 4.7. Flowchart of PSO	53
Fig. 4.8. Social hierarchy in grey wolves	54

Fig. 4.9. Social hierarchy of grey wolves and their functions.	54
Fig. 4.10. Position update of wolves in GWO	55
Fig. 4.11. Flowchart of GWO algorithm.....	57
Fig. 4.12. The performance of developed MGWPSO on different functions.....	63
Fig. 5.1. Different forecasting horizon and their relation	65
Fig. 5.2. Classification of the short-term forecasting model.....	66
Fig. 5.3. Linear regression plot of the inputs and the solar photovoltaic power.....	67
Fig. 5.4. Experimental setup for SPV power forecasting	69
Fig. 5.5. Structure of developed ANN solar energy forecasting model.....	72
Fig. 5.6. Regression line of training phase of developed model.....	73
Fig. 5.7. Cloudy day prediction response of developed model.....	74
Fig. 5.8. Sunny day prediction response of developed model	75
Fig. 5.9. Functional block diagram of the proposed hybrid intelligent model.....	76
Fig. 5.10. Variation of irradiance and linke turbidity for a highly polluted day.....	79
Fig. 5.11. Performance of GWO model	80
Fig. 5.12. PV power forecasting for high τL condition	82
Fig. 5.13. Comparison of various forecasting models (NRMSE, NMBE and NMAE)....	83
Fig. 6.1. Components and functions of MG.....	86
Fig. 6.2. A distributed generation system for the proposed site	87
Fig. 6. 3. Variation of kl , km , and kb	88
Fig. 6.4.(a) Hourly load demand (b) Monthly load demand.....	89
Fig. 6.5. The developed method for sizing of the off-grid based MG	91

Fig. 6.6. (a) Monthly solar energy generation (b) Monthly wind energy generation	95
Fig. 6.7. The total cost of investment in the initial year	96
Fig. 6.8. Variation of the loading factors for a day.....	101
Fig. 6.9. Flowchart of MGWPSO	102
Fig. 6.10. Power generation from SPV over a year for the site	103
Fig. 6.11. Power generation from wind energy conversion system for the site.....	103
Fig. 6.12. Consumption of power of various loads for different seasons r.....	107
Fig. 6.13. Performance of BESS when $LF_{per} = 0\%$ for different seasons	108
Fig. 6.15. Price of electricity and exchange of grid energy (%) for a day	111
Fig. 6.16. Performance of (a) Simple EMS (b) Optimal EMS with uncertainties.....	113
Fig. 6. 17. Flowchart of the designed MGC	114
Fig. 6.18. (a) Cost of electricity (b) Load profile.....	116
Fig. 6.19. Performance of MGWPSO based EMS on a clear day y	117
Fig. 6.20. Performance of MGWPSO based EMS on a cloudy day	117
Fig. 6.21. Clear day performance (a) Rolling cost (b) Grid usage.....	118
Fig. 6.22. Cloudy day performance (a) Rolling cost (b) Grid usage	118
Fig. 7.1. Power loss in P-V curve during PSC.....	122
Fig. 7.2. Different shading conditions	124
Fig. 7.3. Vector representation of shadow movement on 5x5 PV array.....	125
Fig. 7.4. Irregular irradiance at various instances representing different types of shade	126
Fig. 7.5. Position update of wolves in GWO	128
Fig. 7.6. Flowchart for grey wolf optimizer array reconfiguration (GWO-AR).....	129
Fig. 7.7. (a) BL TCT configuration (b) Proposed BLTCT reconfiguration using GWO	130

Fig. 7.8. I-V curves at different shading conditions for various configurations (a) SP ..	132
Fig. 7.9. P-V curves at different shading conditions for various configurations	133
Fig. 7.10. Effect of different shade due to movement of cloud on the PV array	134
Fig. 7.11. Performance indices (a) Power Loss (b) Fill-Factor (c) PR (d) PE.....	137
Fig. 7.12. Radar plot representing the performance indicators for different topologies.	138
Fig. 7.13. Block diagram of SPV system with MPPT controller.....	140
Fig. 7.14. Structure of the ANFIS based MPPT controller.....	140
Fig. 7.15. Fuzzy subsets membership function for dI/dV	142
Fig. 7.16. Fuzzy subsets membership function for I/V	142
Fig. 7.17. Variation of duty cycle with respect to the inputs	142
Fig. 7.18. Training performance of the designed controller	143
Fig. 7.19. ANFIS based MPPT controller for PV systems	143
Fig. 7.20. Performance of ANFIS controller at constant irradiance and temperature	145
Fig. 7. 21. Performance of ANFIS controller at varying irradiance	146
Fig. 7.22. Performance of ANFIS controller at and varying temperature	148

LIST OF TABLES

Table 1.1 India's power sector at a glance (all data in GW).....	4
Table 1.2 India's renewable energy sector at a glance (all data in MW).....	4
Table 2.1 Summary of EAR application on SPV system	26
Table 2.2 Summary of PR application on SPV system	27
Table 5.1. Daily PV output and it's correlation with the inputs considered.....	68
Table 5.2. Specification of the Solar PV system	68
Table 5.3. Input data for SRFM-ANN	72
Table 5.4. Results of developed ANN predictor technique	74
Table 5.5. Linke turbidity factor and corresponding atmospheric conditions	79
Table 5.6. Performance indices of different training algorithms during training state.....	81
Table 5.7. Parameters of various training algorithms for designing of models.....	81
Table 5.8. Performance comparison of the proposed models for prediction stage.....	82
Table 6.1. General load classification.....	88
Table 6.2. General and cost parameters	94
Table 6.3. Optimal sizing results	97
Table 6.4. The cost of various system components	99
Table 6.5. Technical specifications.....	99
Table 6.6. General load classification.....	100
Table 6.7. Comparison of different RE configurations for MG	105
Table 6.8. Optimal sizing results	105

Table 6.9. Comparative analysis of BESS	110
Table 6.10. Comparative analysis of the developed EMS for MG.....	119
Table 7.1. Current, voltage and power calculation of BLTCT and GWO-BLTCT for different shading patterns.....	131
Table 7.2. GMPP at different shading conditions at 25°C	135
Table 7.3. Performance of the PV array in partial shading conditions due to cloud movement at different instances	136
Table 7.4. Parameter specification of DC-DC boost converter	144
Table 7.5. Comparison of proposed ANFIS with INC MPPT	149

LIST OF SYMBOLS, ABBREVIATION AND NOMENCLATURE

List of Symbols

K_T	Clearness index
D_R	Diffuse ratio
r_{ps01}, r_{ps02}	Random variables associated with exploitation and exploration coefficients respectively
w_{ps0}	Weights of the particle
x_{id}	Position of the particles
τ_L	Linke Turbidity factor
τ_{Lk}	Linke Turbidity factor under clear sky
ρ_{rk}	Rayleigh integral optical thickness
ρ_{ra}	Integral optical thickness by Louche
p_{best}	Personal best value
g_{best}	Global best value
m_a	Atmospheric air mass
h	Sun elevation angle
I_0	Sun constant
I_n	Direct normal solar radiation
X_i	Current value of data X
X_{max}, X_{min}	Maximum and minimum value of the dataset X
c_1, c_2	Exploitation and exploration coefficients respectively
R	Regression coefficient
n_h	No. of hidden layers in neural network

$iter_{max}$	Maximum iterations
tol_{err}	Tolerance error
V_{oc}	Open circuit Voltage(V)
I_{sc}	Short circuit current (A)
V_{pm}	Voltage at maximum power (V)
I_{pm}	Current at maximum power (A)
n_{pv}	Efficiency of SPV system
LF_{per}	Load Flexibility percentage
PV_A	Total area of SPV system (m ²)
$G(t)$	Solar irradiance at time t (W/m ²)
$T_a(t)$	Ambient temperature at time t
E_{pvd}	Daily SPV energy generated (kWh)
$P_{pv}(t)$	SPV power at time t (kW)
$P_{wt}(t)$	Wind power at hour t (kW)
P_{wtr}	Rated power of WT
$P_{dgs}(t)$	Power of distributed generation system at time t
$P_{dl}(t)$	Power demand of the loads at time t
$P_d(t)$	Power deficiency at the time t
u	Wind speed at time t (m/s)
u_{cin}	Cut-in speed of WT (m/s)
u_{co}	Cut-out speed of WT (m/s)
u_r	Rated speed of WT (m/s)
E_{wtd}	Daily wind energy generated (kWh)
$f(x)$	Cost function

f_{iwt}	Design vector/WT fraction for WEGS
f_{ipv}	Design vector/PV fraction for SPV system
S_{bess}	Size of the battery energy storage system (kWh)
C_{bess}	Cost of battery energy storage system (\$/kWh)
C_{iess}	Cost of installation of energy storage system (\$/kWh)
C_{essm}	Cost of maintenance of energy storage system (\$/kWh)
C_{ii}	Initial cost of investment
C_{om}	Cost of operation and maintenance
C_{bess}	Cost of battery energy storage system
C_{ipv}	Unit price of the SPV (\$/m ²)
C_{iwt}	Unit price of the WT (\$/m ²)
k_{ipv}	SPV load demand factor
k_{iwt}	WT load demand factor
D_{em}	Monthly load (kwh)
E_d	Energy to be supplied by the battery (kWh)
E_{pvm}	Monthly SPV energy output (kWh/m ²)
E_{wtm}	Monthly WT energy output (kWh/m ²)
C_{mwt}	Maintenance cost of WT
C_{mpv}	Maintenance cost of SPV
k_{om}	Maintenance factor
ρ	State of charge of the battery
i	Inflation rate
v	Interest rate
y	Number of years

NY	Total number of years
E_{ld}	Daily Energy consumption of loads (kWh)
W_c	Constant loads (kW)
W_l	Lighting loads (kW)
W_b	Building loads (kW)
W_m	Motor loads (kW)
WT_{om}	Operational and maintenance cost for WT system (\$/kWh)
WT_{ii}	Initial investment cost of WT system (\$/kW)
Z_B	Degradation factor of the battery

List of Abbreviations

AI	Aerosol Index
ACI	Annualized Cost of Investment
AOD	Aerosol Optical Depth
ANFIS	Adaptive Neuro Fuzzy Inference System
ANN	Artificial Neural Network
AROI	Annualized Return of Investment
BESS	Battery Energy Storage System
BLDC	Brushless Direct Current
BLTCT	Bridge Linked Total Cross Tied
BP	Backpropagation
BoS	Balance of System
DER	Distributed Energy Resources
DGS	Distributed Generation Sources
ESS	Energy Storage System

FC	Fuel Cell
GFS	Global Forecast System
GWO	Grey Wolf Optimizer
GHI	Global Horizontal Irradiance
HRES	Hybrid Renewable Energy System
kNN	K th Nearest Neighbor
LM	Levenberg Marquardt
LN	Long Narrow
LP	Linear Programming
LW	Long Wide
MG	Microgrid
MGC	Microgrid Control
MGWPSO	Modified Grey Wolf Particle Swarm Optimizer
MILP	Mixed Integer Linear Programming
MLP	Multi-Layer Perceptron
MAPE	Mean Absolute Percentage Error
MABE	Mean Absolute Bias Error
MSE	Mean Square Error
MPPT	Maximum Power Point Tracking
NARX	Nonlinear Auto-Regressive For Exogenous
NE	Normalized Error
NMAE	Normalized Mean Absolute Error
NSE	Normalized Squared Error
NRMSE	Normalized Root Mean Square Error
O&M	Operation And Maintenance

PSO	Particle Swarm Optimization
PE	Power Enhancement
PR	Performance Ratio
P&O	Perturb and Observe
RE	Renewable Energy
RES	Renewable Energy Sources
ROI	Return of Investment
SN	Short Narrow
SOFC	Solid Oxide Fuel Cell
SP	Series Parallel
SPV	Solar Photovoltaic
STC	Standard Testing Conditions
SVM	Support Vector Machine
SW	Short Wide
TCI	Total Cost of Investment
TCT	Total Cross Tied
TSLP	Two Constraints Based Linear Programming
TE	Training Error
ToU	Time of Use
WEGS	Wind Energy Generation System
WT	Wind Turbine

ABSTRACT

The demand for grid power is increasing significantly due to the ever-increasing population and increasing comfort zone and usage of modern household equipment. Climate change and greenhouse gas emissions from conventional power plants are a major concern and it invigorated the use of renewable and green energy resources for power generation. In addition, the energy sector worldwide faces rising challenges related to rising demand, efficiency, changing supply and demand patterns, and a lack of analytics needed for optimal management. The power sector in a developed nation has incorporated artificial intelligence and related technologies for sizing and communication between modern grid with renewables, smart meters, and other connected devices. These intelligent approaches and their integration in the electrical systems have the potential to improve energy efficiency, cost reduction, and user comfort. Therefore, it is of key importance to develop intelligent optimization-based techniques for their applications in different solar photovoltaic systems.

It is essential to develop an optimization-based solar photovoltaic power forecasting model with improved performance. A number of mathematical models have been developed for the assessment of solar power and energy under cloudless skies and cloudy conditions. However, there is a scope for developing a novel artificial intelligence-based solar power forecasting considering aerosol particles. A comparative performance of the developed forecasting model is done with other techniques considering various performance indices.

Various methods have been proposed for the optimal capacity of SPV, wind turbines, and other energy storage devices. A novel approach to integrate the various

aspects and characterization of energy consumption in a deregulated electricity environment is presented. This approach not only focuses on the economic aspects for designing an SPV-based microgrid but, also on the performance of the batteries and its interaction with the grid power at different times of the day.

The stochastic nature of SPV hampers the I-V and P-V characteristics in varying meteorological conditions. This stochastic nature results in a mismatch of power produced from panels especially during different shading conditions. Hence, in this research the performance of the SPV system is enhanced by two methods firstly, an array reconfiguration method and secondly, using maximum power point tracking algorithms. The developed grey wolf optimizer-based array reconfiguration and artificial neural fuzzy inference-based maximum power point tracking (MPPT) algorithm perform significantly well under varying meteorological conditions.

CHAPTER 1

INTRODUCTION

1.1 GENERAL

The requirement for electrical energy is increasing exponentially because of urbanization, population expansion, industrialization, ease of living, etc. The utilization of various sources of renewable energy (RE) such as solar, wind, geothermal, hydro, and tidal are being explored to meet the growing demands of an ever-increasing population. This switch from conventional to RE boasts of a lot of advantages, some of them are listed as below:

- Sustainability
- Economic growth
- Abundant availability
- Minimal carbon footprint

The worldwide growth of electricity generation over the last decade has been almost 110% because of their numerous benefits [1]. In 2020 the worldwide generation capacity using RE was 2800 GW and the capacity of RE sources throughout the world in the last decade is given by Fig. 1.1. Among the various RE sources solar photovoltaic (SPV) have been gaining the most attention worldwide. The main reasons for high growth in SPV systems and advancement in SPV technologies are due to unobtrusive nature, silence, no rotatory part involved, and source i.e., the sun is readily available. This worldwide growth in the generation of SPV in the last decade has exponentially increased

by 9.833 times. The growth in SPV capacity of the world is shown in the last decade is shown in Fig. 1.2.

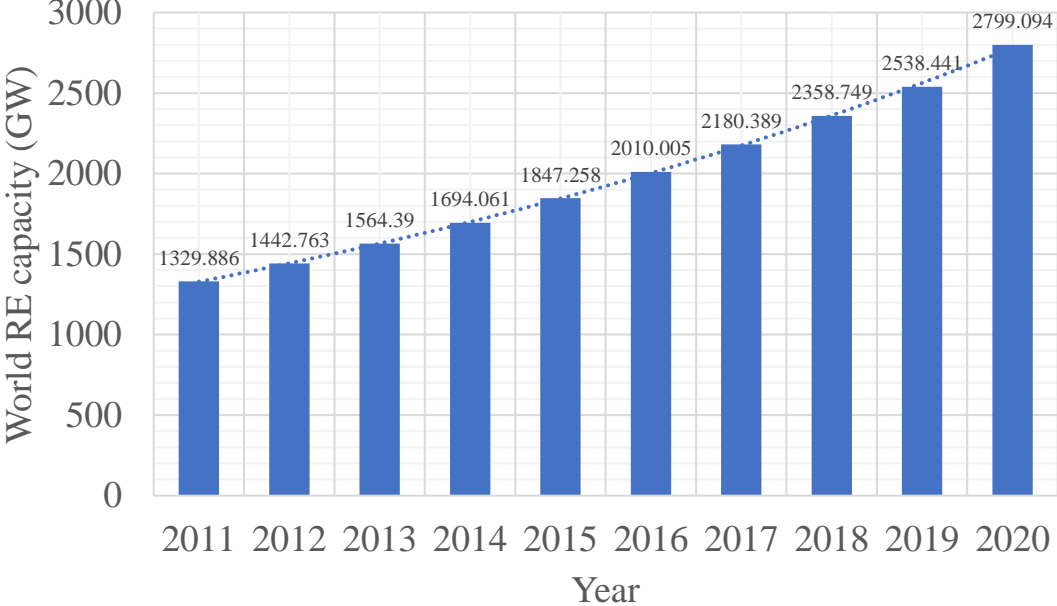


Fig. 1.1 Worldwide RE capacity in GW during 2011-2020

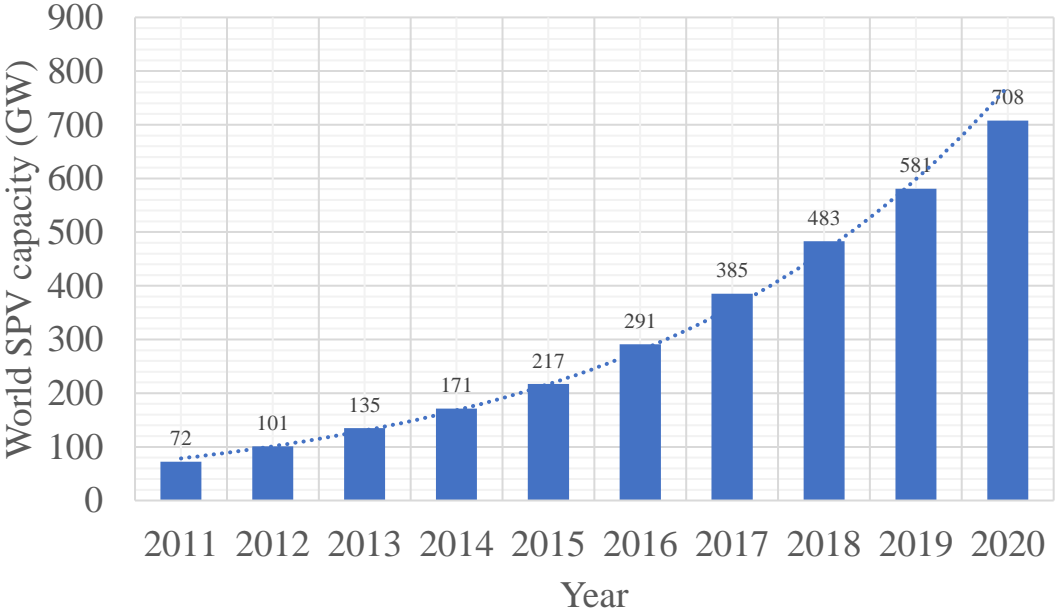


Fig. 1.2 Global SPV capacity in GW during 2011-2020

This meteoric rise in utilization of the SPV system is also due to the declining cost of investment and incentives provided by governments worldwide. This has led to the integration of SPV systems in the existing power grid causing high penetration of the SPV systems into already established electric power systems. This integration of RE sources has further created systems known as microgrid (MG) to effectively provide uninterrupted power supply for a small/local area with or without coordination from the power grid. Moreover, MG and high penetration of RE have negatively impacted the voltage profile and power quality.

The stochastic nature of the RE is the other factor that hampers the potential of clean energy. As RE sources are majorly dependent on the geographical and meteorological parameters, any variation in wind speed or sunlight results in fluctuation of the output power from these RE sources. The rated power must be provided to the various consumer demands by forecasting the RE resources. The adequate sizing of various components such as SPV systems, batteries, inverters, and loads should be kept in mind for efficient working of the modern electrical power system.

1.2 RENEWABLE ENERGY STATUS IN INDIA

The growth in energy demand, ever-increasing population, over exploitation of fossil fuels, and economic policies are the driving factors for RE in the Indian power sector. This led to the setting up of the Ministry of New and Renewable Energy (MNRE) in 1982 by the Indian government to promote and form policies regarding energy generation using RE sources. The total installed capacity of India considering central, state, and private sector cumulatively is at 388.689 GW as of 31st August 2021 and is further elaborated in

Table 1.1. The pie chart in Fig. 1.3 gives an insight into the total installed RE capacity of India as of 31st August 2021. The RE capacity of India constitutes about 25.26% of the total installed capacity. Among the RE sources, SPV has the maximum installed capacity of 45.611 GW followed by wind power with 39.691 GW. Small hydro and bio-powered energy are at 4.807 GW and 10.571 GW respectively in India. Table 1.2 represents the breakdown of different renewable energy power sources in India as of 31st August 2021. By 2030 India aims for achieving 40% of power from renewables.

Table 1.1 India’s power sector at a glance (all data in GW)

Thermal			Nuclear	Renewable	
Coal	Gas	Diesel		Hydro	Other Renewables
209.425	24.924	0.51	6.780	46.367	100.683

Table 1.2 India’s renewable energy sector at a glance (all data in MW)

Bio-Power	Waste to Energy	401.84
	Biomass	10170.61
Small Hydro		4807.81
Wind Power		39691.15
Solar Power		45611.91
Total		100683.32

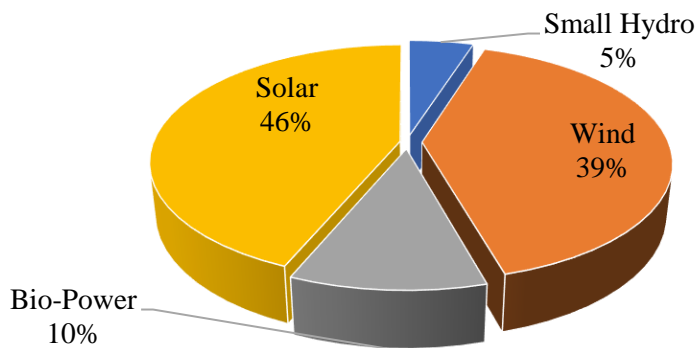


Fig. 1.3 India’s RE sources installed capacity

The growth of SPV power has been tremendous in India in the past decade. In 2011 the installed capacity was 0.563 GW whereas by the end of 2020 it was 38.983 GW. The growth in SPV in India during 2011 – 2020 is depicted in Fig. 1.4.

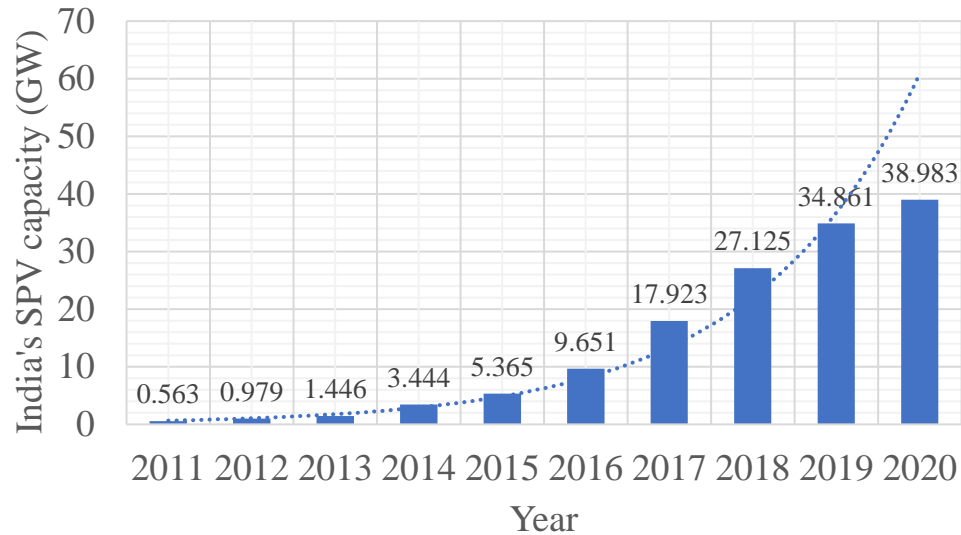


Fig. 1.4 India's SPV growth during 2011 – 2020

1.3 RENEWABLE ENERGY INITIATIVES IN INDIA

India is endowed with huge potential for solar energy, 5,000 trillion kWh/year is incident over the land area that mostly receives 4-7 kWh/m²/day. The vision of the Indian government is to reach 227 GW capacity using RE by 2022, this target is 30% more than the target proposed in Paris Agreement [2]. Among this 227 GW capacity, an ambitious target of 100 GW capacity from solar installations is further envisioned by the Indian government. India has a relatively low per capita energy and electricity consumption. According to India Brand Equity Foundation (IBEF) report, per capita electricity consumption in India is 1208 units for the year 2019-20 [3]. As the economy grows the

electricity consumption is projected to reach 15,280 TWh in 2040, this is a massive increase from 4,926 TWh in 2012.

India is ranked 5th in wind power capacity, 5th in solar power capacity and 4th in cumulative RE installed capacity in the world. India is ranked 3rd based on RE investment and plans and 3rd in Ernst and Young (EY) Renewable Energy Country Attractive Index. These aforementioned rankings are only possible due to the progressive planning, investment, and sustainable policies of the Indian government. Various projects to add to RE capacity are under development such as the 2255 MW solar power plant in Rajasthan, which will be the world's largest when completed. As per Central Electricity Authority (CEA) by 2029-30 the renewables will contribute to about 44% while dependency on the thermal power plants will be reduced from 78% to 52%.

The scheme for “Development of Solar Parks and Ultra Mega Solar Power Projects” was rolled out by the Ministry of New and Renewable Energy on 12-12-2014. Under this scheme, it was proposed to set up at least 25 Solar Parks and Ultra Mega Solar Power Projects targeting over 20,000 MW of solar power installed capacity within 5 years starting from 2014-15. The capacity of the Scheme has been enhanced from 20,000 MW to 40,000 MW vide this Ministry's order dated 21-03-2017. These parks are proposed to be set up by 2021-22 [4]. A scheme under the name of Jawaharlal Nehru National Solar Mission (JNNSM) is now in its Phase II, it facilitates the setting up of over 5000 MW grid-connected SPV projects [5]. Grid-connected rooftop SPV projects by the year 2022 have to reach a cumulative capacity of 40 GW and central financial assistance is provided to the residential sector for up to 3 kW_p plant by the government of India [6].

The off-grid SPV application program focused on installing 118 MW of solar application-based equipment such as street lights and study lamps. Some other schemes initiated by the Government of India promoting off-grid solar power are Atal Jyoti Yojana (AJAY II) and Pradhan Mantri Kisan Urja Suraksha Evam Utthaan Mahabhiyaan (PM KUSUM).

1.4 BASICS OF SPV SYSTEM

SPV system comprises one or more solar panels that are working in coordination with the inverters/converters, batteries, and grid. These vary in size from a rooftop and portable systems to massive grid-connected plants. A solar cell is a building block of an SPV system, these cells when connected in series and parallel form a solar panel/modules, which in turn form solar arrays. The other components apart from photovoltaic panels/modules are considered as the balance of systems (BoS). These include the inverters, converters, switches, battery packs, wirings, controllers, meters, and mounting systems.

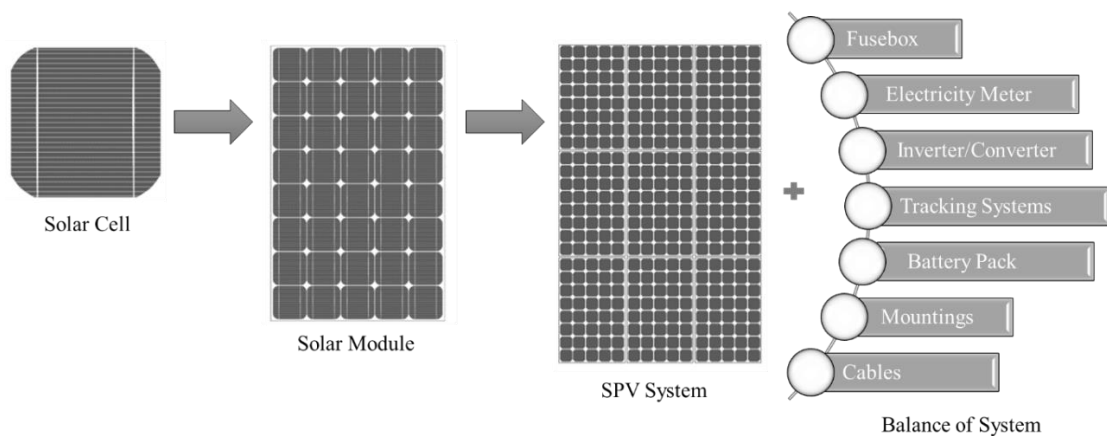


Fig. 1.5 Basic composition of an SPV system

1.5 DESIGNING OF SPV SYSTEM AND APPLICATION

The designing of the SPV system involves various aspects of the SPV system as the solar power depends on meteorological parameters as well as physical constraints of the location. These factors must be kept in mind before designing the SPV system for various applications. The types of SPV systems for different applications are:

1.5.1 Grid Connected SPV System

A grid-connected solar PV system uses solar modules as the power generation source. The power produced is fed into an inverter which changes the DC power output of the solar array to AC power compatible with the regional power grid regulations at the installation site. The system allows for any on-site loads to be powered by a combination of power generated by the PV system and power drawn from the mains power grid [7]. Excess power generated by the PV system will be exported to the power grid. Fig. 1.6 shows the on-grid SPV system and its functioning.

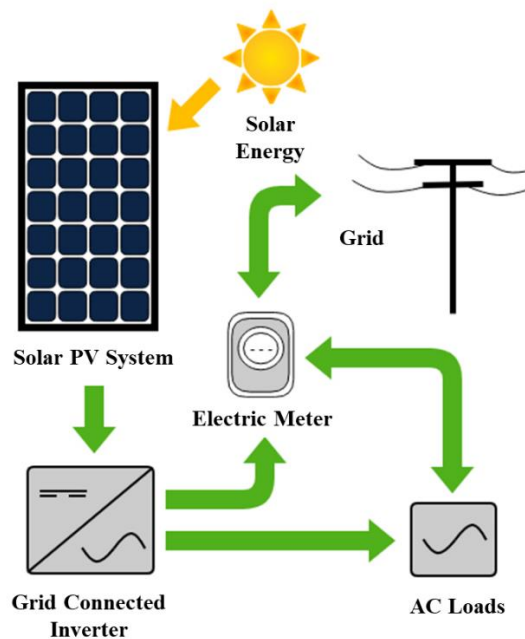


Fig. 1.6 Grid-connected SPV system

1.5.2 Standalone SPV System

A standalone or off-grid SPV system is one where no power exchange from the grid is occurring. This type of system is mainly used for remote areas or in areas where grid power penetration is very low and sporadic. In the off-grid system, the SPV power is fed to the converters for the battery energy storage system and to the inverters for meeting the AC loads requirement [8]. This system is shown in Fig. 1.7.

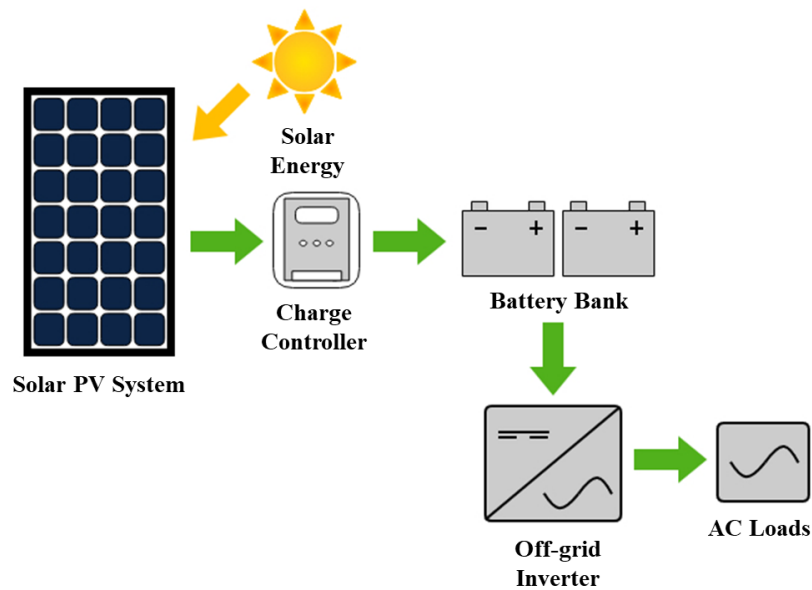


Fig. 1.7 Standalone SPV system

1.5.3 Hybrid System

A system with different power and energy sources working in coordination to meet the power demand is known as a hybrid system. The different sources are solar thermal, SPV, wind energy generation system, batteries, grid, fuel cell, and other renewable energy resources.

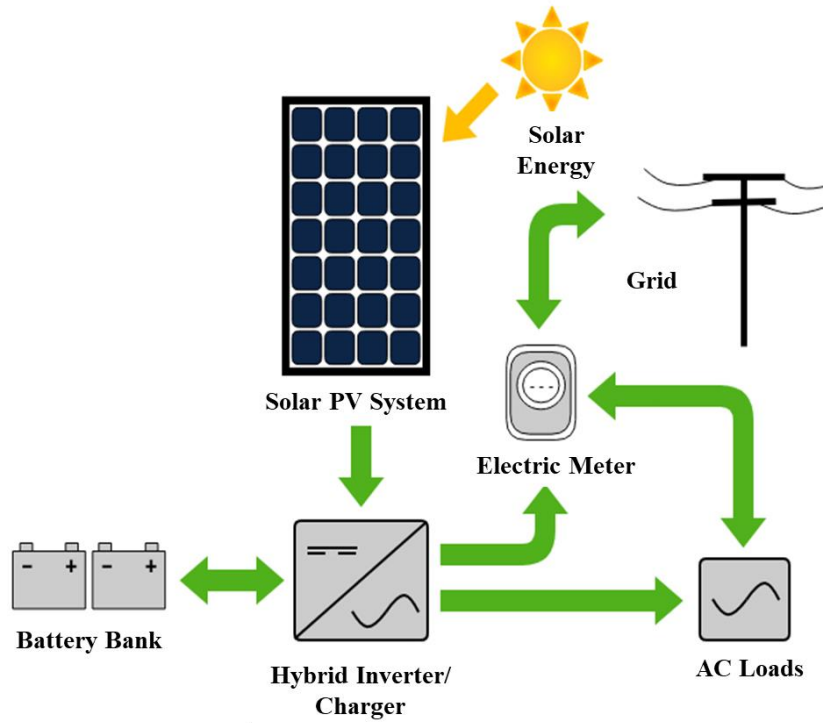


Fig. 1.8 Hybrid system

1.6 PROBLEM FORMULATION

Solar penetration in RE resources as well as in the overall power sector is increasing day by day. In addition, SPV power is stochastic and irregular as it depends on various factors such as irradiance, wind speed, relative humidity, cell temperature, latitude, longitude, angle of inclination, movement of clouds, and many more factors.

Efficient use of the fluctuating energy output from SPV systems requires reliable forecast information. This intelligent model for forecasting SPV power must overcome the drawback of effective prediction during hazy and smoggy conditions especially occurring in highly polluted locations for certain periods.

Due to drawbacks of numerical and computational methods and techniques the formulation of modern meta-heuristic techniques for the optimal designing of the SPV

system and its forecasting is required. A modified grey wolf optimization-based optimal sizing algorithm needs to be designed for the RE sources especially SPV. The deregulation in the Indian power sector is to be kept in mind while designing the algorithm. Moreover, user preference and ease of comfort must also be addressed.

The SPV power is affected by the various nonlinearities thus impacting its efficiency. Performance enhancement is another aspect of the SPV system that requires the designing of modern intelligent methods. Utilizing a modern intelligent technique for designing a robust maximum power point tracking controller is one of the methods. In addition, there is a scope for implementing a novel artificial intelligence-based SPV array reconfiguration method to maximize the performance of the SPV system under changing meteorological conditions.

1.7 OUTLINE OF THESIS

This thesis comprises eight chapters including introduction, literature review, modeling of renewable energy-based microgrid components, study and analysis of intelligent techniques, GWO-ANN based approach for short term SPV power forecasting, design and analysis of SPV based microgrid for a selected location, performance enhancement of SPV system using array reconfiguration and MPPT, conclusions and future scope followed by references.

Chapter 1: This chapter gives a brief insight into the current scenario of RE in the world and India with a focus on SPV. The initiatives and policies formulated by the Indian government to promote SPV, and a brief introduction about the types of SPV systems and their basic components.

Chapter 2: The literature survey is presented in this chapter. This literature review presented is on SPV modeling, intelligent techniques focusing on short-term SPV power forecasting, sizing, and designing of hybrid RE-based microgrid. Moreover, a comprehensive literature analysis on maximum power point tracking techniques and array reconfiguration techniques is presented in this chapter. Based on this, knowledge gap analysis is presented in the last section of the chapter.

Chapter 3: This chapter presents the modeling and designing of RES-based components. The focus is on design elements of the SPV system, wind energy generation system, batteries, inverters, converters, energy balance model.

Chapter 4: This chapter focuses on the study and analysis of the meta-heuristic optimization techniques. This chapter gives a brief overview of population-based optimization techniques such as particle swarm optimization, GWO. A hybrid meta-heuristic technique using GWO and PSO, MGWPSO has been designed and is discussed in detail when applied on different benchmark functions. Artificial neural networks and adaptive neuro-fuzzy techniques are also discussed in this chapter.

Chapter 5: The chapter presents GWO-ANN based approach for short-term SPV power forecasting. It gives an insight on the importance of SPV power forecasting, the SPV site considered for collection of data. Performance evaluation of GWO-ANN based model is presented with comparative analysis in the last section of the chapter followed by the conclusion.

Chapter 6: This chapter presents the design and analysis of an optimal hybrid microgrid for a specific location. The chapter describes the site location in detail followed

by the use of linear programming, MGWPSO based algorithm, and an intelligent energy management system for SPV based microgrid.

Chapter 7: The enhancement of power using array reconfiguration and maximum power point tracking method is presented in this chapter. A comparative analysis of the GWO based array reconfiguration technique with other topologies is discussed in detail. The chapter also comprises modeling and analysis of ANFIS based MPPT for a standalone application.

Chapter 8: The conclusions of the research work are presented in this chapter of the thesis. Moreover, the future scope of the research work is discussed in brief.

CHAPTER 2

LITERATURE REVIEW

2.1 INTRODUCTION

This chapter comprises a brief review of the previous work done on the topics of SPV system, microgrid, maximum power point, array reconfiguration, and other concerned areas of study. Based on the literature survey some research gaps have been identified and problems have been formulated accordingly.

2.2 MATHEMATICAL MODELLING OF RES AND MICROGRID

Integration of SPV array with the grid requires various power electronic-based components. These components include DC/DC converter and inverter. A DC/DC converter is used to implement maximum power point tracking (MPPT) controller to track the maximum power of the SPV array. An inverter provides conditioning in the SPV output and makes this able to match the grid requirements. This section presents a brief literature survey mathematical modeling of various components such as SPV array, wind energy generation system, power electronics converters required for grid integration, fuel cell and pumped hydro storage, etc.

V.J. Chin et al. presented a review paper focusing on the PV cell modeling and model parameters using estimation techniques [9]. It provides the concepts, features, and highlights the advantages and drawbacks of three main PV cell models, namely the single diode R_S -, R_P - and the two-diode. The authors carried out a critical evaluation to summarize the performance of the models. The paper is useful for providing comprehensive studies in

the field of PV modeling and simulation. The comparison of different SPV models is presented based on speed, accuracy, and convenience. Few other literatures focusing on the review analysis of the PV cell parameter identification are [10], [11], [12].

Extraction of parameters of a single diode model for PV cell and its modeling is presented by M. Rasheed et al. The authors proposed a Newton Raphson method (NRM) and modified NRM to solve the equation for parameter extraction of a single diode PV cell [13]. R. Kotla et al. designed the parameters of the SPV arrays using the parasitic effect to find the values of R_{sh} and R_s . The simulation and experimental verification are also presented using IB Solar-36 polycrystalline modules with varying T and G values [14].

C. Lupangu et al. performed a review analysis on the technical issues of SPV systems. The present paper aims at reviewing some technical challenges on the present state of PV systems supported energy policies, numerous cell technologies, MPPT and converter/inverter technology, energy management, and programming techniques, reliability, power quality, and management systems issues [15]. Furthermore, in-depth modeling of SPV systems in a grid connected scenario is presented by [16], [17], [18].

Wind energy conversion system (WECS) is a key aspect as RE source in a microgrid. A. Merabet et al. designed a DFIG based WECS using a sliding mode controller [19]. A review is presented by R.A. Badwawi et al. for the sizing and design optimization of SPV and wind energy system [20]. The sizing of the batteries and energy balance equations for a hybrid microgrid system is presented by [21], [22], [23], [24]. Y. Kumar et al. designed an efficient microgrid considering 422 kW peak load with HOMER software. The authors designed a hybrid RE-based microgrid with 6.18% of annual cost savings and 38.3% of reduced CO₂ emissions [25].

Somaiah et al. [26] investigated and compared the mitigation of low frequency (LF) current ripples by using a cascaded converter with conventional push-pull converters for FC applications. A single-stage, single phase FC for grid connected as well as the standalone mode is proposed based on boost inverter by Jang et al. [36]. Bensmail et al. [37] presented modeling of a hybrid PV/FC system, which utilized a power conditioning unit (PCU) for effective management. Akin et al. [38] proposed a soft-switched space vector PWM controlled parallel resonant DC link-based inverter for fuel cell applications. Further, the authors used the proposed converter with an induction motor to evaluate the results of a controller.

For an off-grid application of SPV system [27], [28] there are various topologies of DC-DC converter including buck, boost, push-pull, half-bridge, full-bridge, flyback, buck-boost, etc. The choice of topology depends on system requirements and its applications. M. Kumar et al. presented a comparative analysis of DC-DC converter topologies for an SPV-based water pumping system considering a BLDC motor [29]. Ahmed H. El Khateb et. al [30] presented a combination of cuk and buck DC-DC converter for a standalone PV system. An MPP tracking control approach is devised with the converter to supply a fixed voltage/current to the battery system under varying environmental conditions. The proposed system has been tested under different irradiance and temperature conditions.

2.3 OPTIMIZATION TECHNIQUES

There are numerous optimization algorithms present in the literature and their performance is dependent on the nature of the problem that is chosen for the optimization. G. Venter [31] presents an in-depth review of different types of optimization methods such

as local optimization problems, global optimization problems, evolutionary algorithms, deterministic algorithms, and many more. The literature presenting the review of different nature-inspired and evolutionary algorithms are [32], [33], [34], [35].

The swarm-based optimization techniques have better results and fast convergence. I. Trelea analyzed the standard results from dynamic system theory and derived graphical parameter selection guidelines for particle swarm optimization (PSO) [36]. A Nickabadi et al. designed a novel PSO algorithm by changing the inertia weight characteristic of standard PSO [37]. Similarly, multiple variations of the PSO have been proposed in the literature such as self-regulating PSO [38], dynamic inertia weight PSO [39], social learning PSO [40], PSO with Levy flight [41], multi-vector PSO [42].

In modern times modifications to the population-based or swarm-based optimizations have led to the development of evolutionary algorithms (EA). These algorithms can be implemented for other applications than optimizations. EA is further referred to as soft computing or intelligent algorithms [43]. The different types of EA are simulated annealing [44], hybrid fuzzy genetic algorithm [45], hybrid PSO genetic algorithm [46], fuzzy evolutionary optimization [47], whale optimization [48], grey wolf optimizer [49].

2.4 SHORT TERM SOLAR POWER AND ENERGY FORECASTING

SPV power forecasting is one of the key tools for this paradigm and plays a vital role in the efficient integration of renewable power generation and reduction in volatility to distributed generation systems. Precise and accurate forecasting of PV power helps massively in planning and scheduling of power demand-supply for the consumers as well

as various distribution companies (DISCOMs). It further enhances system reliability and power quality issues due to uncertainty in PV power generation. It is also an essential tool for creating a modern transactive energy framework in a grid connected microgrid system [50], [51], [52], [53]. PV power prediction not only reduces the number of units required in hot standby but also minimizes the operational costs. Therefore, the prediction of PV power has become crucial for grid stability, optimal unit commitment, and economic dispatch.

Recently, many studies have been performed to obtain accurate forecasts using different approaches such as mathematical modeling, regression models, and intelligent techniques-based approaches. There are two major approaches to predict solar PV output such as direct and indirect approaches [54], [158].

C. Wan et.al [55] comprehensively reviewed the theoretical prediction methods of solar energy resources and photovoltaic power generation. The application of solar forecasting in smart grid energy management is also studied in detail. The author submits relevant research papers on the development of solar and photovoltaic energy prediction methods. Solar and photovoltaic forecasting models are divided into four categories: statistical models, artificial intelligence-based models, physical models, and hybrid models. This article briefly discusses the advantages and disadvantages of different types of forecasting methods. This article has thoroughly studied the application of solar energy forecasting in smart grid energy management. The proper solar forecasting method can be selected according to the specific application to ensure performance [159].

M. Diagne et al. [56] carried out an in-intensity overview of the present-day techniques used to expect sun irradiance with the intention to pick the right prediction

approach in line with the needs. Machine learning algorithm like k^{th} Nearest Neighbor (kNN) regression algorithm, Support Vector Machine (SVM), Adaptive Fuzzy algorithm, Markov Chain, Cluster evaluation are present in this for solar forecasting.

M. Giorgi et al. [57] studied statistical regression methods to develop the Elman-ANN model to predict the performance of the grid-connected 960 kWp photovoltaic system in Italy. In order to evaluate the accuracy of the prediction method, various statistical error measures were evaluated. In order to determine the amplitude and phase errors, the standard deviation error decomposition was carried out. Parameter skewness and kurtosis allow detailed analysis of distribution errors. Elman's artificial neural network is implemented using three different input vectors as input training data sets. The forecast horizon is from 1 hour to 24 hours and authors used the error distribution and various statistics to carefully check the accuracy of the PV prediction.

J. Antonanzas et al. presented an extensive review of solar PV power forecasting techniques focusing on latest advancement and future trends. It is concluded that mostly forecasting horizon considered is day ahead and statistical approach is superior in most occasions [58]. D.K. Chaturvedi et al. also presented a review of solar forecasting based on various time horizon and classified as intra-hour, intra-day, and day ahead [59]. Martinez-Anido et al. discussed the impact of PV power forecasting in improving the power system operations and the cost of electricity generation [60].

Time horizon (t_h) of forecasted PV power output plays an important role in management of the PV systems and its control, for different locations like schools, hospitals etc. Y.K. Sanusi et al. performed a study considering clearness index (K_T) and diffuse ratio (D_R) for feasibility of solar energy utilization in tropical stations of Nigeria.

In the study, eleven-year data of solar radiation, maximum and minimum temperature was collected and compared with monthly variations of K_T and D_R . The authors therefore suggested that the output of the solar PV system needs evaluation under different conditions, especially considering spatiotemporal variations thus, necessitating the need to monitor grid connected PV plants by installers and investors [61]. Y. Chu et al. has proposed a PV power reforecasting model using ANN model based on three baseline model- ARMA, cloud tracking and kNN for 5-, 10- and 15-min time horizons [62]. The effect of aerosols over northern and eastern China were studied by X. Lia et al., their study showed that 1.5kWh/m^2 per day was an annual reduction in solar radiation when compared with a pollution free environment [63]. The correlation between atmospheric aerosols on the reduction of PV power is to be studied. Thus, there is a need for a solar PV power forecasting model that adapts to this change in the atmosphere.

To help in the study of solar power output characteristics authors have used multiple linear regression analysis with various weather data and solar irradiance data. Garba et al. have studied the prediction of global solar irradiance using relative humidity, temperature and modified sunshine duration factor [64]. Amrouche et al. has proposed MLP based ANN model to forecast global horizontal irradiance (GHI) for two different locations. The adaptability of proposed ANN-MLP model by predicting GHI using unfamiliar data is highlighted by them [65]. A. Mellit et al. discussed various artificial intelligence techniques for the sizing of various PV systems, PV-wind hybrid systems, and also modeling of 24-hr solar forecast system in Trieste, Italy [66].

R.M. Ehsan et al. proposed a 24-hr ahead PV power forecasting model using MLP and discussed the use of different training algorithms and transfer functions for different

layers to map the input-output database [67]. A fuzzy logic-based neural network model is designed by Chen et al. [68] to estimate solar radiation forecast using time series data of radiation and temperature for different sky conditions. The mean absolute percentage error (MAPE) based on the fuzzy logic algorithm is between 13.87% and 20.22% for the solar radiation forecast. The MAPE of the neural network prediction model ranges from 10.85% to 20.33%. the results obtained from ARIMA models shows MAPE is about 30% during the forecast studies of solar radiation [69]. NE ranges from [-10%;10%] for the various empirical and persistent models to estimate PV power, the use of optimized training algorithms along with MLP tool helps in further reducing it [70], [71], [72]. K. Basaran et al. have proposed a new approach of ensemble tree learning algorithm to improve the SVM, ANN and DT techniques in predicting solar radiation with RMSE between 4.6 and 14.6% [73]. M.R. Douiri modelled a self-tuning solar PV power model based on takagi-sugeno type neuro fuzzy technique. The model simulates the I-V characteristics to predict global maximum power point with 1.4% average error [74].

2.5 DESIGN AND SIZING OF HYBRID MICROGRID

There are various challenges in the adoption of the microgrid concept such as the proper selection of distributed energy resources (DERs) along with their optimum size. Various methods have been proposed for the optimal capacity of SPV, wind turbines, and other energy storage devices. A review of the different techniques for sizing problems in a hybrid MG system is discussed in [75] and concluded that a hybrid of two or more meta-heuristic techniques gives better results. In [76], [77] studies have been performed considering the different objective functions. These objective functions can be related to the economics of the system, environmental impacts of the system, and operational factors.

Research has been done using numerical methods for sizing as well as cost optimization of SPV, WT, and small hydro systems. The use of meta-heuristic techniques has also been proposed by many authors, but these techniques are complex and need more memory for a quick and effective solution [78], [79], [80], [81].

A standalone microgrid on Dongfushan Island, is designed using the multi-objective genetic algorithm for realistic and practical sizing of the site [82]. The authors verified the results of the proposed GA method using the operational data from the microgrid developed. The issue related to energy storage systems during an islanded operation of an MG is presented by K. Lai et al. [83]. In this paper, a new battery storage sizing algorithm for microgrids to limit load shedding is proposed. The modeling and performance of hybrid MGs in islanded mode are discussed in the literature [84], [85].

A case study of grid-connected MG using two algorithms for sources sizing and battery sizing and optimal solutions is presented by U. Akram et al [86]. A mathematical model is proposed by J. Aguado et al. [87] for the battery storage system in a market-driven scenario. The developed system is tested on the IEEE-24 bus system and performed well. R. Blanco et al. proposed a large-scale integration of grid-connected energy storage in the locality with a high penetration of RE resources and a centralized perspective of reducing operational costs along with the investment cost of energy storage has been considered [88]. A dynamic programming algorithm is employed to design the hybrid wind power plant with energy storage elements in a real-time electricity market [89].

According to the modern power system, the load profile is becoming uncertain, key factors being advancement in power electronic devices, evolution of EVs, planning and management of MGs. Further, the sizing of the complete system from RE resources to

energy storage system may not be optimal in case of uncontrolled load. Some related literature for RE integration with the existing grid without any consideration of the smart controller is found in [90], [91]. However, to design a hybrid MG for optimum performance and reduced cost, the load needs to be flexible. The electrical demand considered should be flexible for accommodating high levels of RE. A multi-objective MG operator for a smart grid with different RE sources like SPV, WES, fuel cell, and a battery energy storage system was designed and presented [92]. A demand response concept was considered for the optimization problem and a mixed-integer linear programming-based optimization for DERs is provided [93] for MG environment with opportunities for load management. A two-step novel real-time BESS for smoothing of PV/WES generation is proposed by X. Li et al [94]. These aforementioned studies are rule-based i.e.; they are specifically designed for the operation strategies. On the other hand, short term scheduling of grids for instant energy dispatch and load management has been the key focus in [95], [96].

R. Atia et al. have tried to investigate the effect of the electrical load flexibility on the component size of the hybrid MG system in a residential area in Okinawa. They had considered a different level of uncertainty and loading parameters for the same area to meet the demand optimally and effectively [97]. This paper investigates the impact of load flexibility on the overall sizing of the different components under different cases. The authors have also tried to model the usage of different appliances according to the resident's usage.

2.6 POWER ENHANCEMENT IN SPV SYSTEM

A report presented by S. Ong et.al for the solar land usage metrics in the USA considering SPV and concentrating solar power (CSP) facilities. Some of the drawbacks of the SPV system are listed below, the land used for the PV system compared with CSP is 8.4% more [98]. Furthermore, the PV arrays have a low conversion efficiency of with 24% being the highest for the most common silicon crystalline module [99]. It becomes even more critical and challenging to improve its performance in different conditions. In the SPV systems, the power enhancement is achieved mainly by tracking the maximum power point. With the help of various literature related to the power efficiency improvement of SPV systems, there are two main approaches for this. Firstly, using array reconfiguration (AR) methodology and secondly designing maximum power point tracking controllers (MPPT).

2.6.1 Array Reconfiguration Method

Reconfiguration of the PV arrays aims to redistribute the shade to create a uniform row current or equal irradiation. The reconfiguration can be performed either via physical relocation (PR) [100] or via electrical routing of the arrays i.e., electrical array reconfiguration (EAR) [101], [102], [103]. PR methods suffer from excessive interconnecting ties and skilled labor [104]. EAR techniques are also the dynamic reconfiguration technique requiring sensors to determine the partial shading and faulty conditions. Whereas, in PR methods fixed interconnection of the PV modules is performed according to the physical location. The significant difference among them is the use of sensors and thus the cost of the system.

Several techniques have been proposed to work effectively in tracking GMPP of PV array with PS [105], [106], [107], [108]. Different configurations of PV array reconfiguration such as series-parallel (SP), series (S), parallel (P), total cross-tied (TCT), bridge link (BL), and honey-comb (HC) are analyzed in [109] and performance has also been compared. The hybrid configuration of the PV system is superior when compared to the conventional topologies based on power maximization [110]. The topologies derived from SuDoKu game theory have limitations that it can be implemented where the PV array has an even number of rows [111]. In a real-world scenario, the shadow on the PV panels is rarely in the straight lines or a linear pattern, the cloud movement and its modeling are presented by S. Vijayalekshmy et al. for a TCT and rearranged TCT topology [112]. However, the predominant factor for cloud movement and cloud shade due to wind was not taken into consideration.

G. Sagar et al. had modeled the movement of clouds using wind velocity and had further implemented SuDoKu based shade dispersion through PR of 6x6 panels in a BL-TCT configuration [113]. Different techniques have been proposed in the literature for shade dispersion through reconfiguration such as magic square (MS), latin square (LS), and dominance square (DS). R. Venkateswari et al. had proposed Lo Shu arrangement for physical reconfiguration of PV array for different types of shading conditions [114]. It was concluded that these were better than conventional topologies. Table 1 and Table 2 provide a better understanding of EAR and PR respectively by presenting them in a summarized form.

Table 2.1 Summary of EAR application on SPV system

Ref	Reconfiguration Technique	Configuration	Control Algorithm	Sensed Parameter	Total Switches
[101]	Dynamic Link Logical Block	SP: 3x2	Rough Set Theory	I	$2(N_{pv} + 1)$
[103]	Convert SP to TCT	SP: 3x3	Arduino based DAS	V, I, frequency	$(N_{pv} - 2)$
[107]	Switching Matrix	TCT: 9x9	Grasshopper Optimization	V, I, Irradiance	$2(i * j)$
[108]	Optimal Switching Matrix	TCT: 9x9	Marine Predators Algorithm	Irradiance, V	$6(i * j)$
[115]	Switching Matrix	SP: 6x5	Refer [14]	V, I	NS
[116]	Swarm Matrix Dispersion	TCT: 9x9	PSO	V, I	$2(1 \text{ pole m throw})$
[117]	Irradiation Equalization	TCT: 3x4	Hierarchical Iterative Sorting	V, Irradiance	$(i * j)$
[118]	Two phase process	TCT: 9x9	Row current minimization	V, I	$2(1 \text{ pole m throw})$
[119]	Adaptive bank	TCT	Bubble sort	V, I	$2(i * j)$
[120]	Irradiation Equalization	TCT: 4x4	Best worst sorting	V, I	$N_{pv}(i^2 - i)$
[121]	Adaptive	6x4	Fuzzy estimator	V, I	$i + 6$
[122]	Adaptive bank	TCT: ixj	Scanning algorithm	V, I	$2(i * j)$

Table 2.2 Summary of PR application on SPV system

Ref.	Reconfiguration Technique	Configuration	Cloud Movement	Complexity	Types of Shade
[100]	SuDoKu	TCT: 9x9	No	Moderate	SN, SW, LN, LW
[102]	GA	TCT: 9x9	No	High	SW, SN, LN
[104]	Optimal SuDoKu	TCT: 9x9	No	High	Discontinuous shade
[109]	Mitigate MMPL	5x5	No	Low	SN, SW, LW, LN
[111]	Puzzle shade dispersion	BLTCT: 5x4	No	Low	Different patterns
[110]	SuDoKu Puzzle	TCT: 4x4	No	Moderate	Different patterns
[112]	SuDoKu Puzzle	6x6	No	Moderate	Consistent shading patterns
[113]	SuDoKu Puzzle	Hybrid TCT: 6x6	Yes	Moderate	Non uniform shading
[114]	Lo Shu Technique	TCT: 9x9	No	High	SN, SW, LN, LW
[123]	Topsolver program	TCT: 3x3	No	High	SN, LN, LW
[124]	Zig-Zag Arrangement	TCT: 4x3	No	Moderate	Corner patterns with horizontal and vertical shading
[125]	Dominance Square	TCT: 5x5	No	Moderate	SN, SW, LN, LW
[126]	Magic Square	TCT: 4x4	No	Low	Corner patterns with horizontal and vertical shading
[127]	Latin Square	TCT: 4x4	No	Moderate	Corner patterns with horizontal and vertical shading

2.6.2 Designing MPPT Controllers

The performance of the PV systems depends on various meteorological parameters including global horizontal irradiance, efficient MPPT controller, cell temperature, wind speed, spectral density and the dust particle accumulated on PV module. It has been reported that the performance of PV and power output may be increased by 20%. The effect of these non-linear variables is regulated by using control techniques for tracking the maximum power point of the system [128], [129], [160], [161], [162]. There are a number of intelligent approaches like fuzzy logic, ANN, GA, PSO etc. [130], [131] are available in the literature to track the maximum power point of the PV system. N. Karami et al. performed a general review analysis of various MPPT techniques [132]. The authors compared 40 old and new MPPT methods and highlighted the various aspects of each method in a tabular form. The analysis is thorough and presented in such a way that readers can select the most suitable method for his own application.

A. R. Reisi et al. studied the non-linear behavior of PV panels along with the variation of MPP with changing environmental conditions [133]. The authors classified MPPT methods into three categories: online, offline and hybrid methods and simulated results in Matlab/Simulink environment for each method. P&O and INC are some of the most common tracking algorithms for MPPT but have certain drawbacks. I. Houssamo et al. compared INC and P&O techniques experimentally with a dSPACE setup to show the MPPT efficiency [134] and T. Sruthy et al. have developed a fast-converging MPPT for PV system using dsPIC microcontroller [135]. R. Feranda et al. presented a comparative analysis of ten MPPT algorithms on the basis of cost were evaluated, comparison was made on their performance and implementation cost for 12 different types of irradiances, using

MATLAB Simulink namely incremental conductance method, open voltage method, short circuited pulse method, P&O, and constant voltage method, etc. [136].

T. Eswam et al. compared numerous methods and presented an in-depth analysis of the MPPT techniques. Some of the key findings were open voltage and short circuit pulse techniques provide low energy output in comparison with P & O and incremental conductance algorithms [137]. While analyzing different techniques for tracking maximum power point it was noticed by the authors, in P&O technique, the output power keeps oscillating as the controller is unable to find global maxima or minima and is stuck between local minima and maxima. Similarly, in-depth review of MPPT algorithms used in PV has been done [138] and were compared on the features such as tracking speed, complexity, efficiency and relative cost [139].

INC to some extent overcomes this but gives unsatisfactory results under low irradiance and requires harsh detection devices, was analyzed by A. Kumar et al. and proposed a Fuzzy Logic MPPT to overcome INC shortcomings [140]. S. Al-Majidi et al. proposed a novel MPPT using fuzzy logic approach, the efficiency of the achieved was 99.6% under varying conditions. Authors considered EN 5030 standard test to calculate the efficiency of the proposed methodology [141]. F. Kazan et.al have explained the concept of maximum power point and its control and tracking. They have implemented a PID controller with all the detailing explained [142]. K. Kanimozhi et.al developed a hybrid MPPT for improved efficiency during partial shading conditions, the proposed algorithm adjusts the duty cycle of the Cuk converter according to the changing conditions and the simulation results were verified experimentally by the authors using Solartech SMP085P PV modules and RL loads [143].

2.7 KNOWLEDGE GAP ANALYSIS

Modeling of the novel hybrid intelligent technique for the SPV system and its application can be investigated. The above-discussed SPV power models do not consider atmospheric aerosol content in modeling of the ANN or MLP forecasting models and the errors range from 5% to 20%. The use of aerosol particles or air quality index in the solar photovoltaic forecasting system is sparingly available in the literature, especially, considering the Indian scenario. There is a scope for implementing a hybrid intelligent technique for sizing and energy management of a hybrid microgrid system. Furthermore, a seasonal case study can be implemented for the specific site considering deregulation in Indian power systems. Evolutionary optimization-based MPPT algorithms and array reconfiguration are sparsely available in the literature to maximize the PV power Output.

2.8 PROBLEM FORMULATION

The main objectives of the proposed research work based on the above-mentioned research gap are formulated as follows:

- Study and analysis of hybrid intelligent optimization algorithms for SPV application
- Development of the intelligent model for SPV power forecasting
- Designing of SPV based microgrid using the intelligent approach for a specific site
- SPV power enhancement through array reconfiguration and MPPT algorithms

CHAPTER 3

MODELLING OF RENEWABLE ENERGY BASED MICROGRID COMPONENTS

3.1 INTRODUCTION

The various RE resources along with energy storage systems form a hybrid renewable energy system (HRES) and may provide reliable and sustainable power generation. In the deregulated electricity network, the coexistence of RE resources like solar photovoltaic and wind energy conversion systems along with the traditional AC grid is achieved through microgrids (MG). These MGs are touted as the next-generation power system because of their two-way communication with the energy generators and the users. This chapter focuses on various components of the microgrid and its modeling. These components required for optimal designing of MGs are solar PV, wind energy generation systems (WEGS), battery, inverter modelling, and also energy balance equations.

3.2 RENEWABLE ENERGY SOURCES

Renewable energy sources and their applications in the power sector are booming day by day, the extensive research on materials and procurement of these sources is reducing the cost. Thus, promoting the world towards a clean energy future with a comparatively less carbon footprint. The major sources of renewable energy are solar and wind.

3.2.1 Solar Photovoltaic System

A photovoltaic system comprises photovoltaic arrays, which are the combination of series and parallel configurations of the PV modules. The Photovoltaic cells are the building blocks of the PV system. The PV cells produce very low voltage and current so these are configured, in series and parallel for a higher rating as per the requirement. When increasing the number of cells in series the V_{oc} (open circuit voltage) increases and in the same way, the current rating meets our requirement by increasing the number of parallel branches. In a PV cell, the relationship between voltage and current is non-linear. A single diode circuit model is used for effectively modeling the PV cell to represent its exact characteristic [144] [145]. In an ideal PV module, a single diode is connected in parallel with a light-generated current source as depicted in Fig. 3.1.

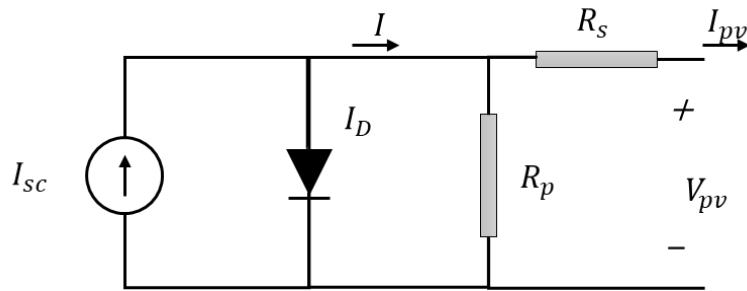


Fig. 3.1. Single diode model of PV cell with R_s and R_p

$$I = I_{sc} - I_D \quad (3.1)$$

Where,

$$I_D = I_{scref} \left[\frac{\exp(qV_{oc})}{kAT} - 1 \right] \quad (3.2)$$

$$I_{sc} = [I_{scref} + K_i(T - T_{ref})] * G/1000 \quad (3.3)$$

Where,

I= Solar cell current (A)

I_D = Module diode saturation current

I_{SCref} = Module short circuit current at 25°C

q= electron charge

V_{OC} = Module open circuit voltage

G= Irradiation on the device surface (W/m²)

A= Ideality Factor

T= Actual Module operating temperature (K)

I_{SC} = Photocurrent (A)

T_{ref} = Reference temperature (K)

k= Boltzmann Constant

$$I_{SC} = I_D + \frac{V_D}{R_P} + I_{PV} \quad (3.4)$$

Reverse saturation current I_{rs} is

$$I_{rs} = I_{SCref} \left[\exp\left(\frac{qV_{OC}}{N_S k A T}\right) - 1 \right] \quad (3.5)$$

The module saturation current I_D , which varies with cell temperature variation, is

$$I_D = I_{rs} \left[\frac{T}{T_{ref}} \right]^3 \exp \left[\left(\frac{qC_g}{Ak} \right) \left(\frac{1}{T_{ref}} - \frac{1}{T} \right) \right] \quad (3.6)$$

The output current characteristics of the PV module [146] is

$$I_{PV} = N_P I_{SC} - N_S I_D \left\{ \exp \left[\frac{q(V_{PV} + I_{PV} R_S)}{N_S k A T} \right] - 1 \right\} - V_{PV} + \left(\frac{I_{PV} R_S}{R_P} \right) \quad (3.7)$$

Where,

V_{PV} = output voltage of the PV module.

N_P = number of parallel cells

N_S = number of series cells

V_D = diode voltage

R_P = Shunt resistance in a practical model of the PV module

R_S = Series resistance in a practical model of the PV module

According to H. Bellia et.al R_P and R_S are calculated in such a way that compute maximum power is the same as experimental maximum power at STC conditions [147]. The above model equations (3.1) - (3.7) aid us in designing of a simplified circuit for the required PV module; the power electronic designers can easily incorporate this model for effective simulation with power converter devices.

The output power from a PV module is mainly dependent on the area of the module, irradiance incident on the plane of the module, temperature of the photovoltaic cells, latitude, and longitude of the selected location using the Eq (3.8). Fig. 3.2 represents the hourly power generated by SPV system during a year.

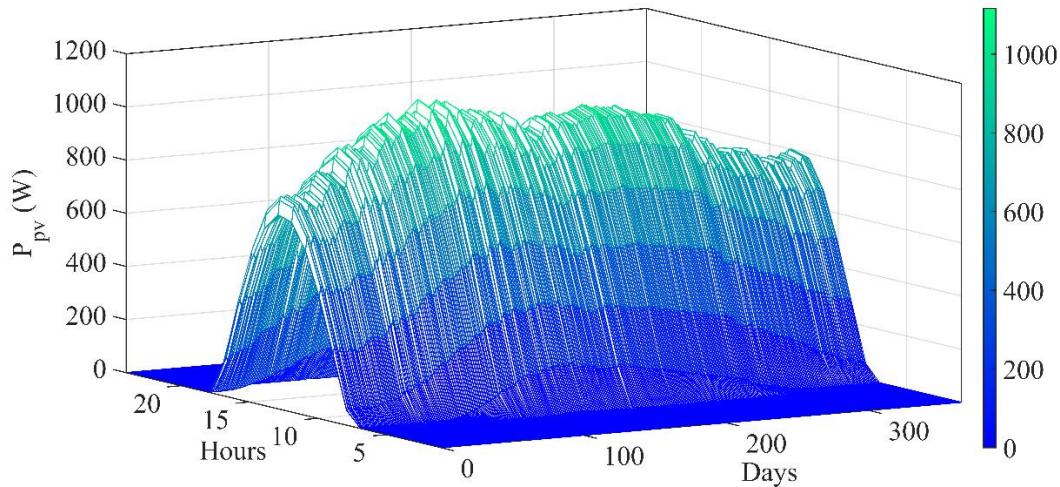


Fig. 3.2. Power generation from SPV over a year

$$P_{pv}(t) = n_{pv}PV_A G(t)\{1 - 0.005(T_a(t) - 25)\} \quad (3.8)$$

Here, $P_{pv}(t)$ is SPV Power at time t (kW), n_{pv} is Efficiency of SPV system, PV_A is Total area of SPV system (m^2), $T_a(t)$ is Ambient temperature at time t and $G(t)$ is Solar irradiance at time t (W/m^2).

3.2.2 Wind Energy Generation System

The wind energy generation systems (WEGS) convert the kinetic energy possessed by the wind into the electrical energy. Equation (3.9) defines the output power of the wind turbine. Fig. 3.3 represents the hourly power produced by wind energy conversion system during a year.

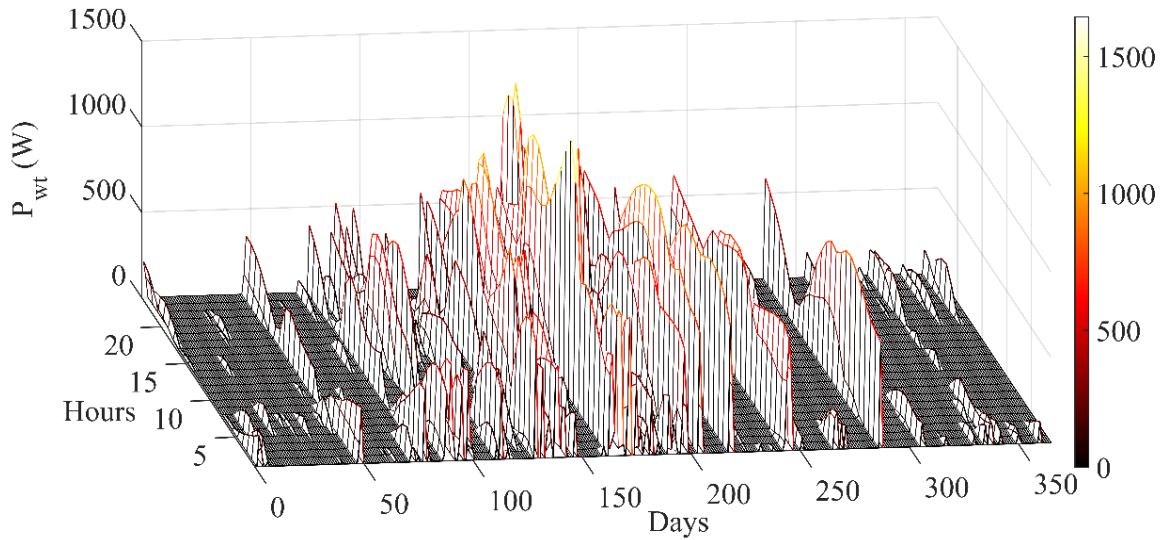


Fig. 3.3. Power generation from wind energy conversion system

$$P_{wt}(t) = \begin{cases} 0 & u < u_{cin} \\ P_{wtr} \times \frac{u - u_{cin}}{u_r - u_{cin}} & u_{cin} \leq u < u_r \\ P_{wtr} & u_r \leq u < u_{co} \\ 0 & u \geq u_{co} \end{cases} \quad (3.9)$$

Here, $P_{wt}(t)$ is Wind Power at hour t (kW), P_{wtr} Rated power of WT, u is Wind speed at time t , u_{cin} is Cut-in speed of WT (m/s), u_{co} is Cut-out speed of WT (m/s), u_r is Rated speed of WT (m/s).

3.3 ENERGY STORAGE ELEMENTS

The storage system is one of the most crucial components since inappropriate design can affect reliability and final costs. Therefore, it is necessary to adopt reliable models for realistically reproducing the working condition of the application.

3.3.1 Battery Energy Storage System (BESS)

The designed BESS is considered for a hybrid microgrid system with active participation from the power grid and other renewable sources such as SPV and WEGs.

The energy change in a battery bank over one hour is given as in Eq. (3.10)

$$E^{bt}(t + 1) = E^{bt}(t) + P_C(t) \cdot \eta_C(t) - \frac{P_D(t)}{\eta_D(t)} \quad (3.10)$$

Here, $E^{bt}(t)$ is Energy of battery at the beginning of t^{th} hour (kWh), $P_C(t)$ is Battery charged power at t (kW), $\eta_C(t)$ is charging efficiency of the battery at t , $\eta_D(t)$ is discharging efficiency of the battery at t and $P_D(t)$ is Battery discharged power at t (kW).

The capacity of the battery bank fades with time as the battery discharges and is known as total capacity fade (E_{tcf}^{bt}) of the battery [148]. This is given by

$$E_{tcf}^{bt}(t + 1) = E_{tcf}^{bt}(t) + Z_B \cdot P_D(t) \quad (3.11)$$

In the above Eq. (3.11) Z_B is degradation factor of the considered BES. The maximum and minimum state of the charge (SoC) allowed is defined as:

$$SoC = 1 - DoD \quad (3.12)$$

$$E^{bt}(t) \leq SoC_{\max} \cdot N_B - E_{tcf}^{bt}(t) \quad (3.13)$$

$$E^{bt}(t) \geq N_B(1 - DoD) \quad (3.14)$$

Here, N_B is Installed BESS capacity (kWh), DoD is Depth of Discharge of the battery. The charging and discharging of the battery are limited by the following:

$$P_C(t) \leq N_B \cdot P_B \quad (3.15)$$

$$P_D(t) \leq N_B \cdot P_B \quad (3.16)$$

Where, P_B is Maximum charge/discharge capacity per hour of the battery (kW). The lifetime of the battery (LoB) is given by the Eq. (3.17). When LoB is unity, it represents the end of battery life.

$$LoB = \sum_{DoD=0.1}^{DoD=0.8} \frac{N_{cyc}(DoD)}{N_{tot}(DoD)} \quad (3.17)$$

3.3.2 Energy Balance

The energy balance in a hybrid MG system is given by the following equations, for the AC bus and another for the DC bus, at every hour $t \in T$

$$P_{PG}^{ac}(t) + \eta_{\frac{dc}{ac}} [P_{pv}^{ac}(t) + P_D(t)] + P_{wt}^{ac}(t) = P_L(t) + P_{SG}(t) \quad (3.18)$$

$$P_{pv}^{dc}(t) + \eta_{\frac{ac}{dc}} [P_{PG}^{dc}(t) + P_{wt}^{dc}(t)] = P_C(t) \quad (3.19)$$

The generation capacity of the PV can be much higher than the power consumed by the electrical load. Thus, the following constraint is defined to limit the dispatching of the power by the maximum available generation at t :

$$\left. \begin{aligned} P_{pv}^{dc}(t) + P_{pv}^{ac}(t) &\leq N_{pv} \cdot P_{pv}(t) \\ P_{wt}^{dc}(t) + P_{wt}^{ac}(t) &\leq N_{wt} \cdot P_{wt}(t) \end{aligned} \right\} \quad (3.20)$$

$$P_{PG}^{ac}(t) + P_{PG}^{dc}(t) \leq u(t) \cdot \overline{P_G} \quad (3.21)$$

$$P_{SG}(t) \leq (1 - u(t)) \cdot \overline{P_G} \quad (3.22)$$

Here, $P_{PG}^{ac}(t)$ is Purchased grid power for the loads at t (kW), $P_{PG}^{dc}(t)$ is Purchased grid power for BESS at t (kW), $P_{pv}^{ac}(t)$ is SPV power dispatched to AC side at t (kW), $P_{pv}^{dc}(t)$ is SPV power dispatched to BESS at t (kW), $P_{wt}^{ac}(t)$ is WT power dispatched to AC side at t (kW), $P_{wt}^{dc}(t)$ is WT power dispatched to BESS at t (kW), $u(t)$ is A binary variable at t and $\overline{P_G}$ is Maximum grid power purchased or sold.

3.3.3 Fuel Cell

A fuel cell works on the electrochemical process and converts fuel (hydrogen) energy into a form of electricity. It works on the principle of chemical reaction between oxidant and the fuel for producing electrical energy with heat and water byproducts. The equivalent circuit of a solid oxide fuel cell (SOFC) is shown in Fig. 3.4. Fuel cells possess several advantages over other renewable energy resources such as high efficiency, high power quality, less or no moving parts which result in lesser noise, low maintenance and fuel flexibility. The efficiency of fuel cells varies 40-60% and in cogeneration applications can be further improved up to 90%. Cost is also lesser nowadays due to high-temperature operation which removes the requirement of precious metal catalysts.

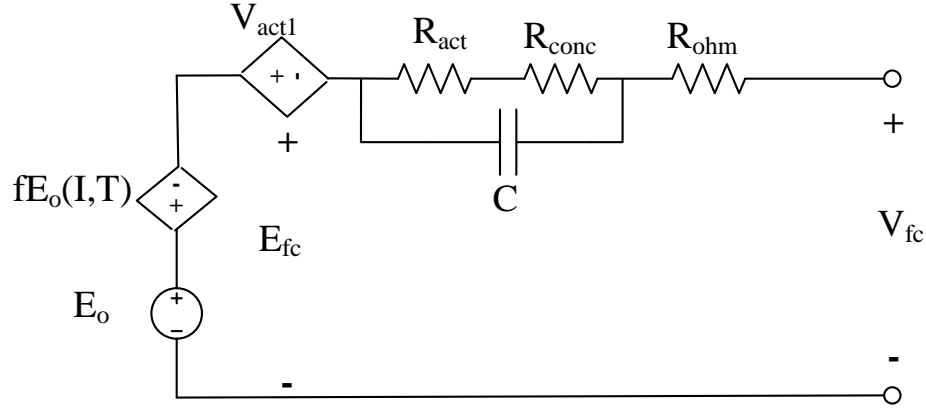


Fig. 3.4. Equivalent circuit of a solid oxide fuel cell (SOFC)

Tafel equation is used to calculate the output voltage of a fuel cell.

$$V_{fc} = E_{fc} - V_{act} - V_{con} - V_{ohm} \quad (3.23)$$

Where, E_{fc} denotes the reversible open-circuit voltage, V_{act} is activation overvoltage, V_{con} shows the concentration overvoltage and V_{ohm} is the ohm voltage. Value of the reversible open circuit voltage (E_{fc}) can be found using Nernst equation:

$$E_{fc} = N \left\{ E^0 + \frac{RT}{2F} \ln \left(\frac{P_{H_2}}{P_{H_2O}} (P_{O_2})^{0.5} \right) \right\} \quad (3.24)$$

Where, E^0 is standard reversible cell voltage, R denote universal gas constant (JK/kmol), T shows the stack temperature in Kelvin, N is the number of cells in stack and $P_i(P_{H_2}, P_{H_2O}$ and $P_{O_2})$ is the mole fraction of species. Ohmic voltage in equation (3.25) is because of electrical resistance of electrodes and the resistance offered due to flow of ions in the electrolyte and can be computed using Ohm's law:

$$V_{ohm} = i_{fc} * R_{fc} \quad (3.25)$$

V_{act} is the voltage due to cell current and hydrogen concentration and can be written as:

$$V_{act} = -A \ln i_{fc} \quad (3.26)$$

Constant A depends on the type of cell used, concentration voltage V_{conc} is ignored by considering the operation in linear region and hydrogen, oxygen flow constant.

3.4 INVERTER MODELLING

Eq. (3.27) and Eq. (3.28) represents the nominal capacity of the bi-directional inverter. It is an extension of Eq. (3.18) and Eq. (3.19) respectively.

$$\eta_{\frac{dc}{ac}} [P_{pv}^{ac}(t) + P_D(t)] \leq N_{inv} \quad (3.27)$$

$$\eta_{\frac{ac}{dc}} [P_{PG}^{dc}(t) + P_{wt}^{dc}(t)] \leq N_{inv} \quad (3.28)$$

3.5 DC/DC CONVERTER

The above-mentioned components were essential for modeling a grid connected hybrid microgrid system. The DC/DC converter is mainly implemented in a standalone application of SPV system according to the feasibility of the application. A DC/DC boost converter is required to boost the PV array voltage and to implement the MPPT algorithm which keeps on tracking the maximum power point of the PV array. The value of input inductor (L_b) is calculated as:

$$L_b = \frac{V_{PV} D}{\Delta i f_{sw}} \quad (3.29)$$

$$D = 1 - \frac{V_{PV}}{V_{DC}} \quad (3.30)$$

DC link Capacitors (C)

$$C = \frac{I_{in}D}{\Delta v f_{sw}} \quad (3.31)$$

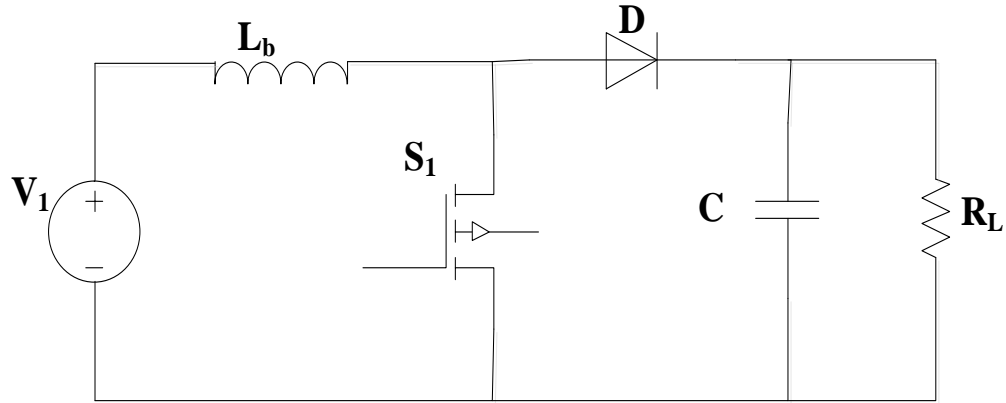


Fig. 3.5. DC/DC boost converter

A circuit of DC/DC boost converter configuration is presented in Fig. 3.5. Input ripple current ΔI_1 is considered as 6% of input current to the DC/DC boost converter and switching frequency (f_{sw}) is chosen as 10 kHz.

3.6 CONCLUSION

Mathematical modeling for various components of the renewable energy-based microgrid components is discussed in detail. The modeling of MG components integrating renewable energy resources include solar photovoltaic system, wind energy generation system, power and energy balance equations involving BESS, and inverter modeling for the grid integrated microgrid. For the stand-alone PV system designing of the DC/DC converter is presented for effective performance analysis of the MPPT for the SPV system.

CHAPTER 4

STUDY AND ANALYSIS OF INTELLIGENT TECHNIQUES

4.1 INTRODUCTION

This chapter focuses on optimization techniques and their mathematical modeling. Due to the large application of renewable energy sources and increased penetration of the SPV system, the need for optimal designing of this system is the need of the hour. The optimization techniques help in finding the optimum solutions or unconstrained maxima or minima for different applications. The chapter mainly discusses the swarm-based optimization techniques such as particle swarm optimization (PSO), grey wolf optimizer (GWO).

In the end, the chapter discusses the design and development of a hybrid technique -Modified Grey Wolf Particle Swarm Optimization (MGWPSO). It combines the exploitation characteristics of GWO and exploration characteristics of PSO. The hybrid technique is seen to outperform both -GWO and PSO techniques. The developed technique is compared with other technique on the basis of computational time, convergence and best solution.

4.2 BRIEF OVERVIEW

The concept of optimization is to execute solutions in iterative form until a satisfactory or optimum solution is reached. The general application of optimization techniques is to minimize the cost or to maximize efficiency. These techniques can broadly be classified into two distinct types:

i. Deterministic Algorithm

These have a set of specific rules for finding one solution to the other. These are traditional techniques also known as classical optimization techniques. They make use of differential calculus for finding the optimum solution.

ii. Stochastic Algorithm

As the name suggests these have probabilistic transition rules derived from nature. These have constraints that depend upon random variables.

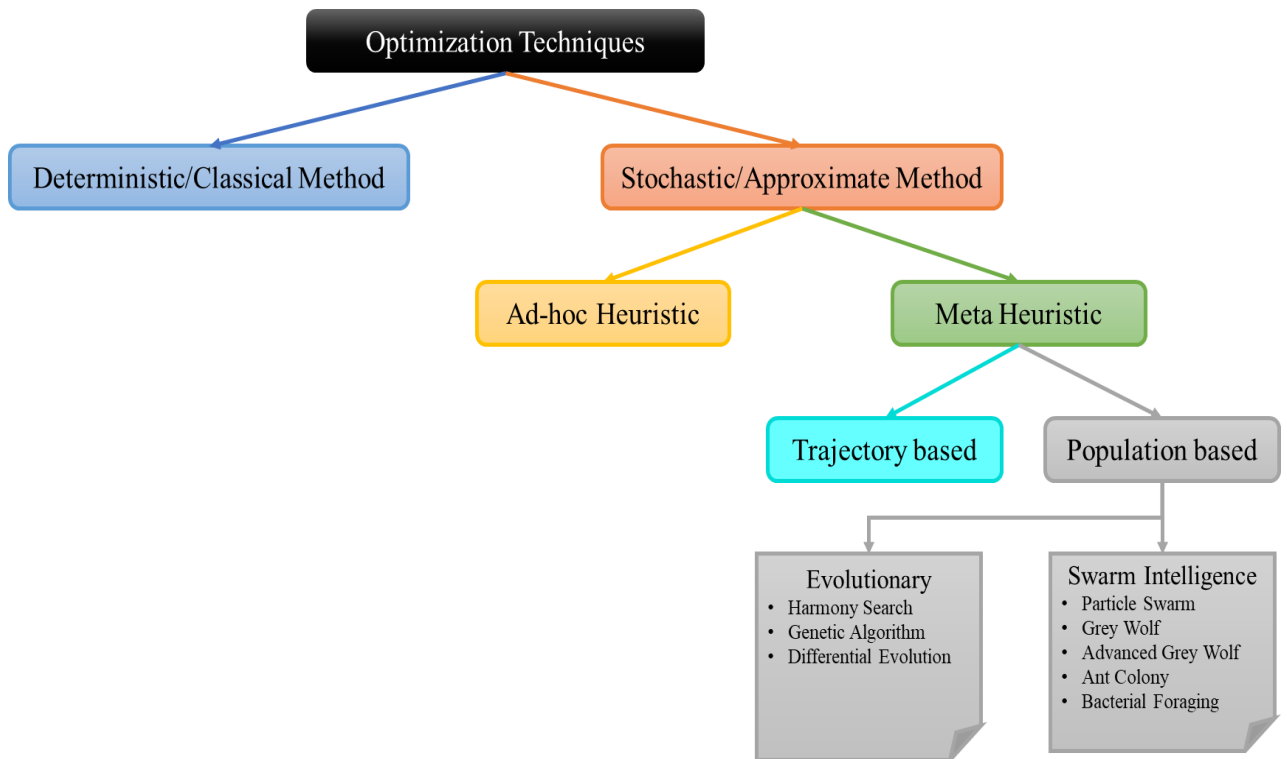


Fig. 4.1. Classification of optimization techniques

The differentiation of numerous optimization techniques is given in Fig. 4.1. An optimal design problem is performed by comparing different solutions obtained using prior knowledge. Thus, the feasibility of each design is first investigated, followed by an analysis

of the solution obtained using estimated objective function of every iteration and the best solution is considered for adoption. Furthermore, it can be added that following a singular procedure for formulation of all electrical engineering design problems is impossible. Fig. 4.2 shows an outline of steps involved in an optimal design problem.

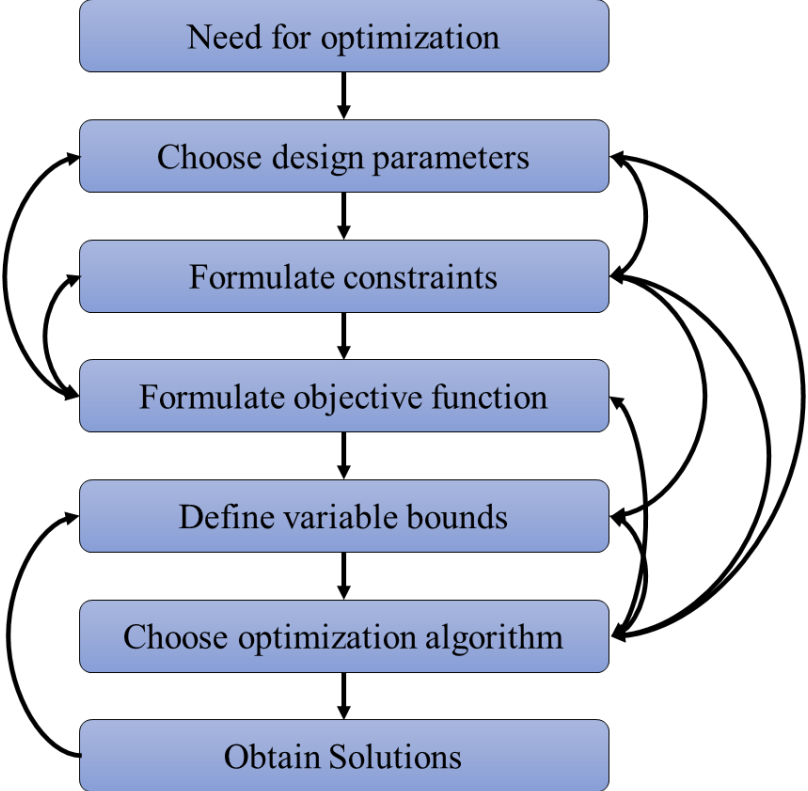


Fig. 4.2. A flowchart for the optimal design procedure

4.2.1 Design Variables

An optimal design problem involves numerous design parameters, among which some are highly sensitive to the proper working of the design. These parameters are known as design variables. These variables remain fixed or vary in accordance with the more important design variables.

4.2.2 Constraints

The constraints define functional relationships among design variables and other design parameters that define certain physical phenomena and certain resource limitations. These are dependent on the users for type and nature. There are mostly two types of constraints:

- a. Inequality type of constraints
- b. Equality type of constraints

4.2.3 Objective Function

To design an optimal problem, formulation of objective function is of key importance. These objective functions are mathematical quantities but still some may not be possible to formulate mathematically. These functions can be either maximized or minimized to obtain the solution.

4.2.4 Variable bounds

The variables defining the maximum and minimum limits of each design variable is known as bounds. In certain optimization algorithms these are not required whereas in some cases these must be defined for optimal solution.

4.3 EVOLUTIONARY ALGORITHMS

The algorithms using heuristic based approach to solve problem with multi-dimensional complexities are known as evolutionary algorithms (EA). It uses mechanism that is typically associated with biological evolution. The weakest solution is eliminated while stronger and more prominent options are retained and re-evaluated in the next step.

4.3.1 Artificial Neural Networks (ANN)

ANN can be described in general terms as a network to process information and this network model is inspired by the architecture of a human brain. ANN are recently being used for nonlinear regression analysis in meteorology as they are very useful in data analysis and prediction. Mostly ANN is used for time series forecasting problems with nonlinear methods. This is a parallel distributed type of architecture, comprising of data processing elements called ‘neurons.’ ANN is generally characterized based on three key factors such as: architecture, training or learning algorithm and activation function.

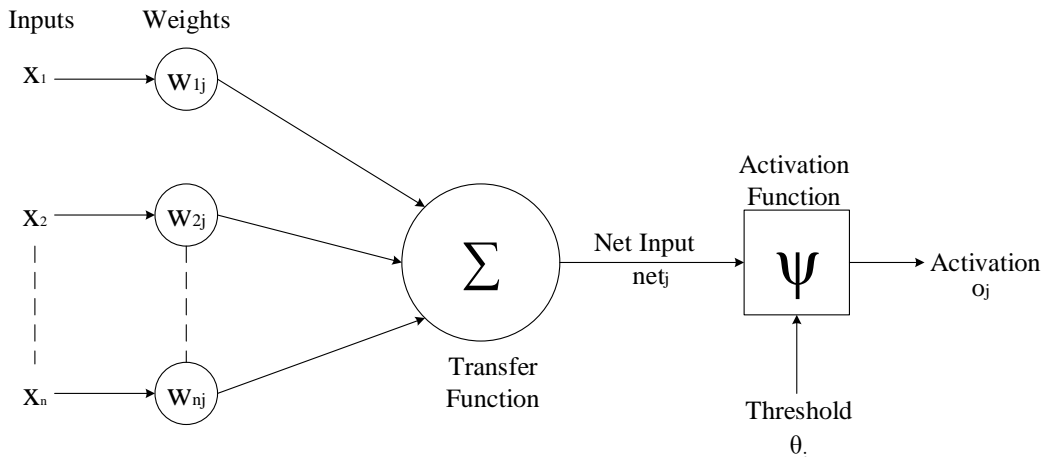


Fig. 4.3. Schematic diagram of ANN

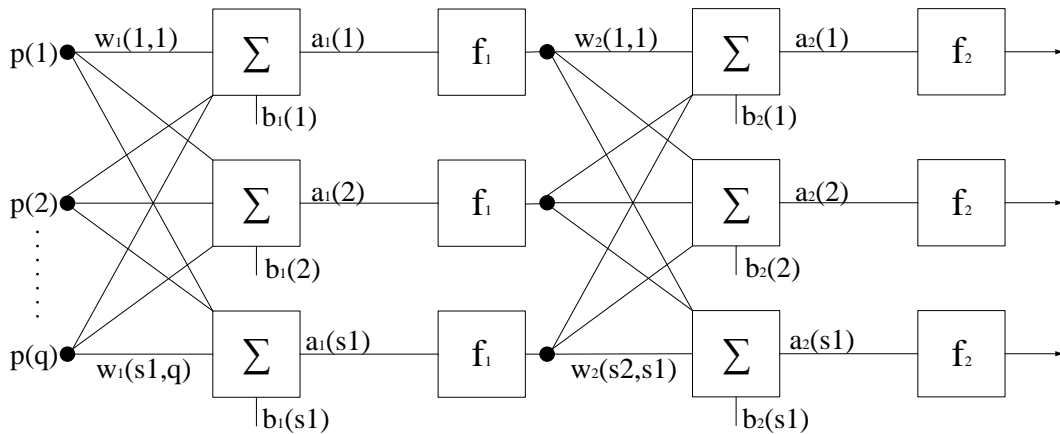


Fig. 4.4. Two layer feedforward MLP neural network

ANN is structured with input layers, hidden layers and output layers. Input layer is the data receiver, data is sent after computation through the output layer. Hidden layer is intermediate layer present between input and output layer, the number of hidden layers depend on convergence speed, generalization capability, neurons present in each layer and training data. These layers in the network are interconnected with help of communication links, these links are associated with specific weights that drive the amount of information passing from them. The transfer function in ANN is chosen according to the properties required. These can be linear or non-linear to form an equivalent single layer or multi-layer network respectively. Activation function is actuated when net_i exceed the threshold to produce the output o_j. ANN working is divided into two steps, firstly, a training process and secondly, network operating process. Schematic diagram of ANN architecture is presented in Fig. 4.3.

Different training algorithms are employed on neural network model to update the weights of the layers, this training and updating of weights occurs using pattern or batch. The training cycle is completed when each training pattern is presented once to multi-layer perceptron (MLP) model. Consider a two-layer MLP neural network, such as shown in Fig. 4.4.

The net input (n) of the unit i in layer $k+1$ is given by

$$n^{k+1}(i) = \sum_{j=1}^{sk} w^{k+1}(i,j)a^k(j) + b^{k+1}(i) \quad (4.1)$$

The output (a) of unit i will be

$$a^{k+1}(i) = f^{k+1}(n^{k+1}(i)) \quad (4.2)$$

for an M layer network, the system equations in matrix form are given by

$$a^{k+1}(i) = f^{k+1}(w^{k+1}a^k + b^{k+1}) \quad (4.3)$$

Here, $k=0, 1, \dots, M-1$, f^{k+1} is activation function of $(k + 1)^{\text{th}}$ layer, w^{k+1} is the weight of $(k + 1)^{\text{th}}$ layer and b^{k+1} is bias of $(k + 1)^{\text{th}}$ layer. From Fig. 4.4, it is observed that the task of the network is to learn associations between a specified pair of input and target pairs $\{(p_1, t_1), (p_2, t_2) \dots (p_q, t_q)\}$, so the performance index for the network is

$$V = \frac{1}{2} \sum_{q=1}^Q (t_q - a_q^M)^T (t_q - a_q^M) = \frac{1}{2} \sum_{q=1}^Q e_q^T e_q \quad (4.4)$$

Where, a_q^M is the output of the network when the p_q input, is presented, the error for the q^{th} input is given by $e_q = t_q - a_q^M$. The performance index is approximated by

$$\hat{V} = \frac{1}{2} \sum_{q=1}^Q e_q^T e_q \quad (4.5)$$

Where the total sum of squares is replaced by squared errors for a single input/output pair.

4.3.2 Adaptive Neuro Fuzzy

This system integrates the benefits of artificial neural networks (ANNs) and the knowledge of fuzzy inference systems (FIS). The novel architecture developed by Jang, uses a set of fuzzy if-then rules with appropriate membership function (MFs) from the input-output data pairs. Though ANFIS system is similar to the fuzzy inference systems, except that the former uses the method of back propagation to reduce the errors. In ANFIS, the process of input passing the input layer and output through the output membership

function is visible in the output layer. The use of neural networks is encouraged to change the parameters till an optimal solution is decided upon. Therefore, ANFIS uses the method of least squares estimation, other than the back propagation method to predict the membership function parameters. The Sugeno fuzzy model, also known as Takagi-Sugeno-Kang (TSK) as in Fig. 4.5, is a systematic approach to generate fuzzy rules based on the available input and output.

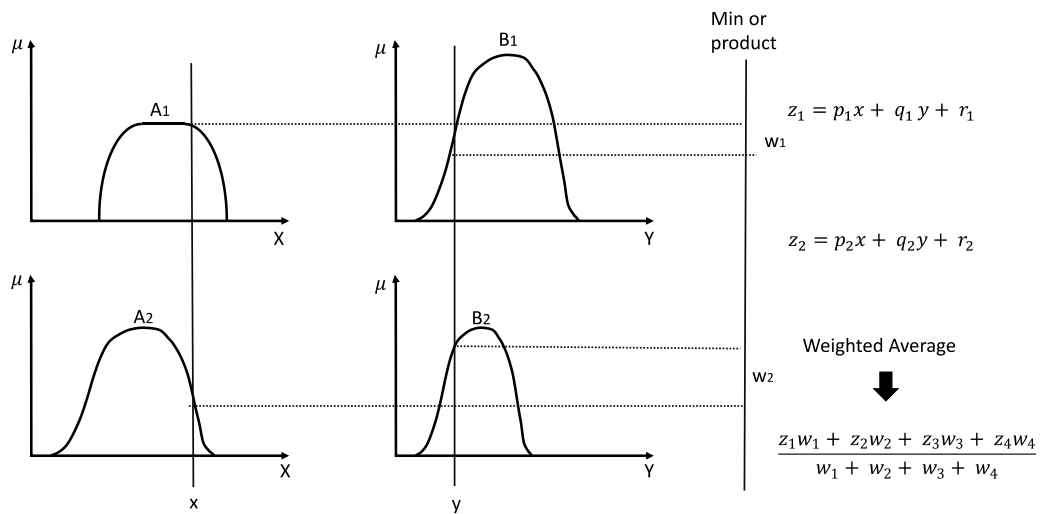


Fig. 4.5. A first-order TSK model with two inputs

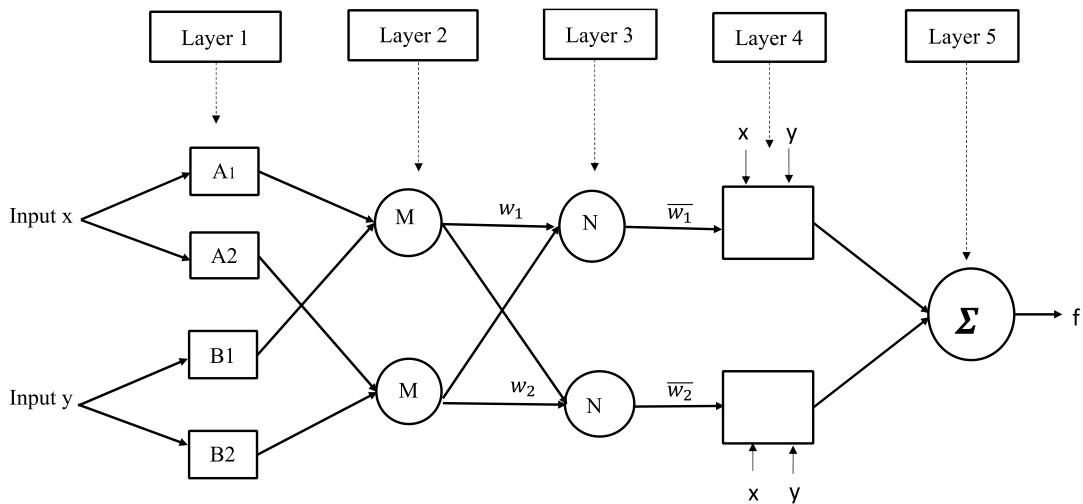


Fig. 4.6. A two inputs architecture of ANFIS model

ANFIS consists of two sets of parameters, adjustable in nature. The first layer contains the premise parameter and the fourth layer contains the consequent parameter. To attain the required response of the fuzzy inference system, the premise and the consequent parameters are adjusted separately during the learning process. This involves a rapid training process and adapting the fuzzy inference system using a hybrid learning algorithm in combination with the least-squares (LS) and the backpropagation (BP) algorithms. Different studies use a unique algorithm based on the requirement of speed, complexity, and convergence.

4.4 POPULATION BASED OPTIMIZATION

In the population based intelligent optimization there are three key factors determining the optimum solution.

- *Inertia Term*: This term forces the swarm/population in the same direction.
- *Cognitive Term*: This forces the swarm/population to move in local search region on its own life experience also known as exploration.
- *Social Learning Term*: This term forces the population/swarm to move to the best previous position of its neighbors also known as exploitation.

4.4.1 Particle Swarm Optimization

PSO algorithm is also a widely used technique to minimize or maximize a cost function. PSO is a population based stochastic, meta-heuristic optimization method developed by Dr. Eberhart and Dr. Kennedy in 1995. It mimics the social behavior of a flock of birds or a swarm of fishes. They [149] have discussed the use of PSO for

multidimensional experiments such as training of weight in feedforward multilayer perceptron (MLP) neural network model. PSO is a technique that lie in between genetic algorithm and evolutionary programming. There are four parameters on which performance of this optimization technique depends: personal best (p_{best}), global best (g_{best}), c_1 and c_2 . Each particle keeps track of its coordinates in the solution space which are associated with the best solution (fitness) that has been achieved so far by that particle. This value is called personal best, i.e., p_{best} . Another best value that is tracked by the PSO is the best value obtained so far by any particle in the complete swarm of the particles. This value is called global best, i.e., g_{best} . The performance (search and exploit) of PSO is dependent on defining of parameters. The movement of the particles to the near global optimum position is described in the following equations.

$$v_{id}(t + 1) = w_{ps0}(t) * v_{id}(t) + c_1 * r_{ps01} * (p_{best} - x_{id}(t)) + c_2 * r_{ps02} * (g_{best} - x_{id}(t)) \quad (4.6)$$

$$x_{id}(t + 1) = x_{id}(t) + v_{id}(t + 1) \quad (4.7)$$

Where,

$v_{id}(t + 1)$ and $v_{id}(t)$ are the velocities of the particles at (t+1) and t instances respectively,

$x_{id}(t + 1)$ and $x_{id}(t)$ are the position of the particles at (t+1) and t instances respectively,

c_1 and c_2 are exploitation and exploration coefficients respectively,

r_{ps01} and r_{ps02} are the random variables associated with exploitation and exploration coefficients respectively,

p_{best} and g_{best} are particle having personal best and global best values respectively.

Each particle tries to modifies its position and velocity by using the following information:

- The current position,
- The current velocity,
- The distance between the current position and p_{best} ,
- The distance between the current position and the g_{best} .

$w_{ps0}(t)$ is the weights of the particle, that are given by equation (3.3)

$$w_{ps0}(t) = w_{max} - \frac{(w_{max} - w_{min})}{T} * t \quad (4.8)$$

Here, w_{max} is 0.9, w_{min} is 0.4, t is the current iteration and T are the maximum number of iterations. A large inertia weight (W) facilitates a global search while a small inertia weight facilitates a local search. By linearly decreasing the inertia weight from a relatively large value to a small value through the course of the PSO run gives the best PSO performance compared with fixed inertia weight settings.

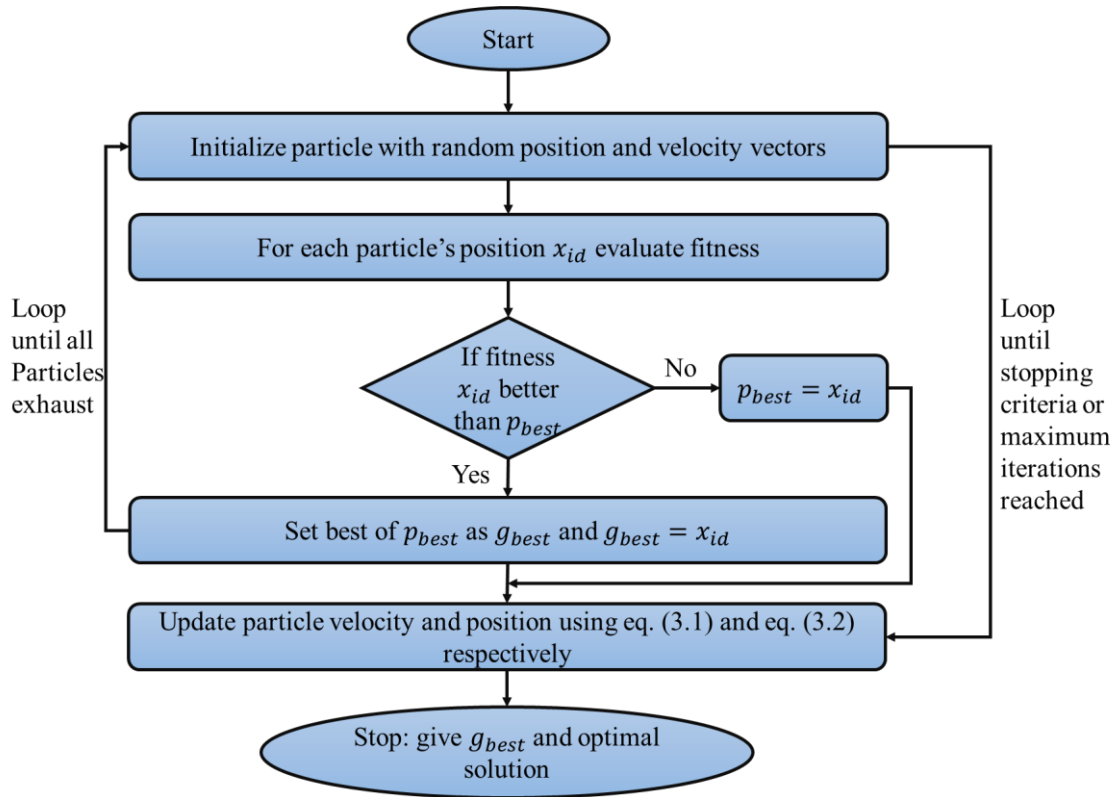


Fig. 4.7. Flowchart of PSO

4.3.2 Grey Wolf Optimizer

The application of the intelligent meta-heuristic technique in solar photovoltaic design is vital because of numerous possibilities of shade dispersion. GWO is a modern nature-inspired optimization technique, capable of solving complex, nonlinear stochastic problems. This algorithm uses the movement of grey wolf for encircling and targeting their prey [49] [150]. The algorithm uses randomly scattered particles in the search space known as wolves. These wolves are classified into four groups; alphas (α), betas (β), deltas (δ) and omegas (ω) as shown in Fig. 4.6.

This classification is performed based on hierarchical order, where the alphas are the lead pack of wolves with least number. The betas follow the decision of the alphas, they are followed by the deltas and the remaining group of wolves are kept in omegas. The

population of wolves increases from alphas to omegas. The different roles of wolves and their social hierarchy is explained in Fig. 4.7. The position and movement of wolves is depicted with the help of Fig. 4.8. In GWO the best solution is given by the alphas (best position) and the entire pack is driven by them. GWO is fast, requires less parameter definition and has comparatively low computational memory. It focuses more on exploration, rather than exploitation, of a meta-heuristic technique.

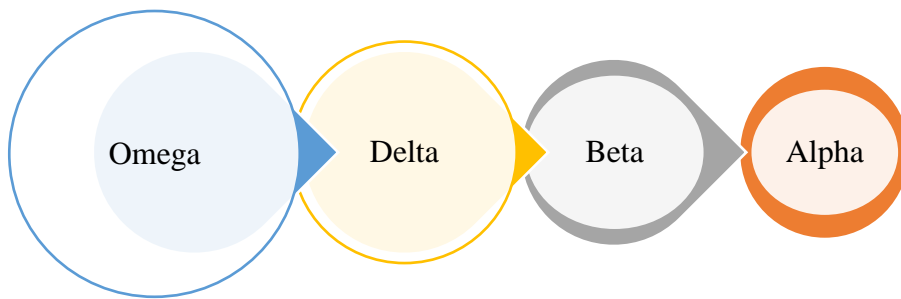


Fig. 4.8. Social hierarchy in grey wolves

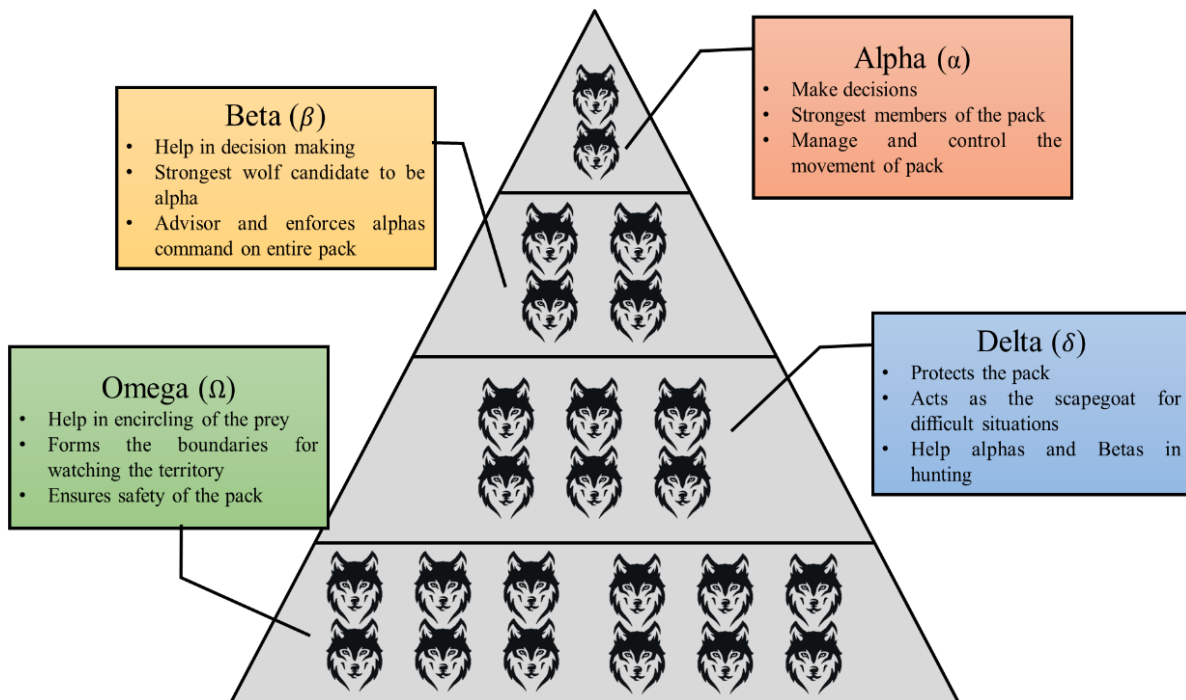


Fig. 4.9. Social hierarchy of grey wolves and their functions.

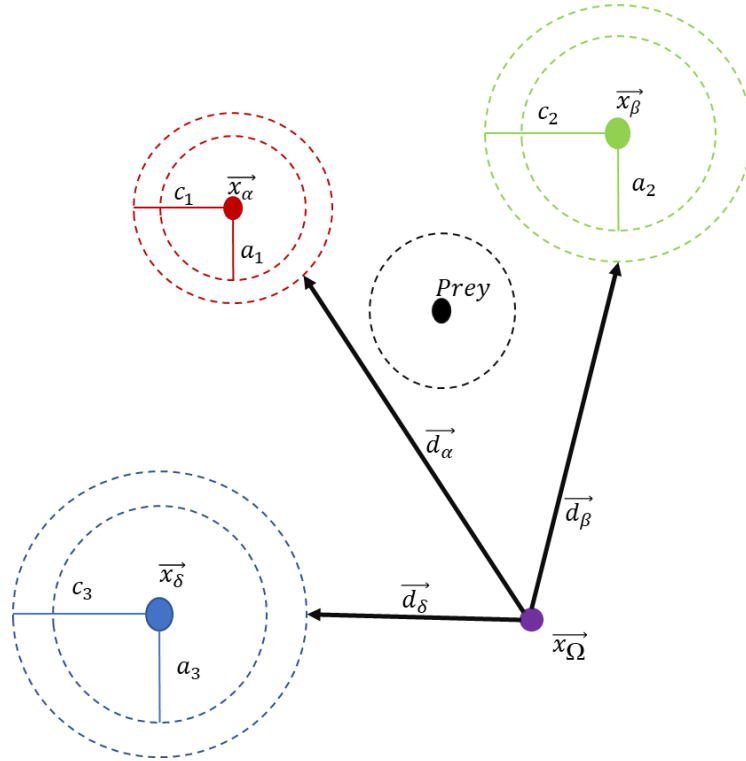


Fig. 4.10. Position update of wolves in GWO

$$\vec{d} = |\vec{c} \cdot \vec{x}_p(t) - \vec{x}(t)| \quad (4.9)$$

$$\vec{x}(t+1) = \vec{x}_p(t) - \vec{a} \cdot \vec{d} \quad (4.10)$$

Here,

\vec{d} defines the encircling behavior,

\vec{x} is the current position of the grey wolf,

\vec{x}_p is the position of the prey that has to be hunted,

coefficient vectors \vec{a} and \vec{c} are given as

$$\vec{a} = 2\vec{q} \cdot \overrightarrow{r_{gwo1}} - \vec{q} \quad (4.11)$$

$$\vec{c} = 2 \cdot \overrightarrow{r_{gwo2}} \quad (4.12)$$

In the above equation, \vec{q} is linearly decreasing from 2 to 0 at every iteration,

\vec{r}_{gwo1} and \vec{r}_{gwo2} are random variables $\in [0,1]$.

The Eq. (4.13)- (4.19) represents the hunting characteristics of the grey wolf.

$\vec{x}_\alpha, \vec{x}_\beta, \vec{x}_\delta$ are the position vectors of alpha, beta and delta respectively.

$$\vec{d}_\alpha = |\vec{c} \cdot \vec{x}_\alpha - \vec{x}(t)| \quad (4.13)$$

$$\vec{d}_\beta = |\vec{c} \cdot \vec{x}_\beta - \vec{x}(t)| \quad (4.14)$$

$$\vec{d}_\delta = |\vec{c} \cdot \vec{x}_\delta - \vec{x}(t)| \quad (4.15)$$

$$\vec{x}_1 = \vec{x}_\alpha - \vec{a} \cdot \vec{d}_\alpha \quad (4.16)$$

$$\vec{x}_2 = \vec{x}_\beta - \vec{a} \cdot \vec{d}_\beta \quad (4.17)$$

$$\vec{x}_3 = \vec{x}_\delta - \vec{a} \cdot \vec{d}_\delta \quad (4.18)$$

$$\vec{x}(t+1) = \frac{\vec{x}_1 + \vec{x}_2 + \vec{x}_3}{3} \quad (4.19)$$

The steps involved in the development of GWO algorithm are given in flowchart and presented in Fig. 4.10. The stopping criterion used in the proposed technique is formulated by i) tolerance error (tol_{err}), ii) error is no longer decreasing or decreasing too slowly, and iii) maximum iteration is reached.

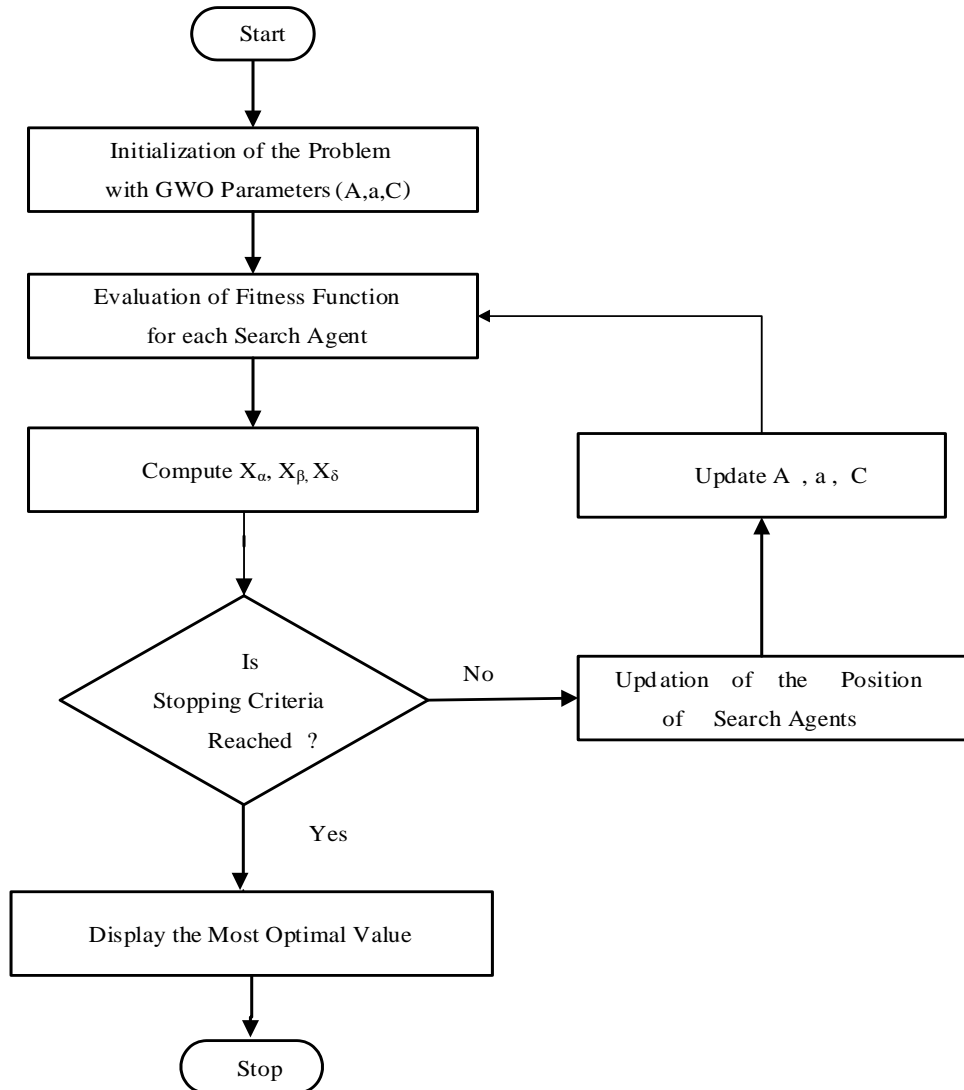


Fig. 4.11. Flowchart of GWO algorithm

4.5 DEVELOPMENT OF MODIFIED GREY WOLF PARTICLE SWARM OPTIMIZATION

The developed optimization technique is a hybrid technique that is inspired by the movement of the grey wolves to attack their prey and swarming action of birds to reach locations for food. In GWO the grey wolf pack is divided into four groups of different hierarchy such as alpha, beta, delta, and omega. The alphas (α) are at the top periphery of

the social hierarchy, thus are the main decision-makers and the remaining entities follow them. The main characteristics of grey wolf i.e., hunting, searching, encircling, and attacking its prey is designed with the help of mathematical equations to perform the optimization. The position update of the wolves is similar to the GWO and briefly described by eq. (4.20) – (4.21).

$$\overrightarrow{x_{1|2|3}} = \overrightarrow{x_{\alpha|\beta|\delta}} - \overrightarrow{a} \cdot \overrightarrow{d_{\alpha|\beta|\delta}} \quad (4.20)$$

$$\overrightarrow{d_{\alpha|\beta|\delta}} = |\overrightarrow{c} \cdot \overrightarrow{x_{\alpha|\beta|\delta}} - w_{ps0} * \overrightarrow{x}(t)| \quad (4.21)$$

$$\overrightarrow{x}(t+1) = \frac{\overrightarrow{x_1} + \overrightarrow{x_2} + \overrightarrow{x_3}}{3} \quad (4.22)$$

The exploitation and exploration of MGWPSO are based on grey wolf optimization and particle swarm optimization respectively. The developed hybrid algorithm is a modified particle swarm optimization with a grey wolf optimizer, thus forming a low-level co-evolutionary algorithm. The modified governing equations for the first 3 wolves are updated using Eq. (4.20) - (4.22). The velocity and updation equation of PSO is modified to Eq. (4.23) - (4.25).

$$x_i(t+1) = x_i(t) + v_i(t+1) \quad (4.23)$$

$$w_{ps0}(t) = w_{max} - \frac{(w_{max} - w_{min})}{T} * t \quad (4.24)$$

$$v_i(t+1) = w_{ps0}(t) * v_i(t) + c_1 \cdot r_{ps01}(x_1 - x_i(t)) + c_2 \cdot r_{ps02}(x_2 - x_i(t)) \\ + c_3 \cdot r_{ps03}(x_3 - x_i(t)) \quad (4.25)$$

Initialization

Initialize iteration (max_iter), coefficient vectors (q and c), weights (w) Evaluate fitness of agents *while* (error_tol < average of value of n iterations) *for* each search agent i.e. alpha, delta, beta and omega

Update the vectors (v) and position (x) end *for*

Update coefficient vectors (q and c), weights (w)

Evaluate fitness of all search agents

Update the position of the first three agents

Increment the counter end *while* return the best search agent position

PSEUDOCODE 1. PSEUDOCODE OF THE PROPOSED MGWPSO

4.6 RESULTS and DISCUSSION

The developed MGWPSO has been tested on various unimodal, multimodal benchmark functions to assess its performance. The functions $F_1(x)$ to $F_9(x)$ have been selected after careful observations to provide a good launchpad for testing the credibility of any optimization algorithm. The performance of the developed MGWPSO is compared with the GWO variant in terms of convergence and accuracy. The algorithms were run for 30 times on every function mentioned above. MGWPSO converges to an optimum solution without getting trapped in local minima and maxima thus attaining a faster convergence rate also. This optimization technique uses the modified error tolerance-based stopping criterion (METSC). This METSC improves the convergence characteristics of MGWPSO and also reduces the computational burden on the processor.

Table 4.1. Benchmark functions used to test the performance of developed MGWPSO

Function	Dimension	Range	f_{min}
$F_1(x) = \sum_{i=1}^n (x_i^2 - 10 \cos(2\pi x_i) + 10)$	20	[-5.12, 5.12]	0
$F_2(x) = \sum_{i=1}^n (x_i^2)$	20	[-5.12, 5.12]	0
$F_3(x) = \frac{1}{4000} \sum_{i=1}^{n-1} (x_i^2) + \sum_{i=1}^{n-1} \cos\left(\frac{x_i^2}{\sqrt{i+1}}\right) + 1$	20	[-500, 500]	0
$F_4(x) = \sum_{i=1}^{n-1} 100(x_{i+1} - x_i^2)^2 + (x_i - 1)^2$	20	[-30, 30]	0
$F_5(x) = \sum_{i=1}^{n-1} ((i+1)x_i^4) + rand[0,1]$	20	[-1.28, 1.28]	0
$F_6(x) = -\sum_{i=1}^n x_i \sin(\sqrt{ x_i })$	20	[500, 500]	-8329.65
$F_7(x) = 20 + e - 20 \exp\left[0.2 \sqrt{\left(\frac{1}{n}\right) \sum_{i=1}^n x_i^2}\right] - \exp\left(\frac{1}{n} \sum_{i=1}^n \cos(2\pi x_i)\right)$	20	[-32, 32]	0
$F_8(x) = (x_2 + x_1^2 - 11)^2 + (x_1 + x_2^2 - 7)^2 + x_1$	2	[-5, 5]	-3.78396
$F_9(x) = \sum_{i=1}^5 j \cos((j+1)x_1 + j) \sum_{i=1}^5 j \cos((j+1)x_2 + j)$	2	[-10, 10]	-186.730

Table 4.1 presents various benchmark functions used to test the capability of the developed hybrid optimization technique. Table 4.1 gives an insight into the modality,

dimensions, randomness, and minimum value (f_{min}) of various benchmark functions along with a 3-D graph of them in Fig. 4.8.

Table 4.2. Comparison of developed MGWPSO with GWO

Function	GWO			MGWPSO		
	Iter	$best_{sol}$	t_{comp} (s)	Iter	$best_{sol}$	t_{comp} (s)
$F_1(x)$ Rastragin Function	1000	$1.23 * 10^{-2}$	1.018	389	$8.34 * 10^{-14}$	0.891
$F_2(x)$ Sphere Function	1000	$8.73 * 10^{-19}$	1.054	1000	$1.251 * 10^{-23}$	1.008
$F_3(x)$ Greiwank Function	1000	$1.459 * 10^{-1}$	1.061	253	$4.211 * 10^{-2}$	0.963
$F_4(x)$ Rosenbrock Function	1000	$6.552 * 10^2$	1.035	1000	$2.717 * 10^{-2}$	1.00
$F_5(x)$ Noise Function	1000	$1.291 * 10^{-1}$	1.052	1000	$3.275 * 10^{-2}$	0.974
$F_6(x)$ Schwefel Function	1000	-5911.983	1.067	1000	-8329.657	1.003
$F_7(x)$ Ackley Function	1000	$8.753 * 10^{-3}$	1.049	1000	$7.81 * 10^{-10}$	1.002
$F_8(x)$ Himmelblau Function	1000	-3.561	1.025	1000	-3.783	1.002
$F_9(x)$ Shubert Function	1000	-186.73	1.084	259	-186.7	1.014

This hybrid meta-heuristic technique's performance is clearly shown based on iterations required for convergence, the best solution ($best_{sol}$) of function and time took (t_{comp}) by the program to give the best solution (TIC-TOC) is shown in Table 4.2. The designed technique outperforms GWO significantly when the dimensions of the functions are large like Rastragin, Sphere, Rosenbrock, Schwefel and Ackley.

4.7 CONCLUSION

This chapter helps in distinguishing the different types of optimization techniques that can be used for optimal solution. The key factors for population based meta heuristic techniques have been discussed. Furthermore, the chapter presented a comparative study between GWO and MGWPSO technique using various benchmark functions. The computational speed and convergence of the developed optimization technique is found to be better. The designed MGWPSO technique outperforms GWO significantly when the dimensions of the functions are large like Rastragin, Sphere, Rosenbrock, Schwefal and Ackley. Moreover, it can be concluded that MGWPSO can tackle the nonlinearity and stochastic nature of the renewable energy sources when modelled mathematically.

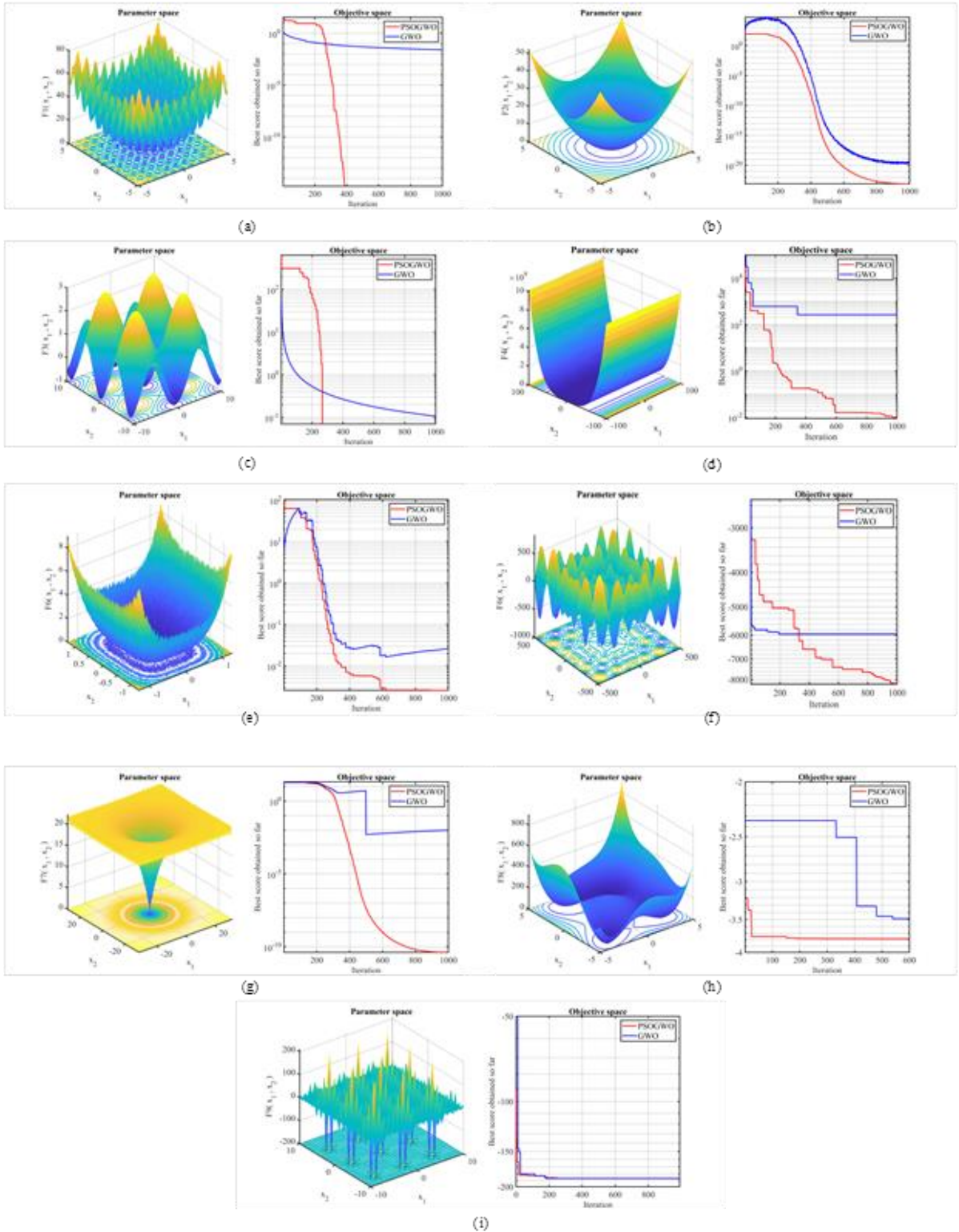


Fig. 4.12. The performance of developed MGWPSO on different functions (a) Rastragin (b) Sphere (c) Greiwank (d) Rosenbrock (e) Noise (f) Schewefel (g) Ackley (h) Himmelblau (i) Shubert

CHAPTER 5

GWO-ANN BASED APPROACH FOR SHORT TERM SPV POWER FORECASTING

5.1 INTRODUCTION

The demand for grid power is increasing significantly due to the ever-increasing population and increasing comfort zone and usage of modern household equipment. Climate change and greenhouse gas emissions from conventional power plants are a major concern and it invigorated the use of renewable and green energy resources for power generation. Based on the literature review, solar energy-based power plants have proven to be the alternative and sustainable solutions for fulfilling such high demands. However, there are certain issues and challenges associated with solar photovoltaic base power plants. These issues and challenges include grid stability, power quality, proper energy management therefore it becomes of utmost importance to forecast photovoltaic power. This chapter primarily focuses on solar photovoltaic power forecasting using the grey wolf optimization-based intelligent approach.

5.2 IMPORTANCE OF SPV POWER FORECASTING

Among the renewable energy sources, the adoption of solar photovoltaic is increasing day by day, because of various advantages such as clean, silent, availability, low running cost, etc. However, the rapid development of SPV systems also brings many challenges in the operation and control of SPV based power systems [151] [152]. Further, the high penetration of solar PV may cause grid stability and reliability issues in the smart grid environment. Therefore, solar PV power forecasting is one of the key tools for this

paradigm and plays a vital role in efficient integration of renewable power generation and reduction in volatility to distributed generation systems. Precise and accurate forecasting of PV power helps massively in planning and scheduling of power demand-supply for the consumers as well as various distribution companies (DISCOMs). It further enhances system reliability and power quality issues due to uncertainty in PV power generation. Further, forecasting is an important tool for grid operators, since they can schedule generation and distribution according to the load profile, also define generation units to act as operating reserve generators [153] [154]. PV power prediction not only reduces the number of units required in hot standby but also minimizes the operational costs. Therefore, the prediction of PV power has become crucial for grid stability, optimal unit commitment, and economical dispatch. Fig. 5.1 shows the different methodologies used for varying spatial and temporal resolutions, and Fig. 5.2 gives brief explanation about the different forecasting horizons (time horizons) and its various applications.

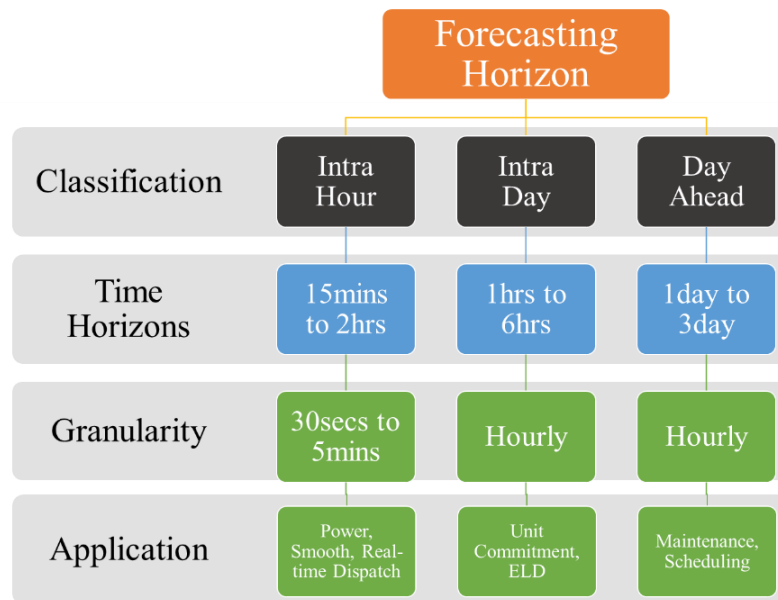


Fig. 5.1. Different forecasting horizon and their relation

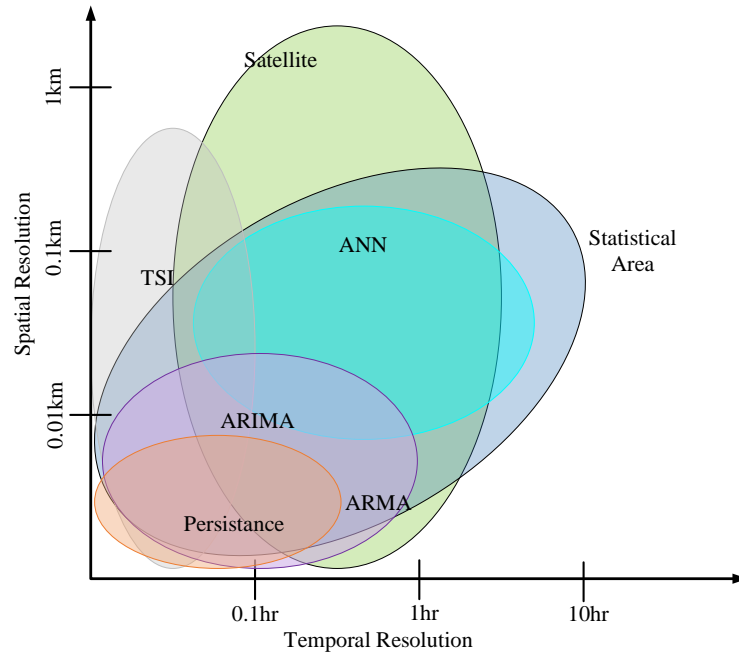


Fig. 5.2. Classification of the short-term forecasting model

5.3 LEARNING/TRAINING ALGORITHMS

Various learning techniques or training algorithms are used for modeling of the neural network-based MLP. These algorithms are namely levenberg marquardt (LM), gradient descent, Newton's method, conjugate gradient and Bayesian regularization. These learning methods help in creating a decision function for weight updation of the neural network. These techniques have few shortcomings of using large memory, high complexity and slow convergence. These learning methods define rules, these rules imply a specific function to update the weights of the neurons after each epoch. The term gradient and backpropagation (BP) can be used interchangeably, BP is a method where error between the network output and the desired output is propagated backwardly. The cost function depends on numerous parameters, so the optimization is single and multi-dimensional. Optimization helps in increasing the computational speed and ~~enhance~~ the convergence rate.

5.4 SITE DETAILS AND DATA PROCESSING

A 5 kW_p grid connected PV system is installed at rooftop of the laboratory and the data of the system is collected through Solar System Analyzer 9018BT during daytime for every 2 minutes. A linear regression study was performed for selection of the various aforementioned inputs on the basis of 1-month historical data. The linear dependence of X and Y is studied using Pearson product moment correlation coefficient, to find the strength of linear dependence of nominal PV power generation output to the inputs. This study is shown in Table 5.1 and Fig. 5.3. The negative correlation shows that larger values of aerosol content (τ_L) and wind speed will result in smaller solar PV output.

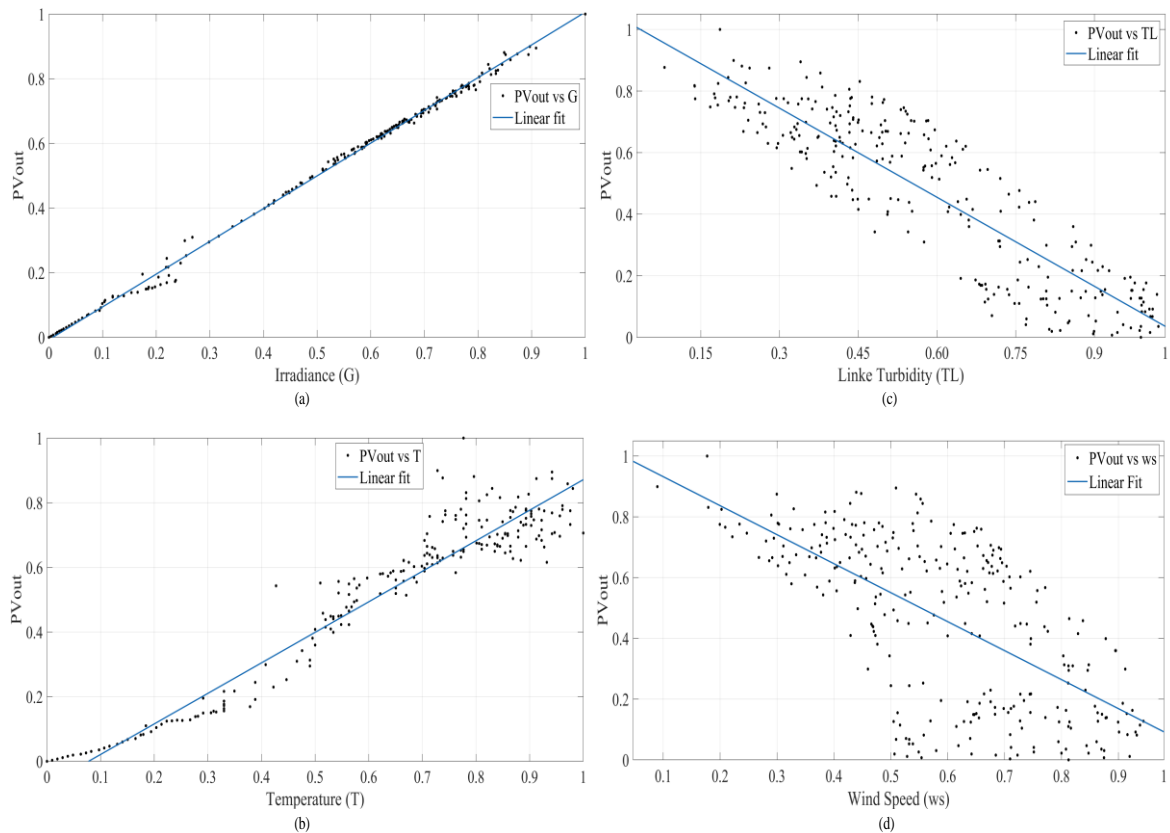


Fig. 5.3. Linear regression plot of the inputs and the solar photovoltaic power (a) PV power vs Irradiance (b) PV power vs Temperature (c) PV power vs Linke Turbidity (d) PV power vs Wind Speed

Table 5.1. Daily PV output and it's correlation with the inputs considered

Inputs	Correlation Coefficient
Irradiance	0.993
Temperature	0.912
Linke Turbidity	-0.382
Wind Speed	-0.191

Table 5.2. Specification of the Solar PV system

Description	Value
Type	Polycrystalline
Maximum Power of module	250 W _p
Open circuit voltage (V _{oc}) of module	37.05V
Short circuit current (I _{sc}) of module	8.580A
Maximum power voltage (V _{pm}) of module	30.74V
Maximum power current (I _{pm}) module	8.15A
Output tolerance of module	±2%
Total number of modules	20
Site layout	10 x 2
Exposure area of a module	1.640m ²
Temperature Coefficients of PV module	
α_{pv}	+0.058%/°C
β_{pv}	-0.330%/°C
γ_{pv}	-0.430%/°C

A large number of samples were collected for training of the neural network based on MLP model. The training data set comprised of 80% of the time series data and 20% of the dataset was used for testing (10%) and validation (10%). The above selection of 80%, 10% and 10% for different stages have been done using trial and error technique. The measured data was verified with the data obtained from NREL and NOAA-GFS model for

the last ten years. The measured irradiance data was in the range of the irradiance obtained from the sources for the selected site. The experimental setup of the solar PV forecasting is shown in Fig. 5.4 and the specifications of the Solar PV system used in this study is provided in Table 5.2.

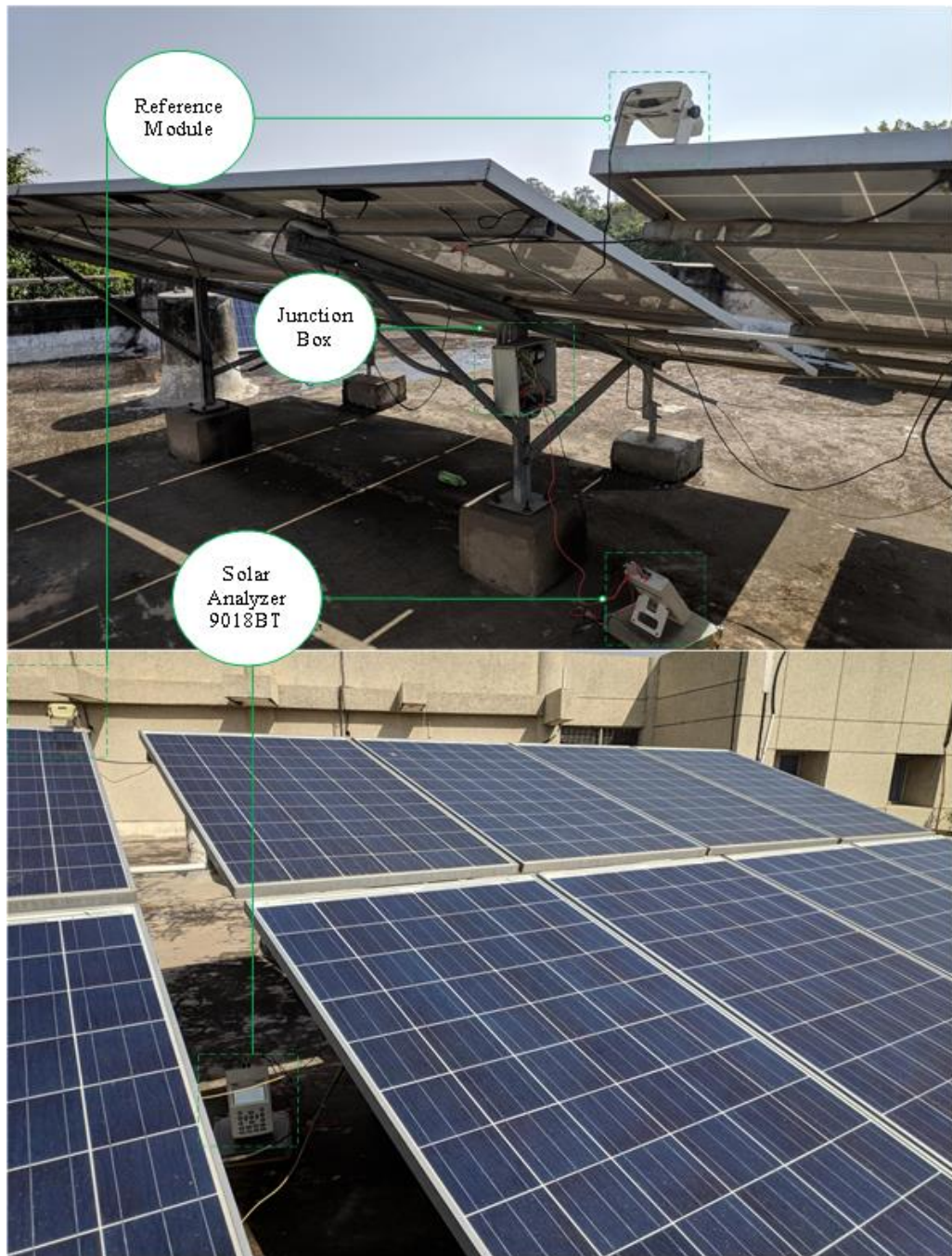


Fig. 5.4. Experimental setup for SPV power forecasting

5.5 SOLAR ENERGY FORECASTING USING AEROSOL INDEX

Aerosol Index (AI) is a measure of the attenuation of the sunlight or solar radiation due to haze, dust and other suspended particles. Particles such as smoke, dust and cloud cover etc. block the sunlight by absorbing, diffusing or scattering light. AI defines the amount of sunlight that is prevented from reaching the ground by aerosol particles. In other words, AI is the number of UV-absorbing aerosols. Studies have shown that a large difference ($\geq 25 \text{W/m}^2$) is observed in Delhi, India and 24.10% of aerosol optical depth from 2000 to 2011 have contributed to the expansion of the aerosol layer over 6 km. Present estimates of the aerosols' forcing on global climate range from minus 0.6 watts per square meter to minus 4.0 watts per square meter, when combining both the direct and indirect effects of sulfate aerosols and biomass burning aerosols. Aerosol Index (AI) is the index that detects the presence of UV absorbing aerosols, this is given by total ozone mapping spectrometer (TOMS) and ozone monitoring instrument (OMI) from NASA Goddard Space Flight Centre, defined as

$$AI = 100 \left[\log_{10} \left(\frac{I_{360}}{I_{331}} \right)_{measured} - \log_{10} \left(\frac{I_{360}}{I_{331}} \right)_{calculated} \right] \quad (5.1)$$

It is noted that, Global Horizontal Irradiance (GHI) and PV power output at earth's surface is adversely affected by the concentration of aerosols. However, the relationship between AI values and radiation data is difficult to obtain due to the complicated relationship of meteorological parameters with AI. Hence the aerosol index data used for training the developed ANN based solar energy forecasting model is collected for the month of May, 2018 at every 3 hours.

If actual monthly data is directly used, this may cause a convergence problem during the learning process. This convergence problem can be avoided if the input and output data are scaled such that they remain within the range of (0.1–0.9). This process to scale the data within a particular range is known as normalization. The following given expression has been used to scale actual dataset for the solar energy forecasting problem

$$L_s = \frac{Y_{max} - Y_{min}}{L_{max} - L_{min}} (L - L_{min}) + Y_{min} \quad (5.2)$$

Where,

L is the actual solar irradiance data,

L_s is the scaled solar irradiance data being used as input to the GNN model,

L_{max} is maximum value of solar irradiance data in a particular column,

L_{min} is minimum value of solar irradiance data in a particular column,

Y_{max} is normalization upper range (0.9),

Y_{min} is normalization lower range (0.1).

5.5.1 NARX ANN based Modelling for Solar Irradiance Forecasting

ANN is inspired from the human neural structure. It makes use of vast number of artificial neurons to imitate capability of living organisms. In recent years, backpropagation neural network is one of the most vastly used ANNs due to the characteristic of making the system simple to understand and implement. The developed ANN model is a feedforward multilayered BP network. Three-layered BP network is shown in Fig. 5.5 where X7 is back propagated Y.

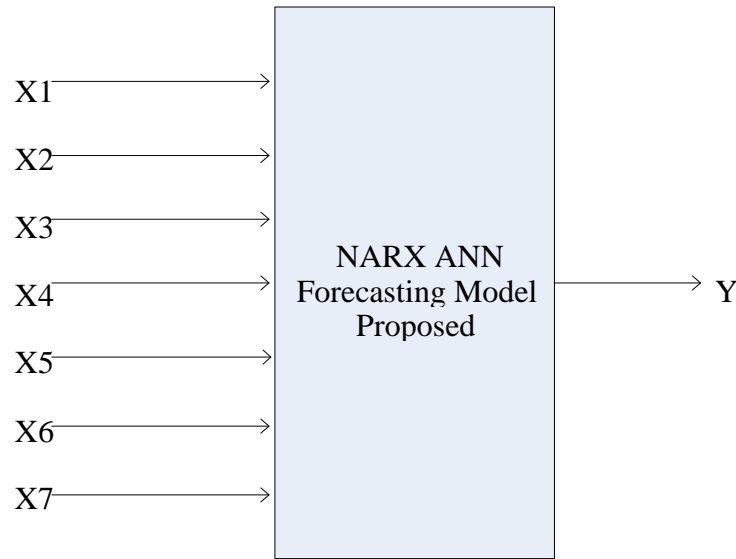


Fig. 5.5. Structure of developed ANN solar energy forecasting model

The above Fig. 5.5 shows the proposed prediction model using seven input variables to forecast the irradiance (Wh/m^2) i.e. denoted by ‘Y’. Here inputs are temperature (K), wind speed (m/s), wind direction, relative humidity (%), pressure (hPa), AI, and historical GHI data (Wh/m^2). It is noted that the temperature and relative humidity is measured at 2 meters above ground, whereas, wind speed is at 10 meters above ground and pressure data is taken at ground level.

Table 5.3. Input data for SRFM-ANN

<i>Input Variables</i>	<i>Meaning of Ambient Variables</i>	<i>Unit</i>
X1	Ambient Temperature	Kelvin
X2	Wind speed	m/s
X3	Wind direction	Degree
X4	Relative humidity	%
X5	Pressure	hPa
X6	Aerosol Optical Depth (AOD)	550nm
X7=Y	Historical GHI Data	Wh/m^2

5.5.2 Results and Discussion

The training data is obtained for the site, Delhi Technological University, with the latitude of 28.74 North and 77.11 East. Before prediction to be performed the historical data is analyzed. The meteorological data is collected every minute but, the AI doesn't vary much every minute or even every hour. Thus, a time horizon considered is 3 hours. Table 5.3 shows the number of data sets used for different stages of modeling of the developed ANN network to accurately predict and forecast solar energy. For training of ANN 80% of the data was used, whereas for validation and testing, 10% each was selected. These values gave satisfactory results as the mean squared error (MSE) is limited to 0.691 (highest in validation phase) and regression factor (R) was always around 0.99.

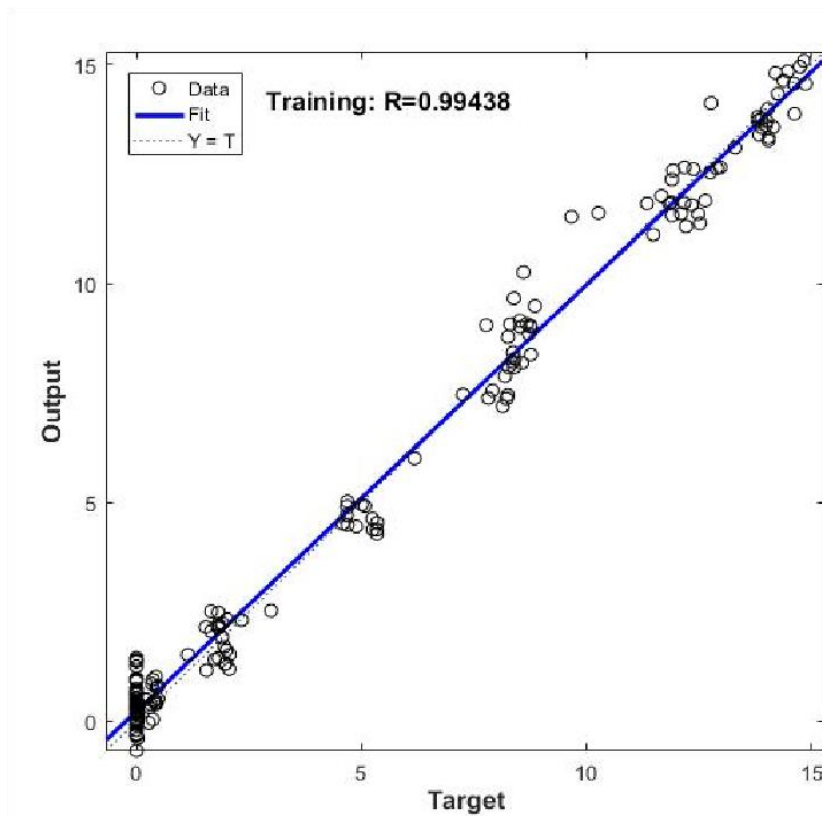


Fig. 5.6. Regression line of training phase of developed model

Table 5.4. Results of developed ANN predictor technique

<i>Phases of ANN model</i>	<i>MSE</i>	<i>R</i>
Training	0.0607	0.998
Validation	0.6910	0.989
Testing	0.1889	0.996

Training of the developed ANN prediction model yields a Regression coefficient (R) of 0.994 considering the above-given variables in Table 5.4. This coefficient defines the rate of change of the independent variable (here it is GHI) for a unit change of dependent variables (here, these variables are wind speed, temperature, humidity, etc). Fig. 5.6 shows the regression line for the training of data.

The predicted PV irradiance for a cloudy day can be performed using the developed model, the forecasted result is shown in Fig. 5.7. From the results, it can be easily seen that error ranges from -0.2 to 0.5. MSE is 2.66% for a cloudy day with 3 hours as the time horizon.

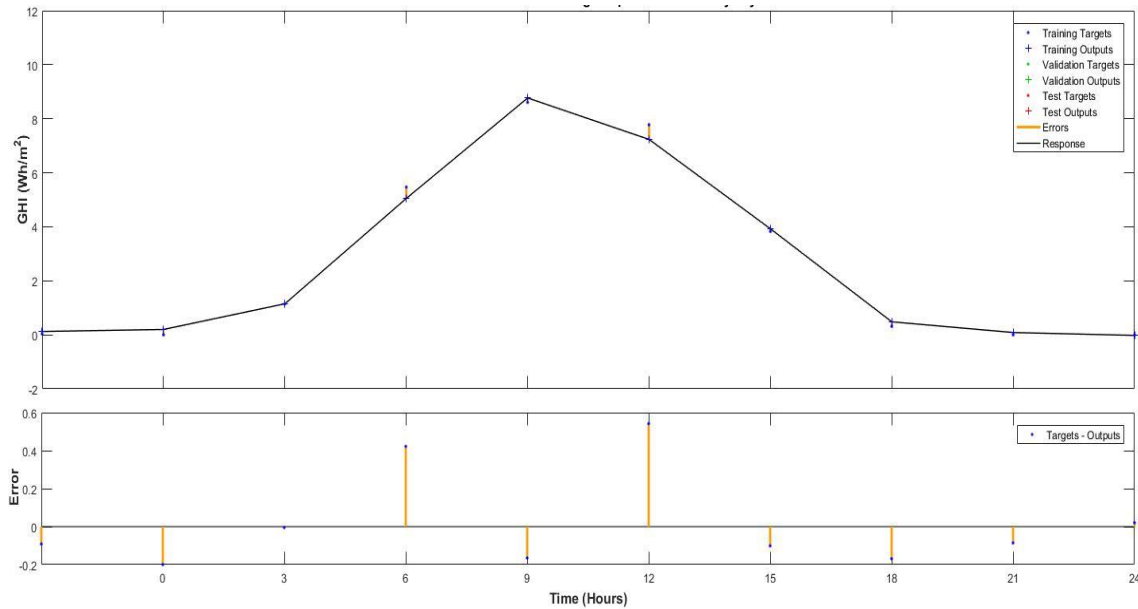


Fig. 5.7. Cloudy day prediction response of developed model

The forecasted values of 3 hourly PV irradiance for the sunny day weather are shown in Fig. 5.8. The results coincide well with the measured values for prediction with the proposed model. Fig. 5.8, shows two consecutive days with sunny weather conditions. The error ranges from -0.5 to 0.4 and MSE is around 2.43%.

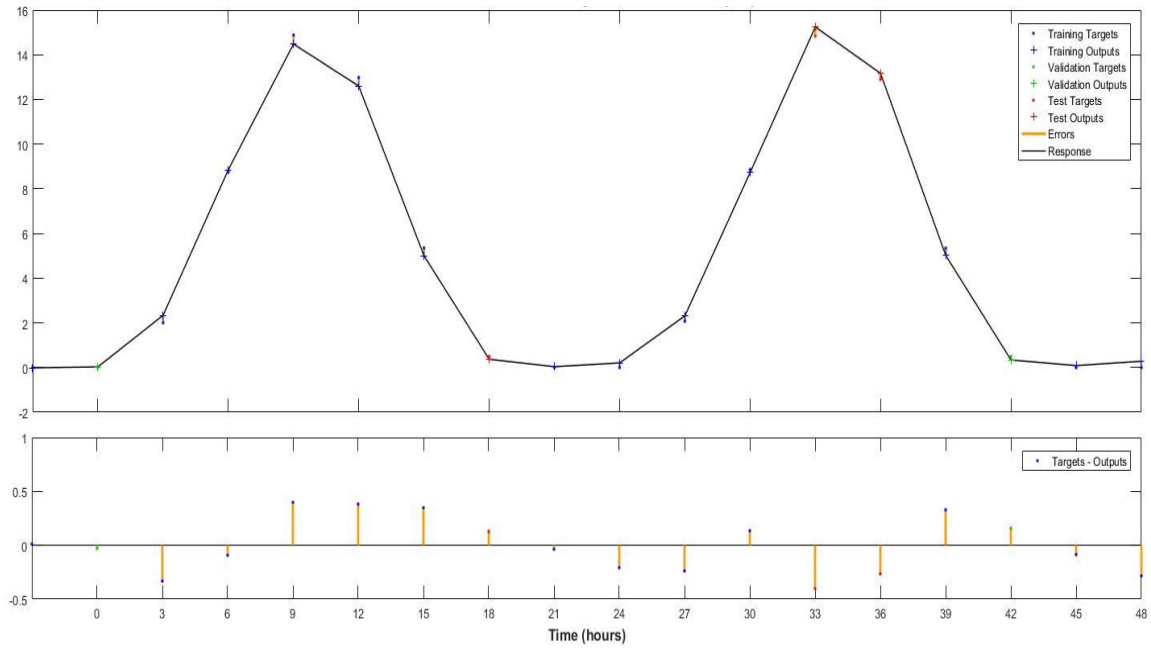


Fig. 5.8. Sunny day prediction response of developed model

5.6 GWO-ANN BASED SPV POWER FORECASTING

This section discusses about the proposed hybrid intelligent model to predict the solar PV power generation for varying aerosol content. Grey wolf optimization (GWO) is used to train weights of the feedforward ANN for mapping meteorological inputs and PV power as output. Solar irradiance (W/m^2) incident on the PV panel, cell temperature ($^{\circ}\text{C}$), Linke Tubidity Factor (τ_L) and wind speed (m/s) have been considered as input parameters and PV power as output of the model. The training and validation stages of the developed GWO based ANN model to predict the PV power, is illustrated in Fig. 5.9. The GWO

algorithm acquires the previous data and assists in effective modelling of ANN network for forecasting the PV power. This meta-heuristic optimization algorithm is used to assign optimized weights to the layers of neural network by minimizing the cost function. The designed hybrid intelligent model uses mean square error as its objective function for a maximum of 1000 iterations, the model comprises of four input nodes with five hidden layers and one output.

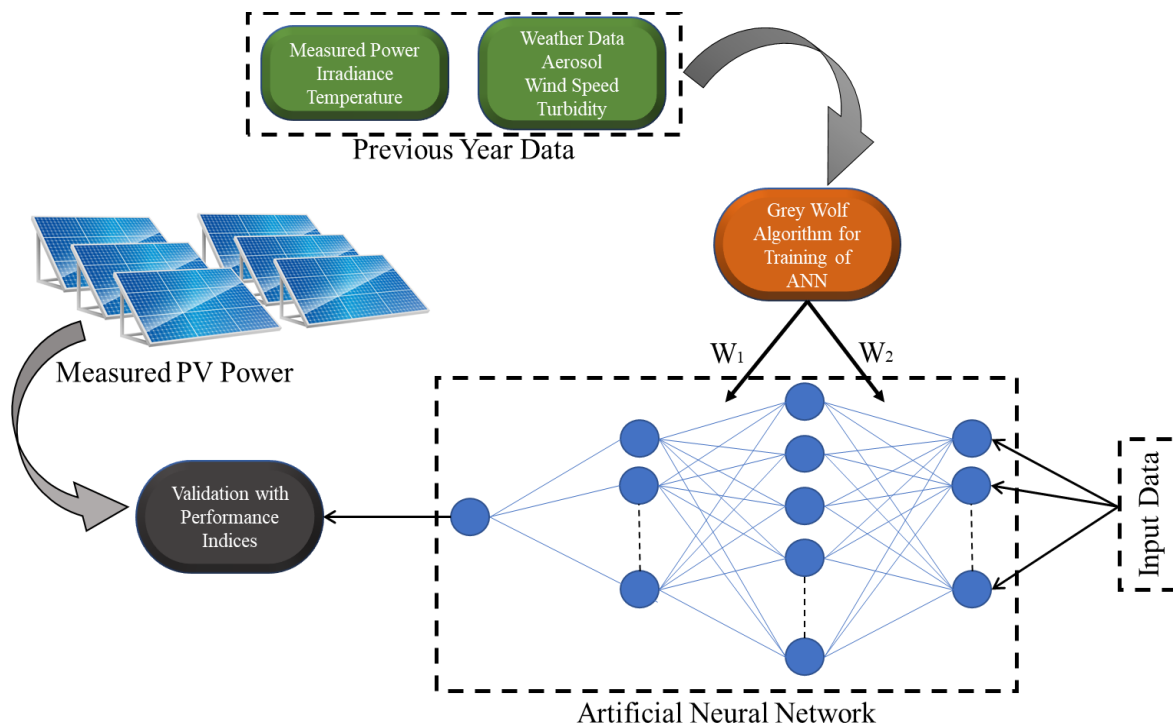


Fig. 5.9. Functional block diagram of the proposed hybrid intelligent model

The solar irradiance and cell temperature have been measured using solar system analyzer and wind speed are collected from National Renewable Energy Laboratory (NREL). The highlights of the designed model are use of GWO technique for training of the neural network. Study for selection of the various inputs and their relationship with solar PV power is performed, giving an insight of dependence on each input considered. The training and prediction of the Solar PV power is done considering τ_L for varying

aerosol content in the atmosphere. Extensive comparative analysis of the proposed model for hourly forecasting of PV power is presented using different performance indices for forecasting such as training error (TE), normalized root mean square error (NRSME), normalized mean bias error (NMBE), normalized mean absolute error (NMAE) and complexity and configuration of the system.

5.6.1 Statistical Indicators

The performance of the developed hybrid intelligent forecasting model is analyzed using the statistical indices. The performance indicators used for proposed PV power forecasting model are normalized error (NE), normalized squared error (NSE) and training error (TE) or mean square error (MSE). The training error is said to be the error obtained when the trained model is again trained for target values. The accuracy of the prediction is evaluated considering these metrics.

$$NE = \frac{P_{out} - P_e}{Max_{i=1}^M(P_{out})} \quad (5.3)$$

Here, P_{out} and P_e are actual PV power and estimated power output at every t_h , and M is the total number of samples.

$$NSE = (NE)^2 \quad (5.4)$$

NSE is calculated for easier calculation of normalized root mean square error (NRMSE).

$$NRMSE = \sqrt{\frac{1}{M} * \sum_{i=1}^M (NSE)} * 100 \quad (5.5)$$

Normalized mean bias error (NMBE) (%) and normalized mean absolute error (NMAE) (%) are also considered as performance indices.

$$NMBE = \frac{100}{M} * \sum_{i=1}^M (NE) \quad (5.6)$$

$$NMAE = \frac{100}{M} * \sum_{i=1}^M |NE| \quad (5.7)$$

$$TE = MSE = \frac{1}{n} \left(\sum_{i=1}^M (x_i - \hat{x}_i)^2 \right) \quad (5.8)$$

Where, x_i is the output of the trained model, \hat{x}_i is target value, and M is the number of samples of data.

5.7 PERFORMANCE EVALUATION OF GWO ANN BASED MODEL

The performance of the developed model has been assessed with changing air quality and is shown in Fig. 5.10. This figure shows the variation of irradiance and linke turbidity for a highly polluted day. The mean τ_L for the day is calculated to be 8.5 (very polluted condition), the density of aerosol particles during the morning and evening hours is very high and gradually decreases and is constant for the afternoon hours, for the selected site. A high value of τ_L indicates a higher number of aerosol particles in the atmosphere and thus increasing the diffused radiation and reducing the direct radiation. Table 5.5 shows the relation of varying sky conditions with respect to τ_L .

Table 5.5. Linke turbidity factor and corresponding atmospheric conditions

Linke Turbidity Factor (τ_L)	Sky Conditions
$\tau_L = 1$	Dry and clean
$1 < \tau_L < 3$	Deep blue (water vapour content high)
$3 < \tau_L < 5$	Turbid atmosphere
$5 < \tau_L < 7$	Polluted atmosphere
$8 < \tau_L$	Hazardous

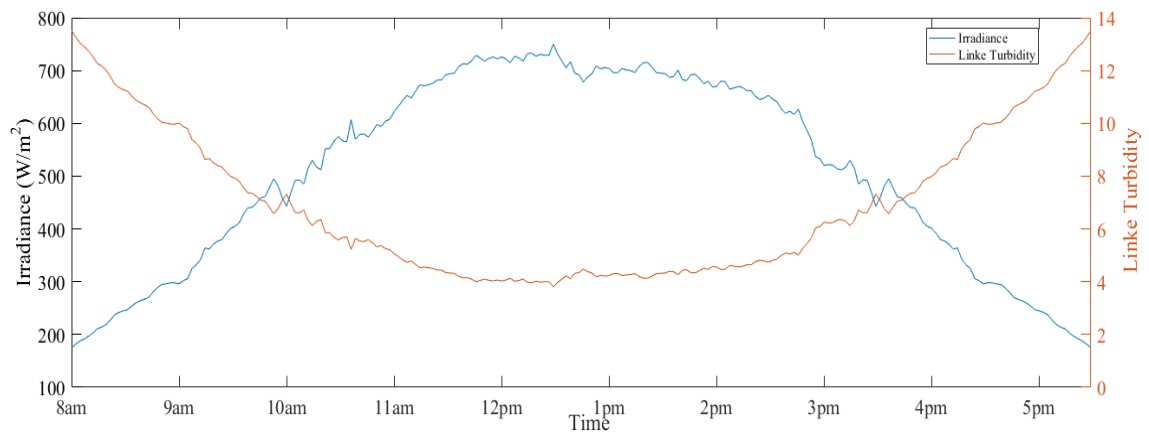


Fig. 5.10. Variation of irradiance and linke turbidity for a highly polluted day

The forecasted PV power output from GWO-MLP model is also compared with the actual solar PV power measured using 9018BT Solar Analyzer. The measured PV power (P_{out}) and forecasted PV power using GWO model is presented in Fig. 5.11(a). From Fig. 5.11(a), it can be observed that the forecasted PV power is very close to the measured data during the afternoon (i.e. high sunshine hours). However, the performance of the developed model is deteriorated in case of more diffuse solar irradiance. The NE for the designed model ranges from 0.27 to -0.12 as can be seen from Fig. 5.11(b). GWO technique being more of an exploration based computational technique, hence can readily forecasts the variations of PV power. NRMSE, NMBE and NMAE of the developed GWO model is 6.67%, 2.267% and 4.681% respectively.

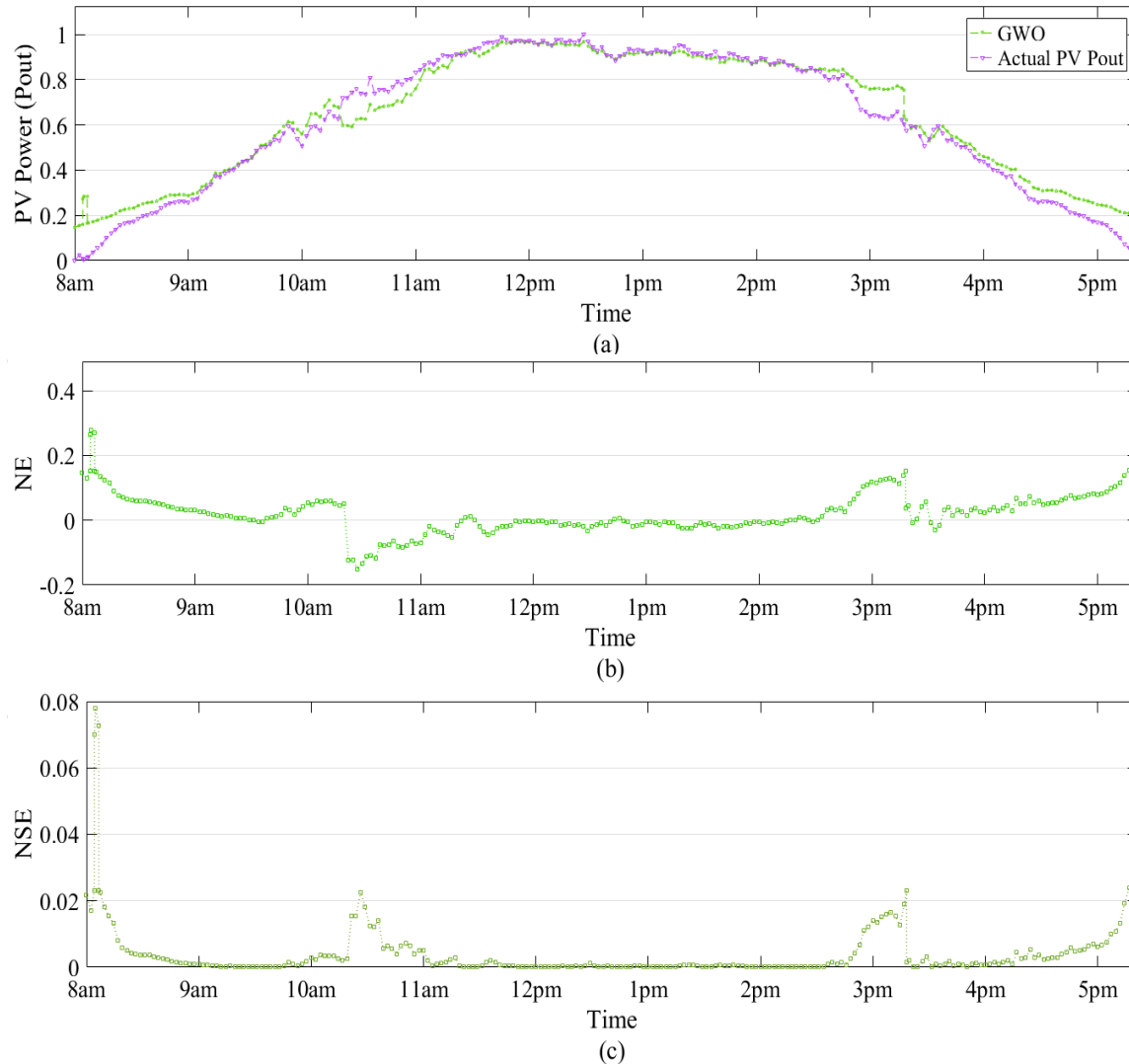


Fig. 5.11. (a) Performance of GWO model (b) Variation of NE for GWO model (c) Variation of NSE for GWO model

A comparative analysis of GWO, PSO, LM and adaptive neuro fuzzy (ANF) techniques algorithms is done on the basis of TE, iterations required for minimum TE, and regression coefficient (R). Table 5.6 shows that the four training algorithms have been compared based on TE, R and number of iterations required to reach minimum TE. The value of R using GWO based MLP model is found to be 0.99832 with minimum number of iterations i.e., highest computational speed training algorithm. From these results it is revealed that the GWO based model requires less computational time as compared to the

other intelligent algorithms such as PSO. Further, the value of training error is also less for the designed model which is 3.23×10^{-4} .

Table 5.6. Performance indices of different training algorithms during training state.

Technique	Training Error (TE)	Iterations/Epochs	Regression Coefficient (R)
GWO	3.23×10^{-4}	148	0.99720
PSO	4.33×10^{-4}	963	0.98575
LM	1.24×10^{-3}	89	0.98410
ANF	7.68×10^{-3}	678	NA

From Table 5.6, it can be concluded that GWO training technique is relatively better than the other training techniques. This technique has the minimum TE, hence the associativity of inputs to output is also high and the computational speed is faster than ANF and PSO technique. The training parameters for various algorithms are described in Table 5.7. The n_h value for the LM based ANN model is 10 to reach a feasible TE of 10^{-3} order, this value of n_h is maximum in comparison to other techniques used, thus the ANN model with LM approach is more complex than the GWO and PSO based models. The forecasted PV power output obtained from LM, ANFIS, PSO, GWO are compared with the measured data and presented in Fig. 5.14.

Table 5.7. Parameters of various training algorithms for designing of models

GWO					
$iter_{max}$	No. of Hidden Layers in neural network (n_h)		\vec{a} decrease factor	\vec{a} initial	tol_{err}
1000	5		$2 - \frac{iter * 2}{iter_{max}}$	2	10^{-6}
PSO					
c_1	c_2	w_{max}	w_{min}	n_h	tol_{err}
1.9	2.1	0.9	0.4	5	10^{-6}

LM					
No. of delays	$iter_{max}$	μ increase factor	μ decrease factor	n_h	tol_{err}
1	1000	10	0.1	10	10^{-6}
ANF					
Membership function type	No. of membership functions	$iter_{max}$	tol_{err}		
Gaussian bell	[5 5 3 3]	1000	0		

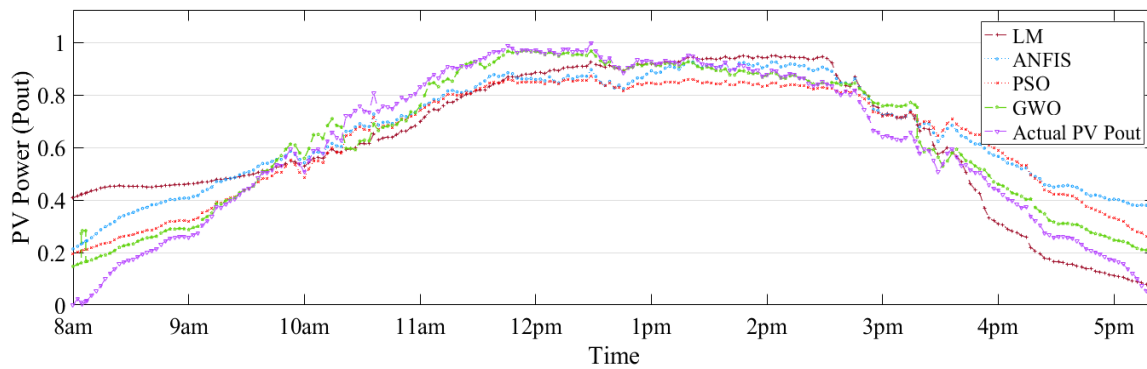


Fig. 5.12. PV power forecasting for high τ_L condition

From Fig. 5.12, it is clearly seen that during morning hours, the PV power generation is low, and the power reaches maximum value in the noon hours and then gradually decreases during the evening hours. However, the performance of the developed model is found satisfactory during sunshine hours. The performance indices can be clearly seen in Table 5.7 for different solar PV forecasting models.

Table 5.8. Performance comparison of the proposed models for prediction stage

Technique	NE	NRMSE (%)	NMBE (%)	NMAE (%)
GWO	[0.27-0.12]	6.67	2.267	4.681
PSO	[0.21-0.10]	10.62	2.532	9.322
LM	[0.41-0.15]	13.37	19.995	10.12
ANF	[0.38-0.10]	12.33	5.112	10.16

When τ_L is very large i.e. ≥ 9 , diffuse irradiance increases significantly as the aerosol particle also increases the atmosphere. As τ_L is in the range of 5 to 7, the impact of aerosol particles does not affect the developed PV power forecasting model as NE is small. However, the performance of the model has been improved significantly during noon hours. The summary of results obtained using Fig. 5.11 (a) and Fig. 5.11 (b) is also provided in Table 5.8. The performance indicators such as NE, NRMSE, NMBE, NMAE for the different approaches are shown in Table 5.8. The value of statistical indicators used in this work is better for the developed GWO model as compared to the other intelligent approaches.

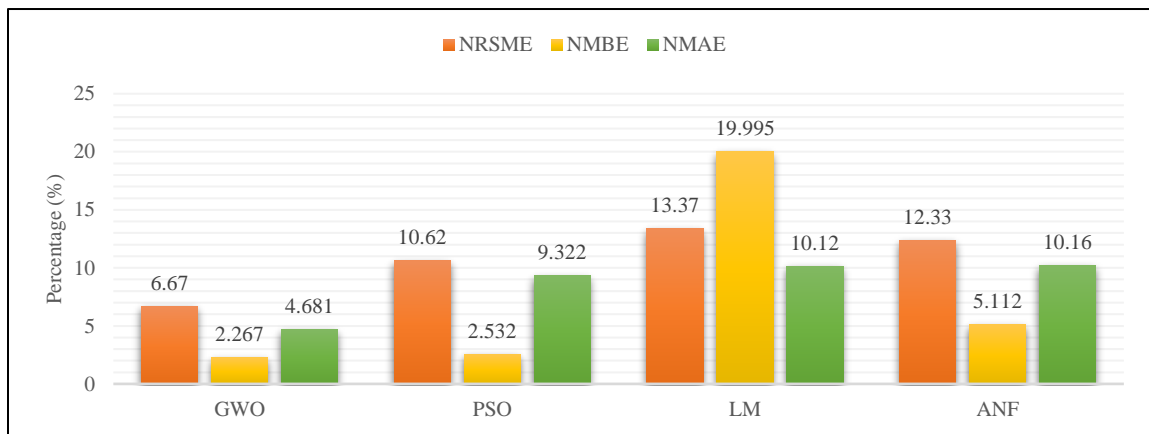


Fig. 5.13. Comparison of various forecasting models in terms of NRMSE, NMBE and NMAE

From Fig. 5.13, it is concluded that the performance of the GWO based approach is found better as compared to the other intelligent techniques.

5.8 CONCLUSION

In this chapter, a new model based on GWO approach for solar PV power forecasting has been developed and presented for smart grid environment. The proposed model is

developed based on meteorological parameters to forecast the PV power output. The performance of the model is evaluated based on statistical indicators and validated from the data set obtained from 5 kW_p PV system installed at the rooftop of the laboratory. The forecasted PV power model performance has also been analyzed for changing air quality. This chapter provides performance analysis of the developed SPV power forecasting model for varying air quality using the linke turbidity factor for the selected site. A comparative analysis of developed GWO-ANN model with other intelligent techniques is also performed and was found better. The performance indicators such as TE, iterations and R were 3.23×10^{-4} , 148 and 0.99720 respectively, suggesting that the developed hybrid intelligent model is better. The designed model also offers relatively fast speed for training of the neurons and is comparatively less complex. The obtained results may be used for smart grid energy management and demand response applications this would help get reliable, load smoothing, and economical electrical energy to consumers.

CHAPTER 6

DESIGN AND ANALYSIS OF SPV BASED MICROGRID FOR A SELECTED LOCATION

6.1 INTRODUCTION

In the present power sector, a large portion of the electrical energy is still generated through fossil fuels such as coal, gas, and oils which results in a large production of harmful greenhouse gases. The various RE resources along with energy storage systems form a hybrid renewable energy system (HRES) and may provide reliable and sustainable power generation. Intensive research has been performed in the field of RE resources and their integration in the existing power system. In the deregulated electricity network, the coexistence of RE resources like solar photovoltaic and wind energy conversion systems along with the traditional AC grid is achieved through microgrids (MG). MGs are the state-of-the-art active distribution networks employing distributed generators (DGs), energy storage systems, and loads, operated in grid-connected or islanded mode, in a controlled and coordinated way [155]. This chapter focuses on designing a hybrid microgrid using intelligent and modified optimization techniques for both on-grid and off-grid applications. The chapter gives readers an insight into the linear programming method and modified grey wolf optimization technique and their application for modeling an optimal microgrid. The load profiling has been incorporated in the chapter for an easier understanding of the load characteristics.

6.2 CONCEPT OF MICROGRID

A microgrid with different renewable power sources is considered to be a hybrid MG system (HMGS). Hybrid microgrid systems are systems comprising of different parallelly connected distributed resources and are capable of performing operations under grid synchronization and islanded mode. The typical framework and components of a microgrid are depicted in Figure 6.1.

The vital components of a modern MG include renewable energy sources, diesel generators, batteries, residential and commercial load, electric vehicles, utility grid and a controller for effective energy management and dispatch. The key component in reducing the cost of the MG and optimal energy management between various sources is the MGC i.e., the energy management controller. The functions of MG for investment deferral according to sale and purchase of the electricity to the grid is controlled by it. Other primary aims of it are reducing the carbon footprint, maintaining an uninterrupted power supply, and increased resilience at the consumer end.

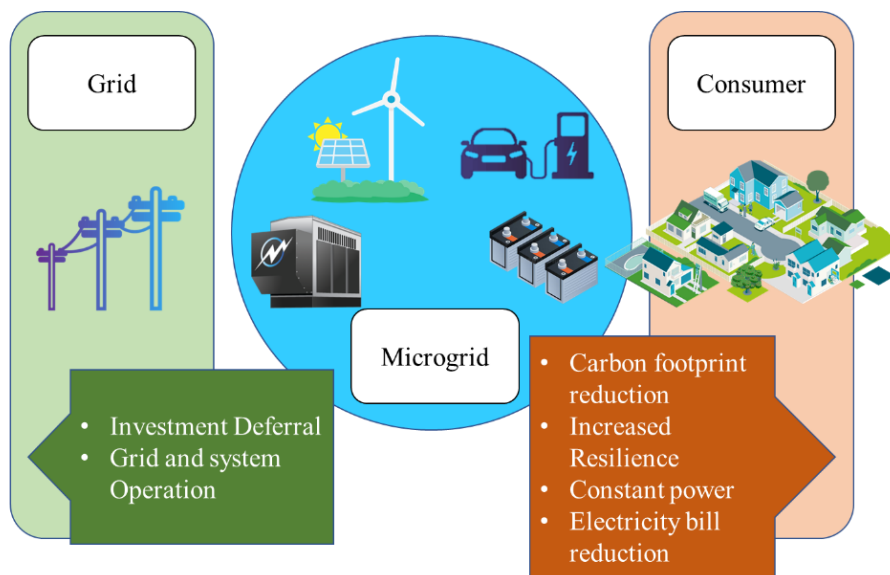


Fig. 6.1. Components and functions of MG

6.3 SELECTION OF GEOGRAPHICAL LOCATION/SITE

The optimal sizing of distributed generation system (DGS) requires proper and accurate procedure for designing of loads. Here, a retail outlet of fuel, in Uttar Pradesh of India is considered as the site for study. The distributed generation system for the optimization of size and cost of SPV and WEGS is shown in Fig. 6.2, for the selected site.

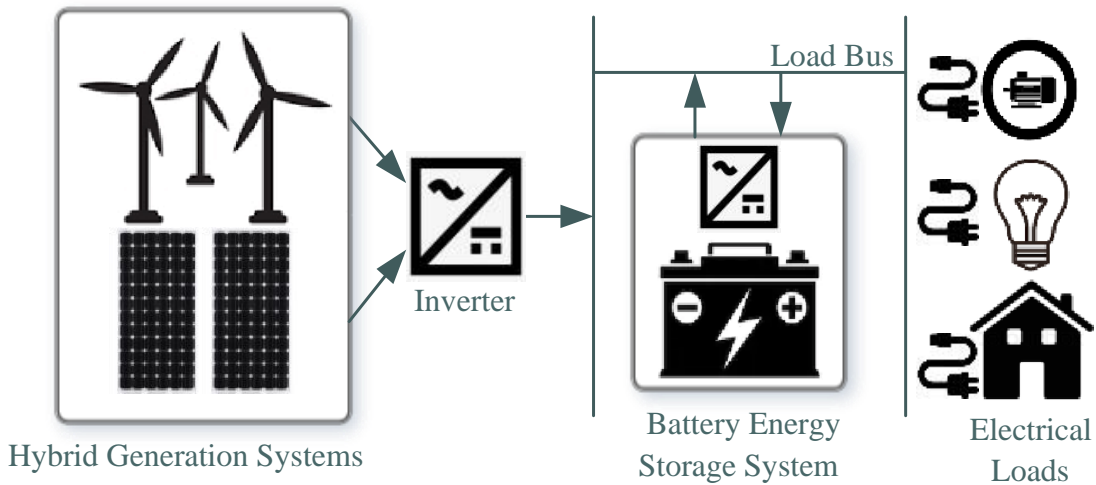


Fig. 6.2. A distributed generation system for the proposed site

The electrical load of site considered for the case study is analyzed using the data of the previous years. The loads for the selected site are classified in two different classes: i) constant load, and ii) variable load. The demand profile for these loads is created for 24 hours for a complete year. The constant load (W_c) are the load that consumes constant power for complete 24 hours. And, variable loads are user-controllable loads, they have varying energy consumption for 24 hours. W_l , W_b , and W_m are light loads, building loads and machine loads respectively. The daily energy consumption profile of the loads is given by Equation (6.1).

$$E_{ld} = \sum_{t=1}^{24} W_c + W_l k_l(t) + W_b k_b(t) + W_m k_m(t) \quad (6.1)$$

Table 6.1 shows the peak power consumption for different types of load for the proposed site. The variable loads W_l, W_b and W_m have loading variables k_l, k_b and k_m respectively. These loading variables are the function of time and help in defining the time of use (TOU) of lighting, building and motor loads.

Table 6.1. General load classification

Type of Loads		Power Consumption (W)
Constant	W_c	6500
Variable	W_l	3700
	W_b	2500
	W_m	31300
Total Peak Load	W_{tp}	44000

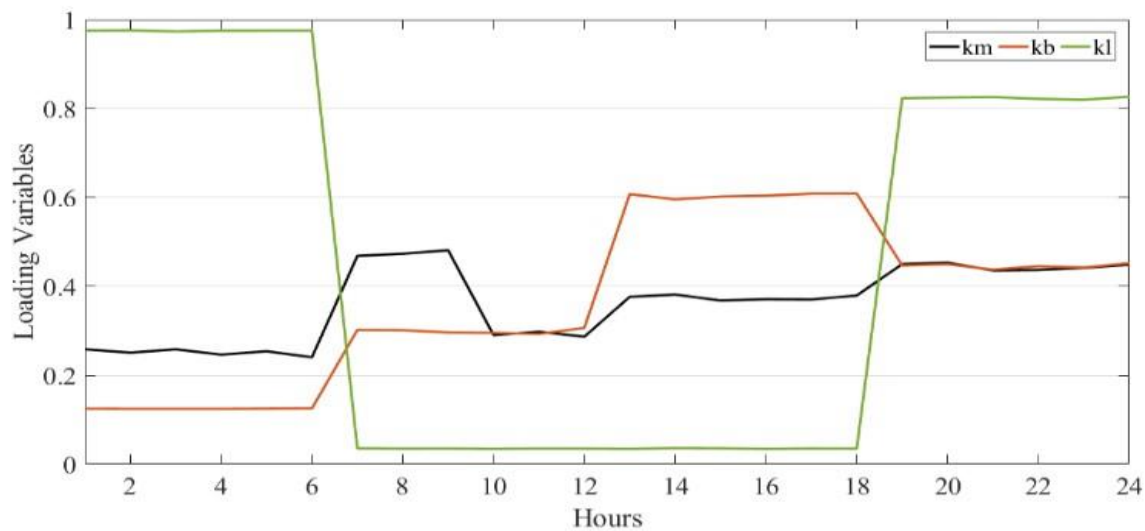


Fig. 6. 3. Variation of k_l, k_m , and k_b

Fig. 6.3 shows the TOU of different loads for the proposed site. The variation of loading variables defined in Figure 6.4 has been obtained by analysis of previous year data of the site.

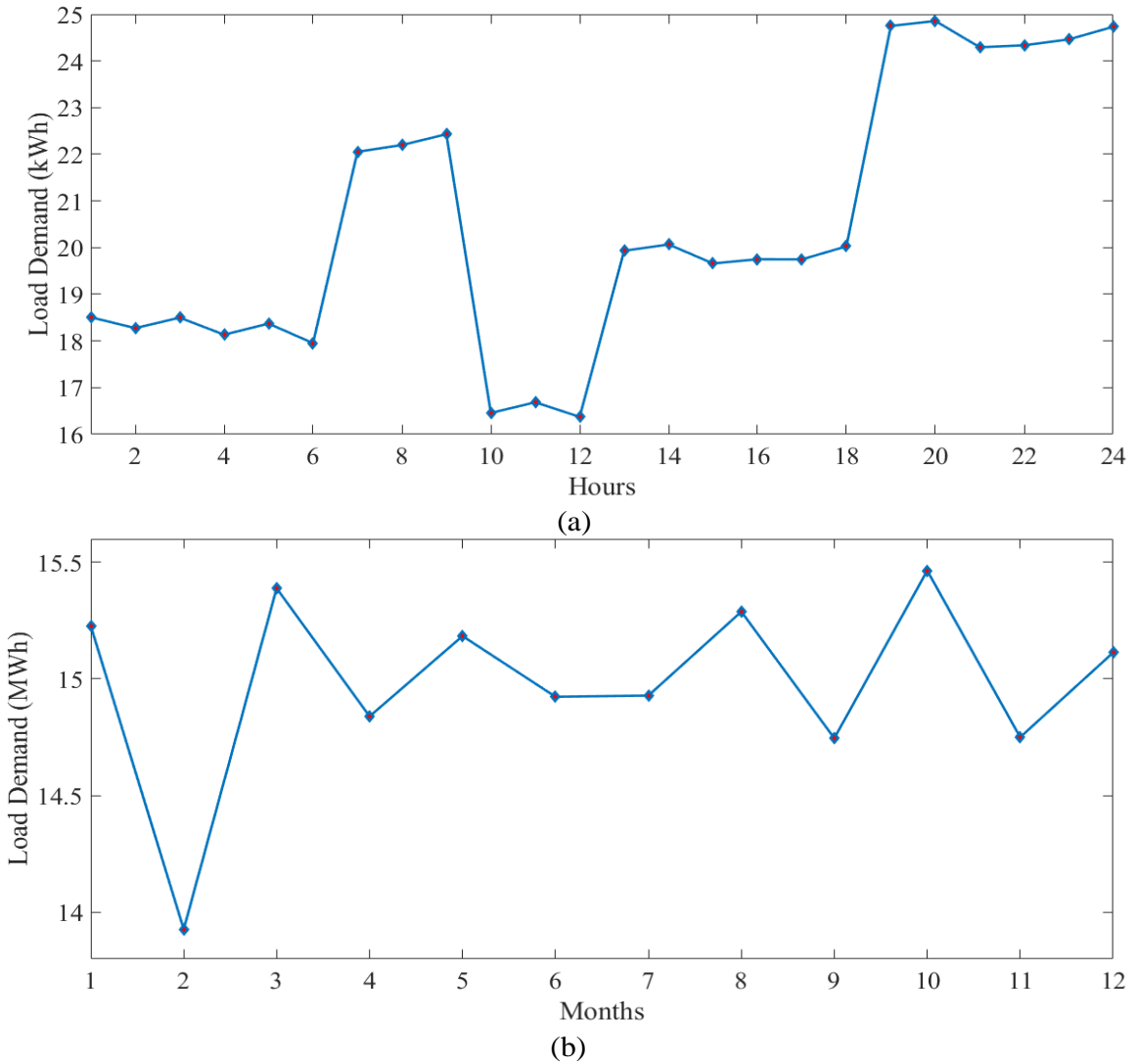


Fig. 6.4.(a) Hourly load demand (b) Monthly load demand

The Fig. 6.4(a) shows the hourly load demand in kWh of the site selected. It is clearly visible that in Fig. 6.4(a), the average hourly load demand is minimum from 10:00 hrs till 12:00 hrs ranging from 16 kWh to 17 kWh. Whereas, the maximum load demand at site is from 18:00 hrs till 24:00 hrs between 24 kWh and 25 kWh. From the hourly load

demand profile, it can be concluded that load demand of the proposed site varies significantly for five different timing zones in a day. The average monthly load (D_{em}) usage in kWh is depicted by the Fig. 6.4(b). The minimum monthly load demand is 13.81 MWh for February and, the maximum monthly load demand is 15.48 MWh for November.

6.4 SIZING OF RE COMPONENTS USING LP

In most of the rural and isolated regions, the grid supply is not available or continuous supply is rarely available. Renewable energy resources as distributed generators can be utilized for such requirements. The appropriate selection of renewable energy resources is of utmost importance for designing the microgrid in distributed power generation systems. This section focuses on the problem of optimal sizing of an off-grid MG by minimization of investment cost. The developed method of optimal sizing is a two-stage linear programming (TSLP) technique.

6.4.1 Proposed Two Stage Linear Programming

Linear programming (LP) is a technique that maximizes or minimizes an objective function. The objective function must be a linear function that may be subjected to linear constraints, these constraints may be equalities and inequalities. LP has three main parameters to be defined effectively for a problem: linear objective function, linear equalities, and linear inequalities [156]. The developed technique follows a two-stage method for designing of DERs. The first stage, it focuses on the probabilistic nature of intermittent RES, where the physical conditions of the site are considered for effective and efficient planning of the system. In the second stage, the load demand profile is compared with the optimally sized DGS for sizing of the BESS. The developed technique aims at

minimizing the total cost of investment (TCI) of designing a system with SPV and WT energy required for the selected site. The load demand of the site is developed considering the load demands for every day for a complete year. The developed objective function and constraints are linear, therefore, the problem of optimal sizing of DGS using *linprog* in MATLAB environment.

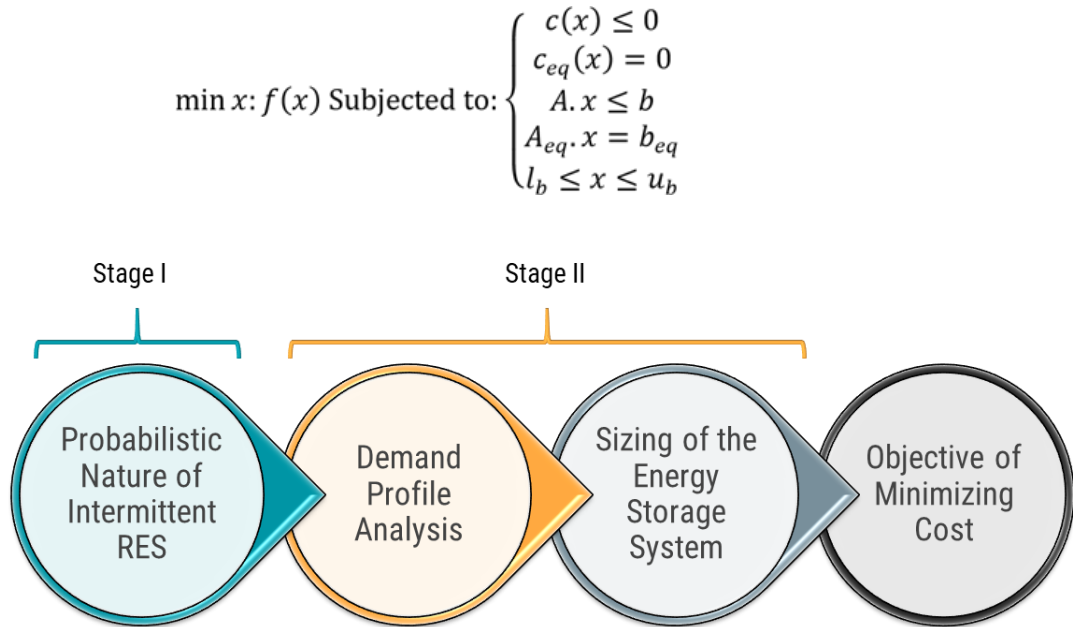


Fig. 6.5. The developed method for sizing of the off-grid based MG

6.4.2 Problem Formulation

In this section, the optimal cost of sizing is formulated considering the total investment cost for meeting the desired load demand. The developed LP method minimizes the cost function $f(x)$, i.e., a function of initial investment cost (C_{ii}), operation and maintenance cost (C_{om}).

$$f(x) = \min(TCI) \tag{6.2}$$

$$TCI = C_{ii} + C_{om} + C_{bess} \quad (6.3)$$

$$C_{ii} = C_{ipv}k_{ipv}f_{ipv} + C_{iwt}k_{iwt}f_{iwt} \quad (6.4)$$

Where, C_{ipv} Unit price of the SPV (\$/m²), C_{iwt} Unit price of the WT (\$/m²), k_{ipv} SPV load demand factor, k_{iwt} WT load demand factor, f_{iwt} Design vector/WT fraction for WEGS and f_{ipv} Design vector/PV fraction for SPV system.

$$k_{ipv} = \frac{D_{em}}{E_{pvm}} \quad (6.5)$$

$$k_{iwt} = \frac{D_{em}}{E_{wtm}} \quad (6.6)$$

Here, D_{em} Monthly load (kWh), E_{pvm} Monthly SPV energy output (kWh/m²) and E_{wtm} Monthly WT energy output (kWh/m²).

$$C_{om} = (C_{mpv} + C_{mwt})k_{om} \quad (6.7)$$

$$C_{bess} = S_{bess}(C_{iess} + C_{essm}k_{om}) \quad (6.8)$$

$$k_{om} = \sum_{y=1}^{NY} \left(\frac{1+v}{1+i} \right)^y \quad (6.9)$$

Where, C_{bess} Cost of battery energy storage system (\$/kWh), C_{mwt} Maintenance cost of WT, C_{mpv} Maintenance cost of SPV, k_{om} Maintenance factor, i inflation rate, v interest rate, y Number of years and NY Total number of years.

Equation (6.2) is the cost function defined to be minimized. Equations (6.3) – (6.9) define the different variables of the objective function of minimizing the TCI i.e., cost function.

6.4.3 Sizing of Battery Energy Storage System

Power of distributed generation system ($P_{dgs}(t)$) at time t is given below

$$P_{dgs}(t) = P_{fiwt}(t) + P_{fipv}(t) \quad (6.10)$$

$f_{ipv} * P_{pv}(t)$, $f_{iwt} * P_{wt}(t)$ are $P_{fipv}(t)$ and $P_{fiwt}(t)$ respectively.

Power deficient ($P_d(t)$), and Power demand ($P_{dl}(t)$) of the loads at time t

$$P_d(t) = P_{dl}(t) - P_{dgs}(t); \quad P_{dl}(t) > P_{dgs}(t) \quad (6.11)$$

Energy to be supplied by the battery (kWh) (E_d)

$$E_d = \sum_{t=1}^{24} P_d(t) \quad (6.12)$$

Size of the battery energy storage system (kWh) (S_{bess})

$$S_{bess} = E_d / (1 - \rho) \quad (6.13)$$

Here, ρ State of charge of the battery.

6.4.4 Constraints

The design vectors in Equation (6.4) f_{iwt} and f_{ipv} are the renewable fractions, these have certain linear equalities and inequalities as defined below, these define the constraints on the distributed generated system.

$$f_{iwt} + f_{ipv} = 1 \quad (6.14)$$

$$0 \leq f_{ipv} \leq 1 \quad (6.15)$$

$$0 \leq f_{iwt} \leq 1 \quad (6.16)$$

At every time step, the power of BESS must be in an allowed range limit according to capacity of battery and the excess demand of the energy.

$$P_d(t) \leq P_{al}(t) \quad (6.17)$$

For discharging cycle, when $(E_{wtd} + E_{pvd})$ is not sufficient to meet the load demand

$$E_d < E_{ld} \quad (6.18)$$

$$0 < \rho \leq 1 \quad (6.19)$$

6.4.5 Results and Discussion

This section presents the sizing results of renewable energy sources using TSLP technique. The results presented in this section are calculated for off grid. Table 6.2 describes the various parameters used for optimal sizing of the DERs using linear programming for the local loads in a standalone MG environment.

Table 6.2. General and cost parameters

Parameter	Value
v	0.015
i	0.020
NY	25
t	0, 1, 2,.....24
C_{ipv}	\$171.512/m ²
C_{iwt}	\$270.716/m ²
C_{mpv}	\$3.357/m ²
C_{mwt}	\$9.103/m ²
ρ	0.2
C_{iess}	\$400/kWh
C_{essm}	\$10/kWh

The Fig. 6.6(a) shows the monthly average of the solar energy generated at the site (E_{pvm}). The solar energy generation is more for March, April and May i.e. 27.9 kWh/m², 28.6 kWh/m² and 29.3 kWh/m² respectively. Whereas, the monthly average of the wind energy generation (E_{wtm}) for the site is represented in the Fig. 6.6(b). The wind energy generation for the month of May, June, and July are more than the rest of the year. For May, June, and July the E_{wtm} is 13.1 kWh/m², 12.7 kWh/m² and 11.2 kWh/m² respectively. E_{wtm} is comparatively less than the E_{pvm} for the selected site.

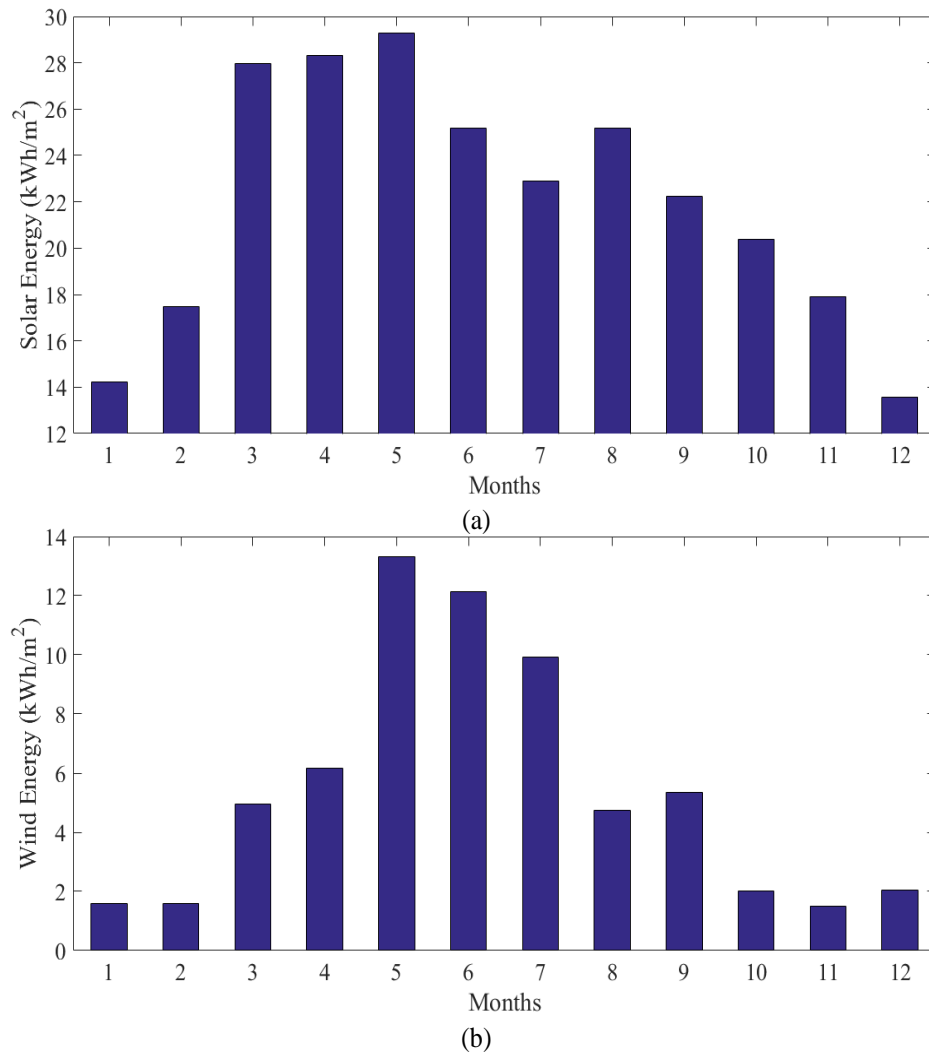


Fig. 6.6. (a) Monthly solar energy generation (b) Monthly wind energy generation

From the Fig. 6.6(a) and Fig. 6.6(b) it is clearly visible that the SPV energy generation is more than the WEGS for the selected site due to demographical and geographical conditions. The optimization tool used for the case study also justifies it with the Fig. 6.7, as it shows that WT system will be costlier than the SPV system throughout the year, considering any month. The trend of TCI for WT system can be easily related to the Fig. 6.6(b), for the months May, June and July the wind energy generated is maximum, so for the same corresponding months TCI is minimum.

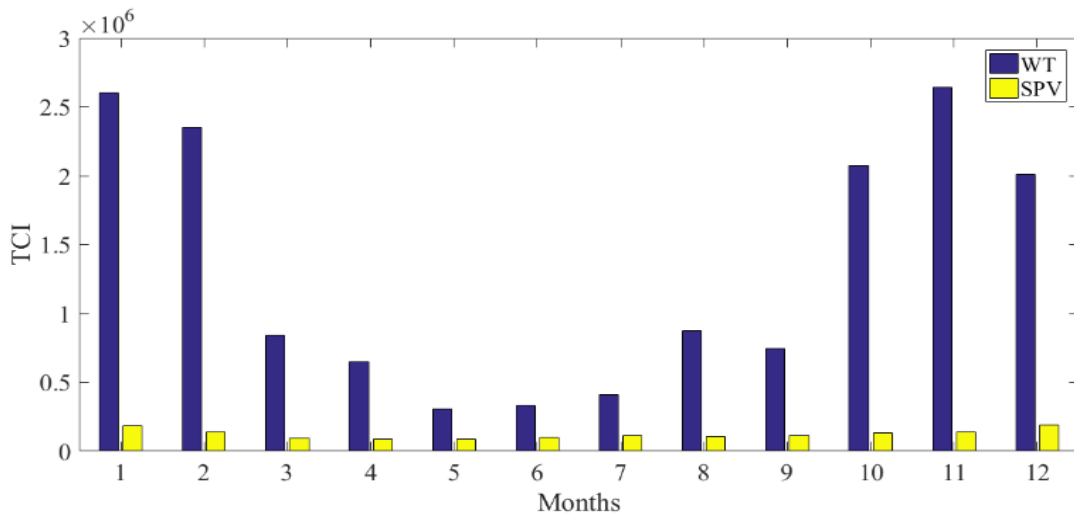


Fig. 6.7. The total cost of investment in the initial year

The developed linear programming technique optimized the cost function ($f(x)$) resulting in significantly less cost of investment for SPV system. Thus, suggesting the DERs to be primarily a SPV system rather than being SPV with WEGS or WEGS. The total cost of investment calculated by the algorithm for the DGS is approximately $\$ 1.77 \times 10^6$. The major area of concern for a completely off-grid MG is the size of energy storage system (ESS), for providing uninterrupted power supply to the load. Table 6.3 reports the optimal sizing results of the SPV and battery energy storage system (BESS). It also shows the optimal total cost of investment calculated by the developed technique. It

is a noticeable factor that in daylight hours the power produced from the SPV system is used to feed all the four loads, and also the charging of BESS is performed during these hours for the proposed system. The amount invested per kW is \$11,190 (TCI/kW) for the proposed case study and payback period for the incentive-based system is calculated to be 6.88 years. The payback period and TCI/kW is significantly less on comparing it with 7.98 years and \$13,233/kW [98].

Table 6.3. Optimal sizing results

Variable	Value
Type of DGS	SPV
TCI	\$1,768,000
Size of SPV	158 kW
Size of BESS	212 kWh
Payback time	6.88 years

It can be seen that the optimal solution to the problem is economical, feasible and has payback period less than five years that is comparatively less considering the initial investment and maintenance cost. The amount invested per kW is \$11,190 (TCI/kW) for the proposed case study and payback period for the incentive-based system is calculated to be 6.88 years. The major advantage of the developed technique is that it prevents the condition of over sizing or under sizing. It is because the designed method analyzes the solar irradiance, temperature and wind speed of the site for the prediction of power from these RES. The developed technique has higher return on investment with significant less TCI/kW in comparison.

6.5 SIZING OF SPV BASED MICROGRID FOR SELECTED SITE IN DEREGULATED ENVIRONMENT

This section provides insight about the sizing problem of MG for modern power systems. This modern power system is represented by controlling the loads, selling and purchase of power from the grid. The load flexibility (LF_{per}) and grid exchange power signify the deregulated electricity environment. In this section, a novel approach to integrate the various aspects and characterization of energy consumption in a deregulated electricity environment is discussed. It focuses on designing a hybrid MG system with ac and dc components such as grid connected inverters and BESS respectively. The key objectives of the proposed work are:

1. To find the optimal sizes of the RE resources considering the geophysical parameters using a nature-inspired optimization technique.
2. Propose a new technique namely advanced grey wolf particle swarm optimizer (MGWPSO), and compare with grey wolf optimizer (GWO).
3. The approach of sizing the MG is designed keeping in mind to maximize the profits and reduce the burden on the grid.
4. Furthermore, the impact of load flexibility on designed MG is to be studied with the help of two different scenarios that are $LF_{per} = 0\%$ and 30% .

6.5.1 Problem Formulation

The objective function of the proposed system is to minimize the annual cost of investment (ACI). In Eq. (6.21) the PV system does not have any replacement cost as in case of the inverter and BESS. The inverter replacement cost and the battery replacement

cost are considered using Inv_{rep} and B_{rep} respectively. The $C_p(t)$ and $C_s(t)$ are considered according to local power commission and the tariff of the design location. The cost of the various system components is mentioned in Table 6.4. The values of constants and technical specifications related to the MG system are given in Table 6.5.

$$f(x) = \min(ACI) \quad (6.20)$$

$$\begin{aligned} ACI = & N_{pv}(PV_{ii} + PV_{om}) + N_{wt}(WT_{ii} + WT_{om}) + N_{inv}(Inv_{ii} + Inv_{om} + Inv_{rep}) \\ & + N_B(BESS_{ii} + BESS_{om}) + B_{rep} \\ & + \sum_{t \in T} \{C_p(t)[P_{PG}^{ac}(t) + P_{PG}^{dc}(t)] - C_s(t)P_{SG}(t)\} \end{aligned} \quad (6.21)$$

Table 6.4. The cost of various system components

Initial Investment Cost				Replacement Cost		O&M Cost
PV \$/kW	WT \$/kW	Batt \$/kWh	Inv \$/kW	Batt \$/kWh	Inv \$/kW	2.5% of initial investment
1500	2500	150	350	150	350	

Table 6.5. Technical specifications

Nominal Interest Rate	Inflation Rate	Project Lifetime	SoC_{mx}	SoC_{mn}	η_{dc}^{ac}	η_{ac}^{dc}	Z_B
3.75%	1.75%	25 years	0.95	0.35	0.95	0.95	3×10^{-4}

6.5.2 Load Management System Considering Load Flexibility

The loads are classified similarly to the electrical load present in section 6.3. The average daily demand for the retail outlet is found to be around 480 kWh for five years. The modeling of the loads and designing of a demand response system is implemented using MATLAB software. For designing a load management system, the

load flexibility (LF_{per}) is considered to be 0% and 30% of the total demand. This flexibility of the load can be achieved by controlling the building loads, lighting loads, and motor loads. The term load flexibility is expressed as the percent of controllable demand to the total demand and is denoted by LF_{per} . The constant load considered are water cooler and air compressor unit. Variable Load can be committed within different shifting of the time window. Table 6.6 defines the rating of the various loads for which MG system has to be designed. The constant load considered are water cooler, and air compressor unit. Variable load can be committed within different shifting of the time window.

Table 6.6. General load classification

Type of Loads		Operating period	Power (W)
Non-Controllable	L_{cnst}	24 hrs	6500
Controllable	L_{exl}	17:00 – 06:00 hrs	3700
	L_{bld}	09:00 – 17:00 hrs	2500
	L_{mtr}	24 hrs	31300
Total Peak Load	P_{Lp}		44000

$$P_L = L_{cnst} + L_{exl}k_l(t) + L_{bld}k_b(t) + L_{mtr}k_m(t) \quad (6.20)$$

The variable loads L_{exl} , L_{bld} and L_{mtr} have loading factors k_l , k_b and k_m respectively. These loading factors are the function of time and help in defining the time of use (TOU) of lighting, building, and motor loads. Fig. 6.8 shows the TOU of different loads for the proposed site for a single day. Here, loading factors can be defined by Equation (6.21), the ratio of A_m/A_i the total number of hours the specific load (motor, building or lights) can be discretely operated. D_{load} defines the task commitment duration in hours for that specific type of loads.

$$k_{l/m/b} = 1 - \min \left(\frac{A_m}{A_i} * D_{load}, 1 \right) \quad (6.21)$$

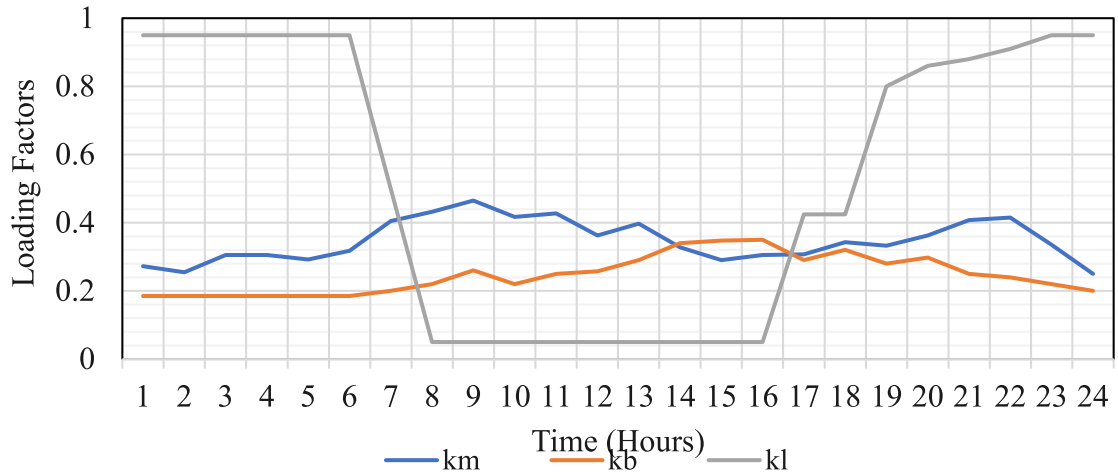


Fig. 6.8. Variation of the loading factors for a day

6.5.3 MGWPSO Sizing Algorithm for SPV based Microgrid

The MGWPSO approach is used to minimize the Annualized Cost of Investment (ACI) of the system. This hybrid meta-heuristic technique is implemented to simultaneously assess the geophysical conditions and size the BESS while optimizing the operations of the battery bank. The hybrid meta-heuristic technique is used because Eq. (20) introduces the nonlinearity as it is variable and stochastic and Eq. (6.21) has $C_p(t)$ and $C_s(t)$ that are time-varying making the function complex. In the main optimization loop, MGWPSO generates random particles of possible solutions, each particle comprises of random sizes of battery. In each iteration, these sizes are sent to the inner loop of the optimization to minimize the daily cost and maximize the consumption of the RE resources. The annual electricity cost is then evaluated for each particle. Fig. 6.9 represents the flowchart for better understanding of the MGWPSO technique in designing the required MG.

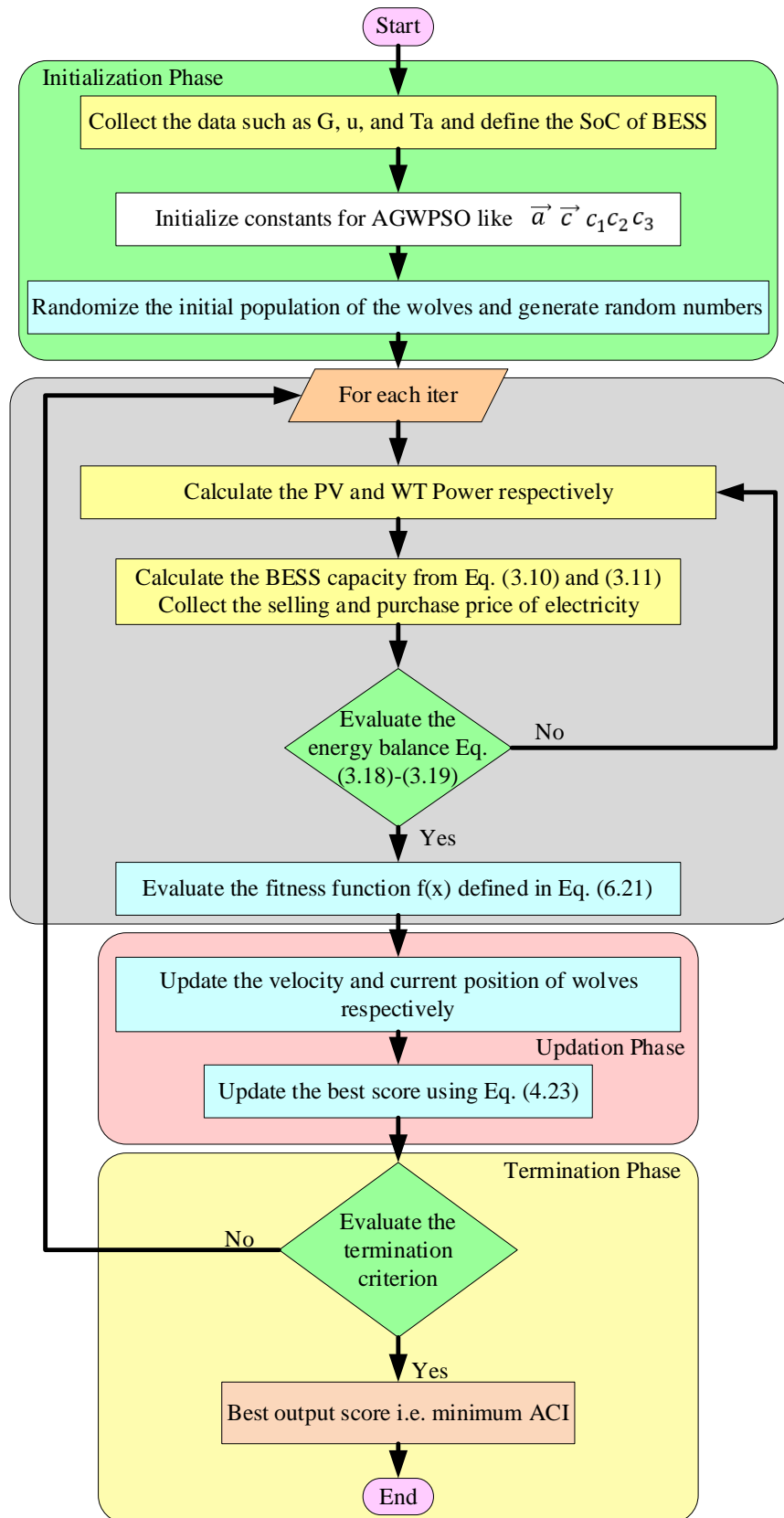


Fig. 6.9. Flowchart of MGWPSO

6.5.4 Results and Discussion

Fig. 6.10 and Fig. 6.11 represents the hourly power produced by SPV and wind energy conversion system respectively during a year. These are calculated using the weather data collected for the site. From these figures it can be concluded that P_{wt} is more erratic and unpredictable than P_{pv} for a similar rated capacity installed at the same site.

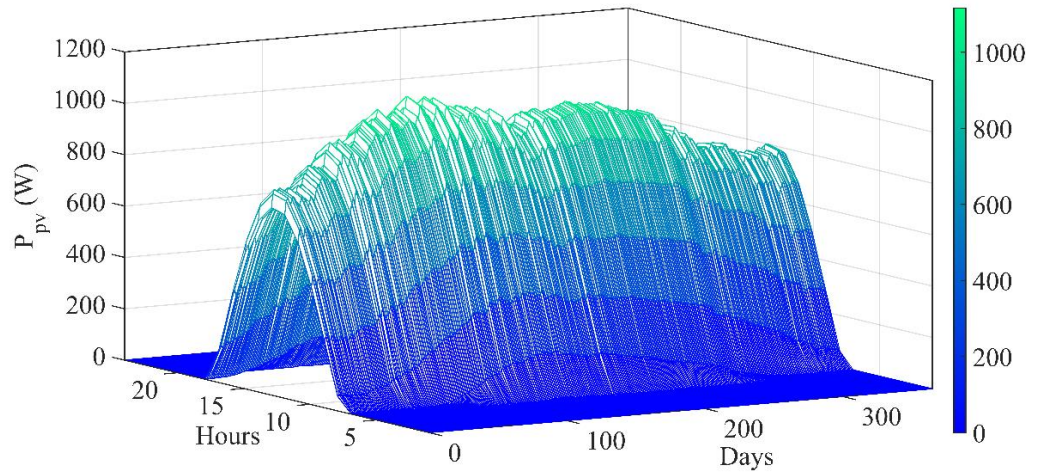


Fig. 6.10. Power generation from SPV over a year for the site

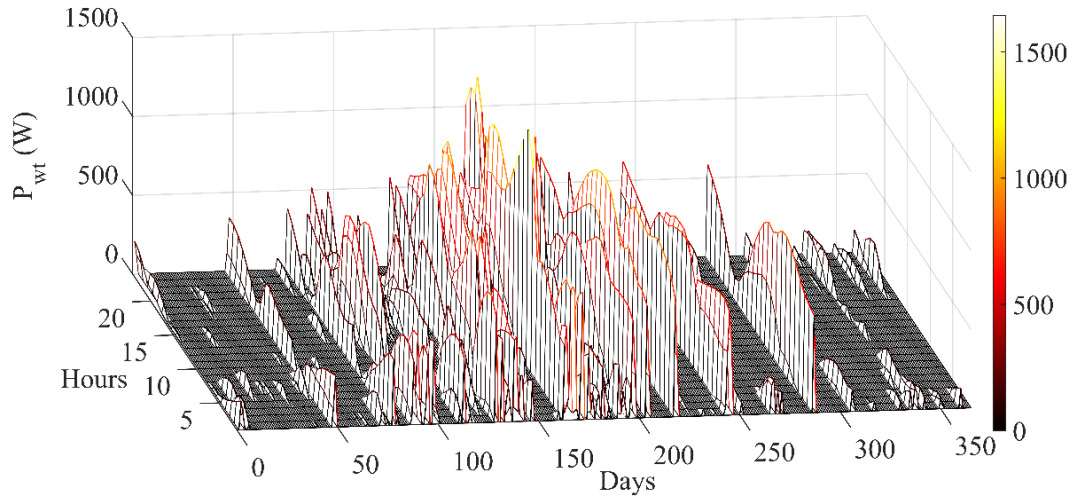


Fig. 6.11. Power generation from wind energy conversion system over a year for the site

This study is done with help of the return of investment (ROI) and annualized return of investment (AROI). ROI is the ratio of gain to investment. The ROI does not depend on the lifetime of the project so AROI is an essential tool to amortize the full investment cost of the system. The life of the project (y) is generally considered to be 25 years.

$$ROI = \frac{\text{Return} - \text{Investment}}{\text{Investment}} = \frac{\text{Avoided Cost}}{\text{Investment}} - 1 \quad (6.22)$$

$$AROI = \left[(1 + ROI)^{\frac{1}{y}} - 1 \right] \times 100\% \quad (6.23)$$

$$\text{Payback Period} = \frac{ACI * AROI}{\text{Yearly savings} + \text{Bonuses}} \quad (6.24)$$

The average wind energy generation through the WES for a complete year is 71.48 kWh/m². The yearly average energy production for the SPV system is 264.78 kWh/m². Thus, the renewable energy available for a complete year at the site is 336.26 kWh/m². Table 6.7 shows the feasibility analysis of the different RE sources that are available for designing hybrid MG and compares the per year investment, payback period, AROI, and annual RE self-consumption of different cases with PV, BESS, and WES.

Case I refers to the use of the only PV in designing of a system and has the highest Investment/year. It is observed that Case III (WES) and Case IV (WES+BESS) are the least favorable scenarios as they both have the highest payback period and least AROI. For case 1, i.e., PV system, Annual RE self-consumption is 38.24%. The addition of BESS to the PV system increases the RE self-consumption by 14.09%. Among Cases II and V

when the comparison is made, PV/WES with BESS has a higher % of RE self-consumption but suffers from a marginally higher payback period and low AROI to a PV with BESS.

Table 6.7. Comparison of different RE configurations for MG

Case	Annual RE self-consumption		Invest/year (\$/year)	Payback Period (year)	AROI (%)
	kWh/m ²	%			
I (PV)	128.59	38.24	515.60	10.1	4.7
II (PV+BESS)	175.95	52.33	401.60	6.67	6.8
III (WES)	41.69	12.38	392.80	10.66	3.3
IV (WES+ BESS)	62.67	18.64	379.60	10.34	3.1
V (PV+WES+ BESS)	216.34	64.34	502.40	7.89	6.2

The optimization for sizing of the hybrid MG considers utilizing only PV as the RE source and a BESS i.e., Case II of Table 6.7. The optimal sizing results are being presented in Table 6.8. It presents the results obtained for sizing the hybrid MG using the MGWPSO approach. During the off-peak hours and also when PV generates maximum power the priority of the designed algorithm is given to the charging of batteries and the surplus energy is exchanged with the grid. This scenario helps in dealing with situations of load flexibility and can supply it when demanded while keeping in mind the electricity market. The $LF_{per} = 0\%$ states that no demand response system is considered.

Table 6.8. Optimal sizing results

Parameters	Scenario 1 $LF_{per} = 0\%$	Scenario 2 $LF_{per} = 30\%$
N_{pv}	164 kW	138 kW
N_B	297 kWh	247 kWh
N_{inv}	87 kW	72 kW
ACI	\$ 33,240	\$ 27,620

6.5.6 Performance Analysis of MGWPSO based SPV Microgrid

The analysis of the daily average consumption of different electrical loads located at the site for every hour is undertaken for four different seasons present in India i.e., summers, winters, spring, monsoon, and is presented in Fig. 6.12. The average load of each hour for each day for a complete year is considered in the case study. The hourly load demand daily average for the winter season is presented in Fig. 6.12(a). The winter season is considered from October till January. During the winter season, the minimum demand or off-peak hours are the afternoon hours of 14:00, 15:00, and 16:00 with 13.96 kW, 13.32 kW, and 14.26 kW respectively. Whereas, the peak demand is observed in the morning hours of 7:00 to 12:00 and at night from 19:00 hrs till 22:00 hrs. The external lighting load is absent from 8:00 hrs to 14:00 hrs. The daily average power required by the load the winter season is 490.866 kW.

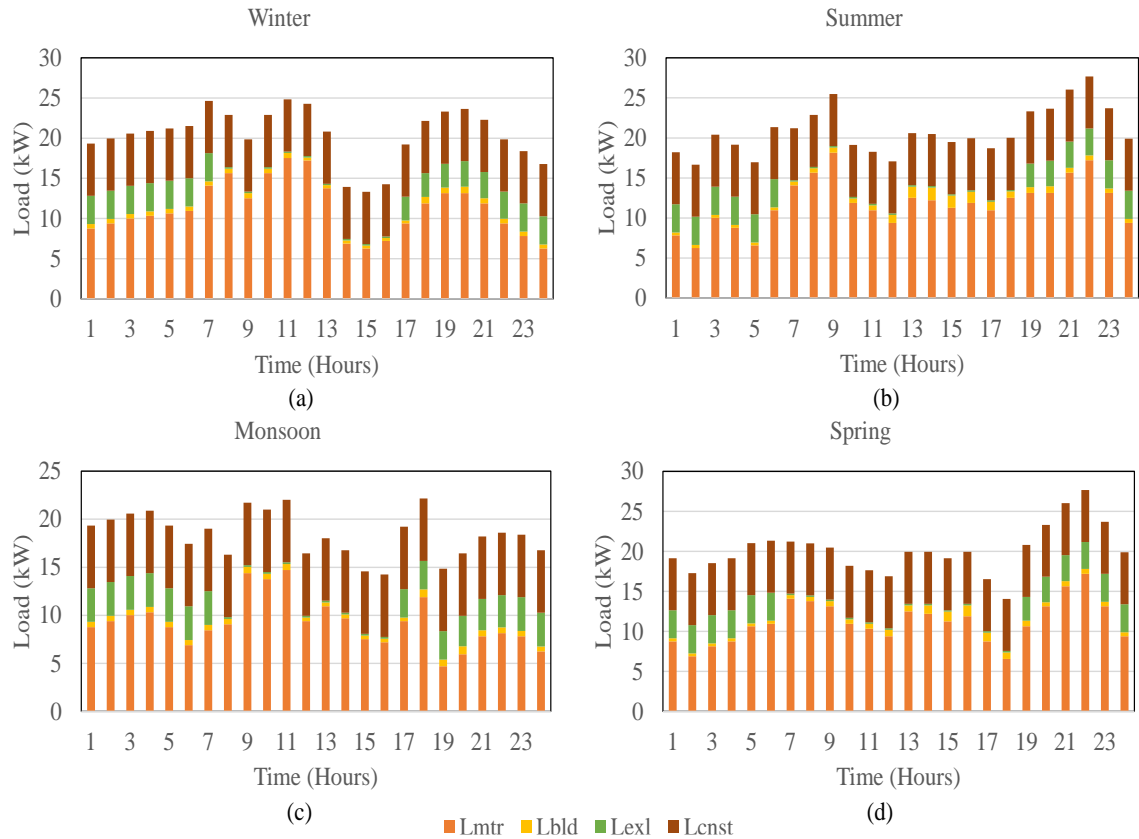


Fig. 6.12. Consumption of power of various loads for different seasons (a) Winter (b) Summer (c) Monsoon (d) Spring

Fig. 6.12(b) represents the daily average of hourly load demand of the summer season. The summer season is considered from March till June. From Fig. 6.12(b) it is observed that peak hours for load demand are prevalent in the morning and night hours, with the maximum power rating going up to 27.86 kW. The off-peak hours are 2:00, 5:00, 10:00, 11:00, and 12:00, but these off-peak hours still have higher power drawing capacity than those of the winter season. The external lighting loads draw negligible power from 7:00hrs till 18:00hrs but there is a slight rise in building loads in the afternoon hours unlike in winters.

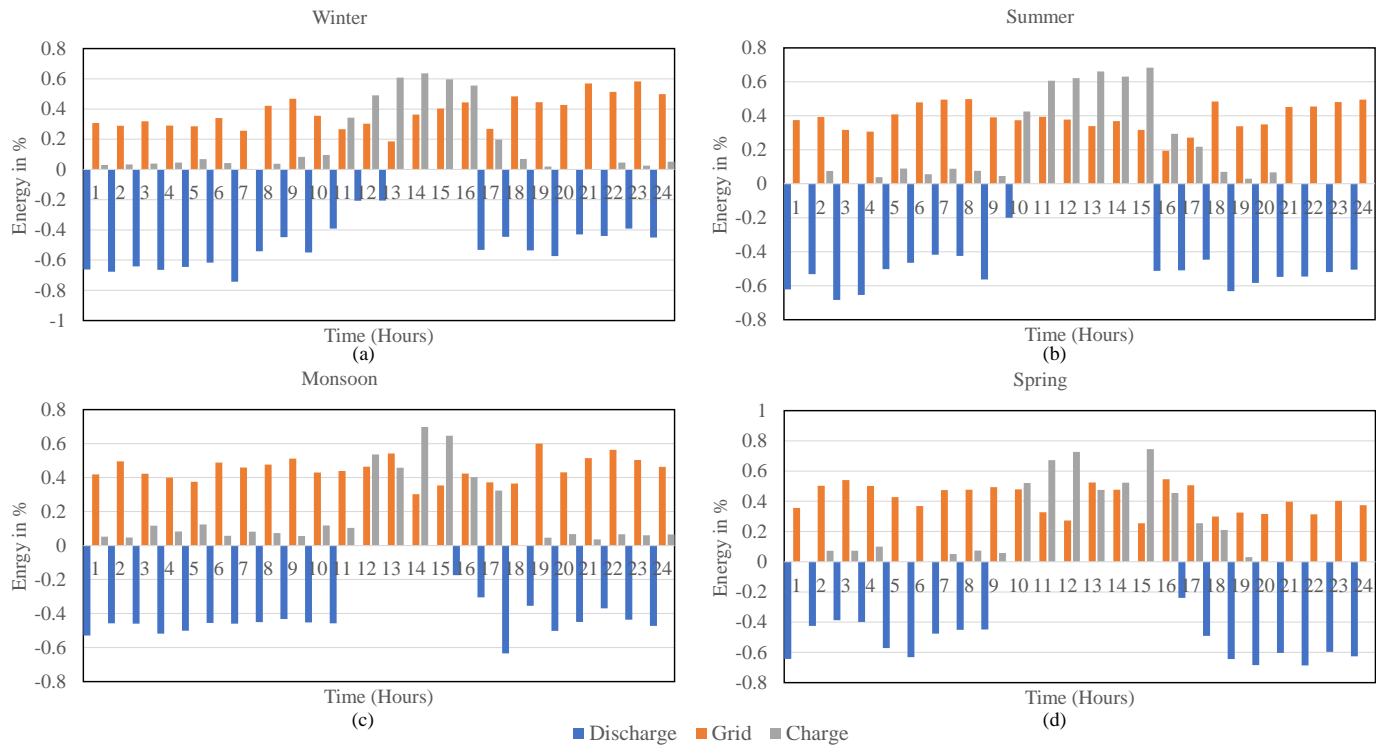


Fig. 6.13. Performance of BESS when $LF_{per} = 0\%$ for different seasons (a) Winter (b) Summer (c) Monsoon (d) Spring

The summer season has the highest daily average load demand of 500.33 kW. The hourly load demand analysis of the monsoon season is shown in Fig. 6.12(c). There is an overall reduction in power consumption when compared throughout all the seasons. The peak hours are less when compared with the other seasons and the power requirement is almost the same throughout the day. The building loads are very less for this season and the total power consumption per hour for this season is the least i.e., 442.35 kW. In Fig. 6.12(d) spring season and its hourly power consumption is depicted. The peak hours can be seen are present in the night time from 20:00 hrs till 23:00 hrs with corresponding powers of 23.38 kW, 26.03 kW, 27.68 kW, and 23.711 kW respectively. There is almost a constant demand for power for rest of the day with 18:00 hrs being the only off-peak time. The trend of the motor loads is similar to the summer season. The total hourly

demand requirement is between the summer and winter season with 472.67 kW. The performance of the BESS for $LF_{per} = 0\%$ is shown in Fig. 6.13.

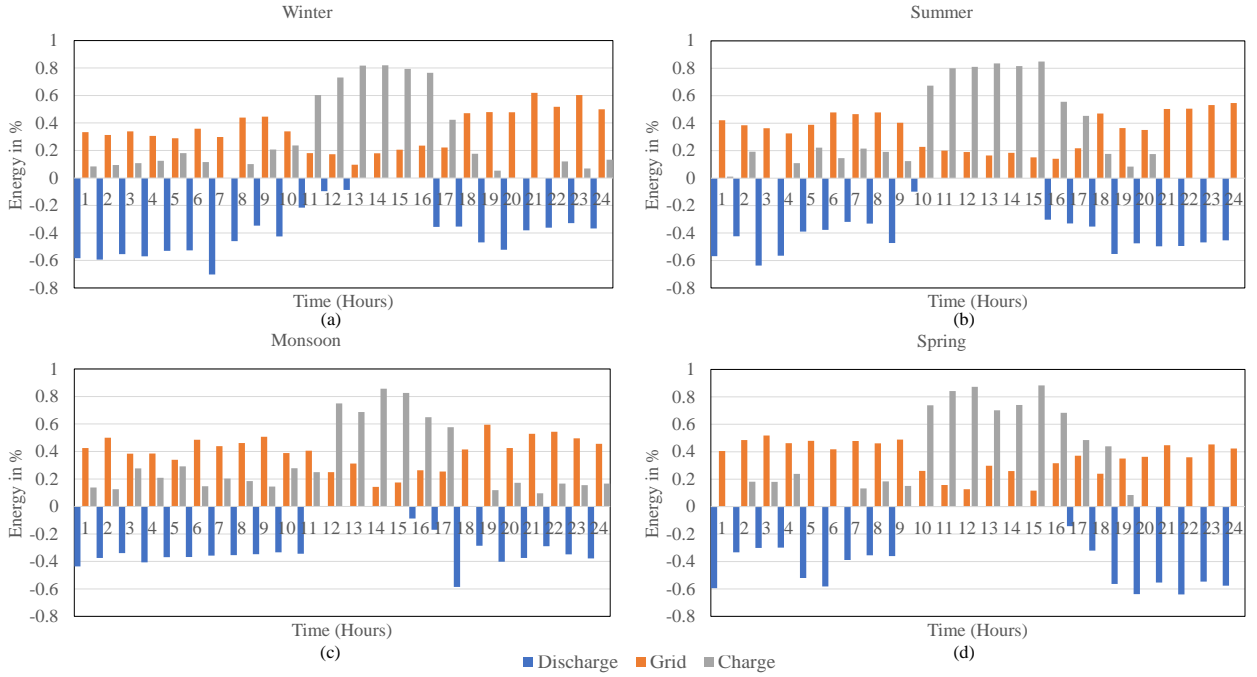


Fig. 6.14. Performance of BESS when $LF_{per} = 30\%$ for different seasons (a) Winter (b) Summer (c) Monsoon (d) Spring

The daily average usage of energy (%) utilized for charging and discharging of the BESS and also the exchange with the grid when considering $LF_{per} = 30\%$ is shown in Fig. 6.14. The performance of the optimal sized of the BESS through the designed MGWPSO approach for the four different seasons, winter, summer, monsoon, and spring is presented in Fig 6.14(a), (b), (c) and (d) respectively. The energy exchange of the grid comprises of energy purchased from the grid as well as sold to the grid. Fig. 6.14(a) shows that charging is highest from 11:00hrs till 16:00hrs during the highest sunshine hours and this energy is surplus for the demand. Whereas, during the night hours when there is no sunshine the discharging characteristics are considerably high. A similar trend is observed

in Fig. 6.14(b) during the summer season, unlike the winters the sunshine hours, are from 10:00hrs till 18:00hrs. The discharging characteristics of the monsoon season are unlike all the other seasons where a constant % of energy is required throughout the day from the BESS with a peak at 18:00 hrs. This is because the energy from the RE source is extremely erratic and sunshine hours are the least i.e., 12:00 hrs till 17:00 hrs. From Fig. 6.14, it can be concluded that during the peak hours of consumption of power, for all the four seasons the discharging of the battery bank is highest when compared for the rest of the day. Similarly, for the off-peak hours of the day i.e., the afternoon hours (10:00hrs to 16:00hrs) the charging characteristics are the maximum, and discharging state is negligible for the 24 hours.

Table 6.9. Comparative analysis of BESS

Season	Condition	Scenario	
		$LF_{per} = 0\%$	$LF_{per} = 30\%$
Winter	Discharge	-44.98 %	-36.77 %
	Charge	17.14 %	28.15 %
Summer	Discharge	-41.10 %	-33.76 %
	Charge	19.92 %	30.98 %
Spring	Discharge	-37.51 %	-32.14 %
	Charge	21.00 %	31.43 %
Monsoon	Discharge	-36.96 %	-28.97 %
	Charge	18.00 %	31.12 %

The performance of the BESS in scenarios when load flexibility is considered both 0% and 30% is shown in Table 6.7. The values of charge and discharge of energy from the BESS are average of the energy (%) shown in Fig. 6.13 and Fig. 6.14 for $LF_{per} = 0\%$ and $LF_{per} = 30\%$ respectively. The negative value in discharge denotes that the energy is

spent out from the battery. It is concluded from the Table 6.9 that when controllable loads are not controlled by the energy management system then stress on BESS is high. This is due to the higher energy spent from the battery to meet the uncontrollable loads. Whereas, when the 30% of the shiftable/controllable loads are controlled then the BESS performance is much higher and higher amount of energy is stored in the charging process. It is a key point that helps in determining the *LoB* of the battery.

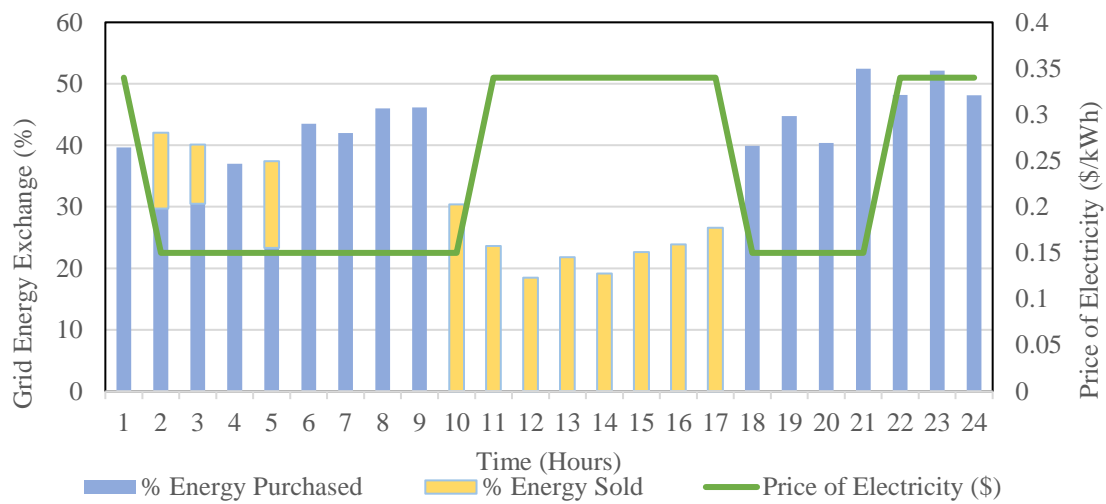


Fig. 6.15. Price of electricity and exchange of grid energy (%) for a day

Fig. 6.15 shows the percentage of energy from the grid purchased and sold for the whole year when averaged for a complete 24 hours. The electricity rates are proposed according to the Time of Day (ToD) Tariffs inspired by the Delhi Electricity Regulatory Commission. The rates of electricity are classified into two groups for off-peak hours and peak hours. It is visible that the designed approach prioritizes the energy exchange with the grid based on load demand, SoC of batteries, and also on the ToD tariffs. During higher tariffs of electricity, the energy is sold to the grid to minimize the ACI and increase the ROI. Fig. 6.15 shows that at 02:00hrs, 03:00hrs, and 05:00hrs, 12.35%, 9.63%, and 14.11% energy is sold to the grid during these off-peak hours. An average of 39.04%

energy is purchased and 21.24% energy is sold to the grid with help of the developed control technique. During the high sunshine hours, i.e., noontime the generation of electricity from SPV systems is relatively very high and feeds this energy to loads and BESS for charging. Some parts of the controllable loads are shifted to the off-peak regions where the rate is cheap. The surplus energy is fed to the grid at higher tariffs. The purchase of electricity from the grid takes place during the night hours and early morning whereas selling takes place during the afternoon hours at higher prices.

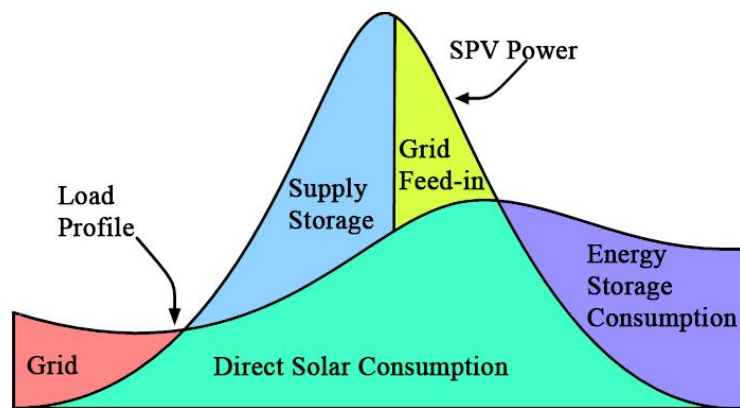
6.6 TECHNO-ECONOMIC IMPACT OF INTELLIGENT EMS IN HYBRID MICROGRID

In this section, an intelligent optimization technique is developed for solving the complex multi-objective function to reduce the operational/rolling cost of the MG. The focuses on a comparative study of this intelligent optimization i.e., modified grey wolf optimizer (MGWPSO) with the linear programming-based (LP) optimization. The main objectives of this section are to integrate the intelligent MGWPSO technique for effective MG energy management strategy for reduced operational cost, present a techno-economic comparative study of the MGWPSO based MGC with LP energy management system and the performance analysis of the developed EMS is presented for a clear day and cloudy day conditions.

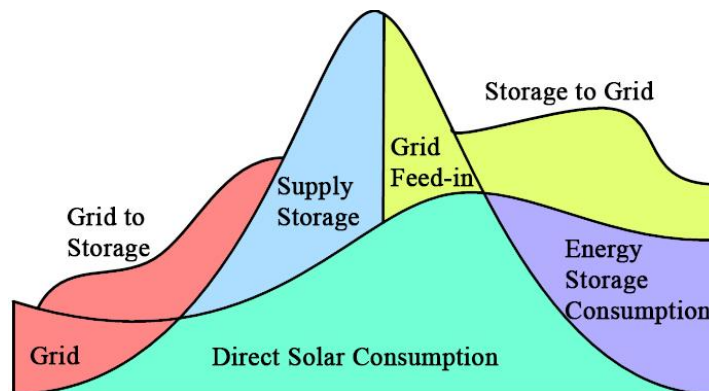
6.6.1 Importance of Energy Management Strategy

The RE sources are stochastic and intermittent, thus not providing electrical power at all times constantly. Hence, it is necessary to control the power from these RE sources.

Fig. 6.16(a) represents a peak demand shift when energy storage is incorporated in a smart energy management system without any variability of loads. Considering, modern power system where the utility grid is experiencing high penetration of the RE sources with higher uncertainties. These variabilities are due to increasing customer awareness and its preferences resulting in variable cost of electricity, and higher exchange of power between grid and RE sources. Thus, designing an optimal energy management strategy is critical to maximize the comfort, savings and productivity for both consumers and operators. Fig. 6.16(b) illustrates a generalized performance of an optimal EMS considering some variations in price and preferences of users.



(a)



(b)

Fig. 6.16. (a) Performance of a simple EMS (b) Performance of optimal EMS with uncertainties

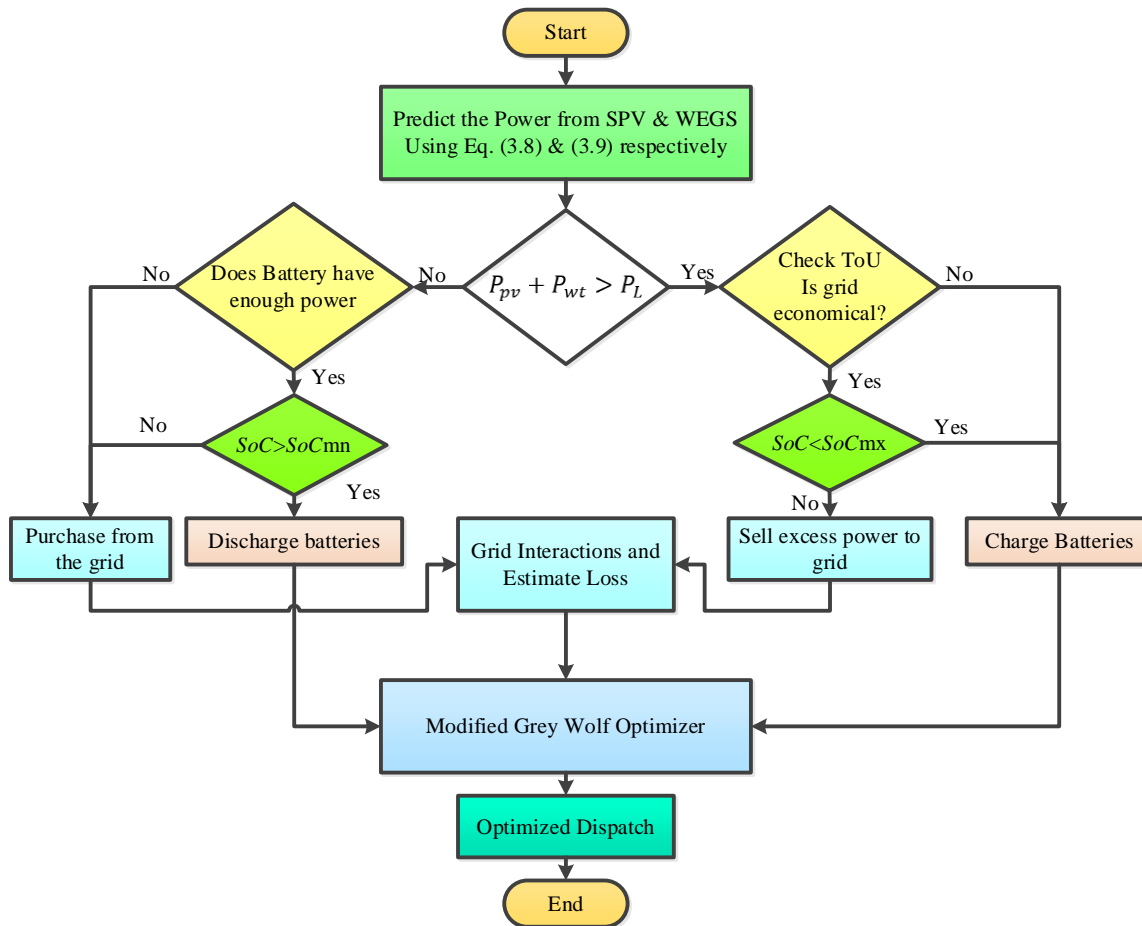


Fig. 6. 17. Flowchart of the designed MGC

6.6.2 Hybrid Intelligent Approach based EMS

Fig. 6.17 shows systematic flow of control to manage the MG. According to this flowchart, the MG with RE sources is initially assessed for the islanding operation with minimal interaction from grid, this helps in estimation of the total power generated by RE. Furthermore, this power is compared with the estimated load demand (P_L), if this is more than the power generated from RE sources and batteries don't have sufficient power/ SoC_{mn} then the deficient power is purchased from the grid. Consequently, if other conditions are satisfied then power is sold to the grid. The battery charging and discharging is also elaborated in the flowchart and is governed by the market conditions and SoC of the

batteries. The prime aim of the hybrid approach-based EMS is to maximize the social benefit by recharging the BESS when electricity cost is minimum and export energy to the grid during high *ToU*. This approach takes benefit from the price gaps between high and low-price hours of electricity from the utility grid. In addition, the transmission losses are reduced as energy is utilized from the RE sources and BESS is recharged accordingly.

6.6.3 Results and Discussion

MG is simulated in MATLAB-Simulink Environment and performance of the developed MGWPSO based EMS is gauged under two different conditions. The two different conditions considered in the work are classified by the day type ratio (R_{dt}) i.e., the ratio of the measured and theoretical clear sky insolation. The different range of R_{dt} has been decided to identify the clear i.e., sunny condition ($R_{dt} > 70\%$) and cloudy condition ($70\% > R_{dt} > 30\%$).

The cost of electricity (cents/kWh) from the utility grid is displayed in Fig. 6.18(a). The load demand graph is given in Fig. 6.18(b). The classification of the regions was done based on the cost of electricity supplied by the utility grid. The cost of electricity is varying from a minimum \$0.09/kWh to \$0.31/kWh and is elaborated in different regions in Figure 6.18.

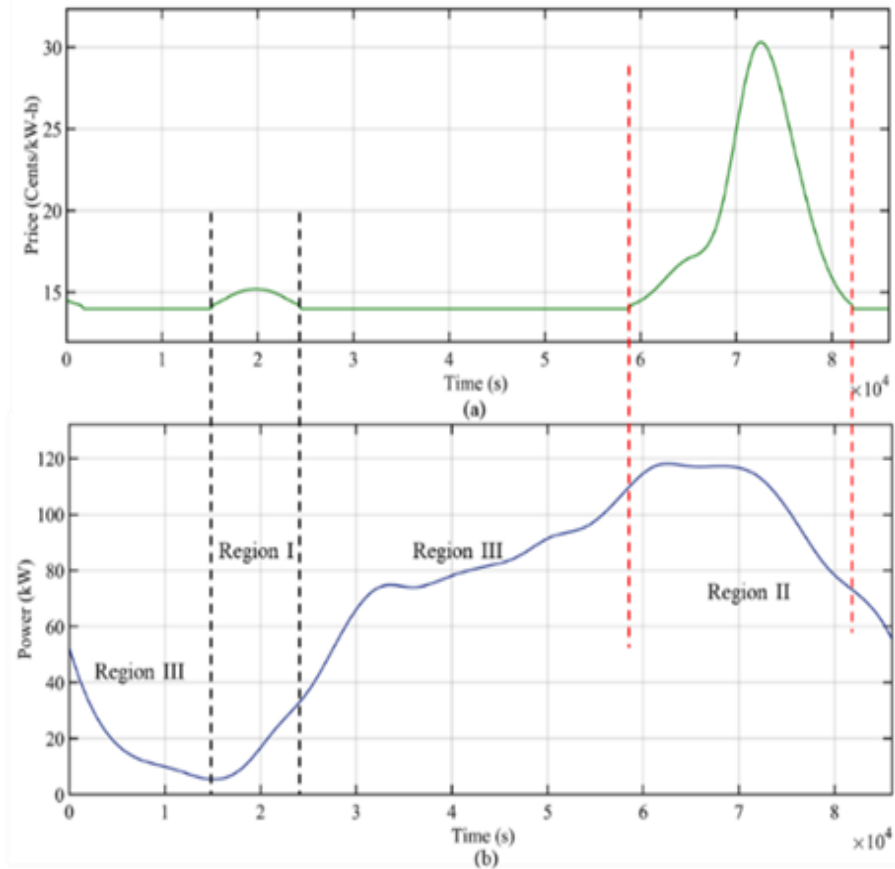


Fig. 6.18. (a) Cost of electricity (b) Load profile

The performance of the hybrid optimization technique i.e., MGWPSO based MGC for energy management on a clear, sunny day is depicted in Figure 6.19. The performance difference is evident because the BESS is charging when the load is least and the cost of electricity is minimum i.e., during some parts of Region I and III. The real time performance of MGWPSO based EMS for a practical situation is discussed in Figure 6.20. Moreover, the performance of SPV system is varying with many fluctuations as shown in Figure 6.20(b). The performance of the BESS is different from the previous condition as, the battery charges till 63% and then following the similar characteristics of the previous conditions as shown in Figure 6.20(c).

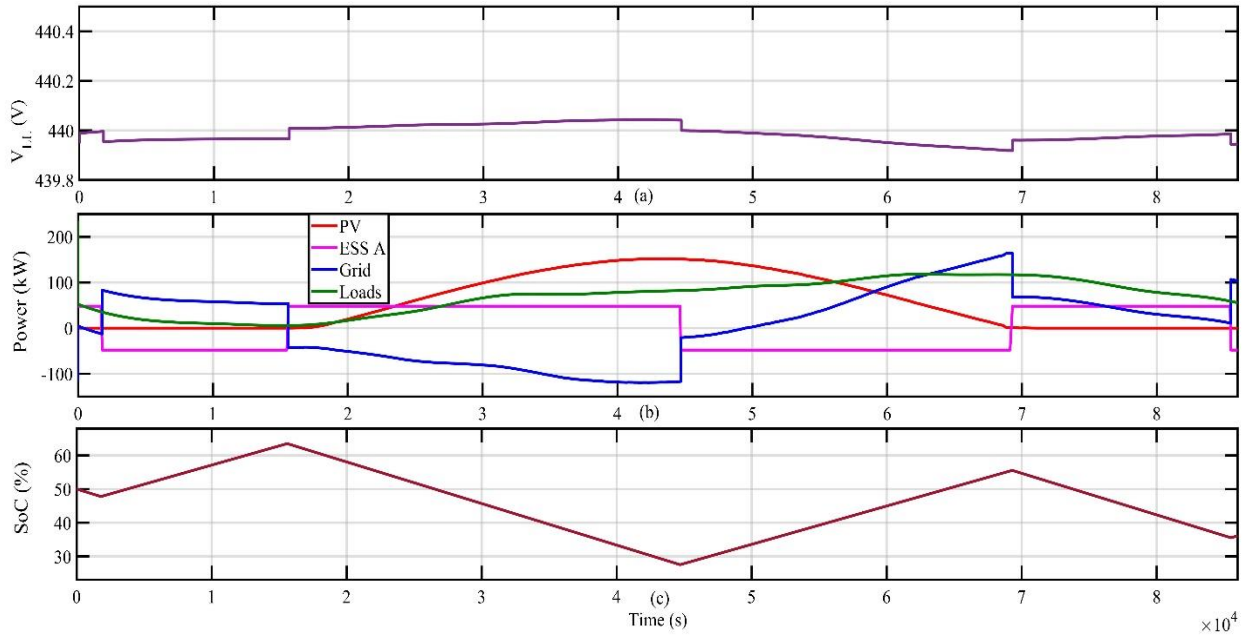


Fig. 6.19. Performance of MGWPSO based EMS on a clear day (a) Line to Line Voltage (magnitude) (b) Power exchange among different sources (c) SoC of the Battery

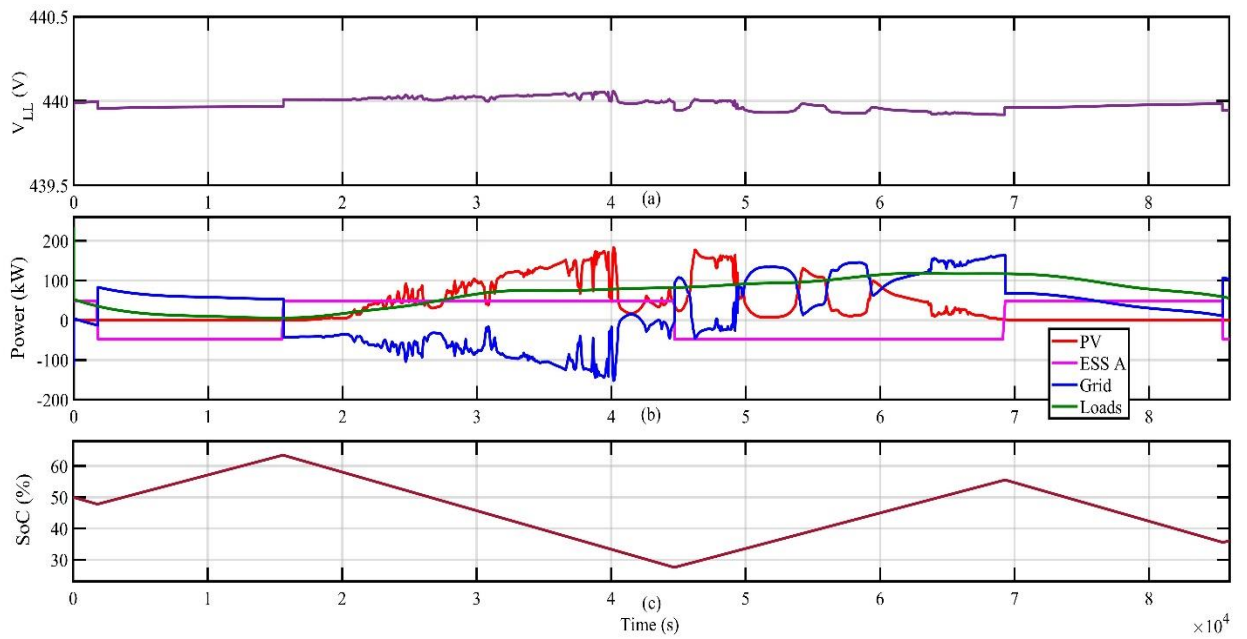


Fig. 6.20. Performance of MGWPSO based EMS on a cloudy day (a) Line to line voltage (magnitude) (b) Power exchange among different sources (c) SoC of the battery

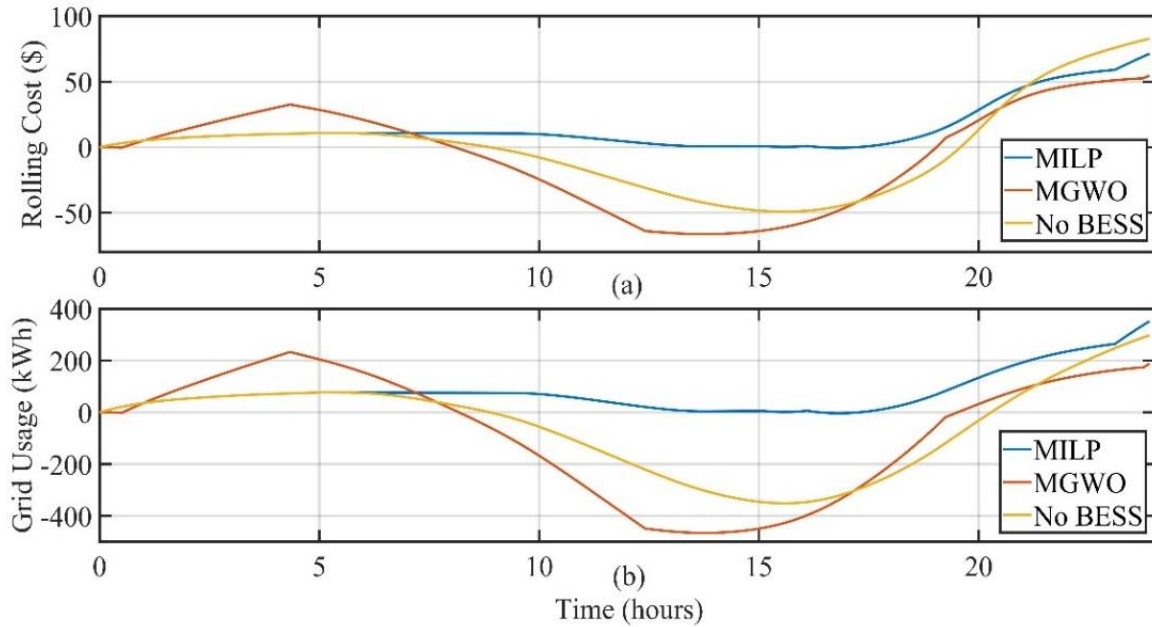


Fig. 6.21. Clear day performance (a) Rolling cost (b) Grid usage

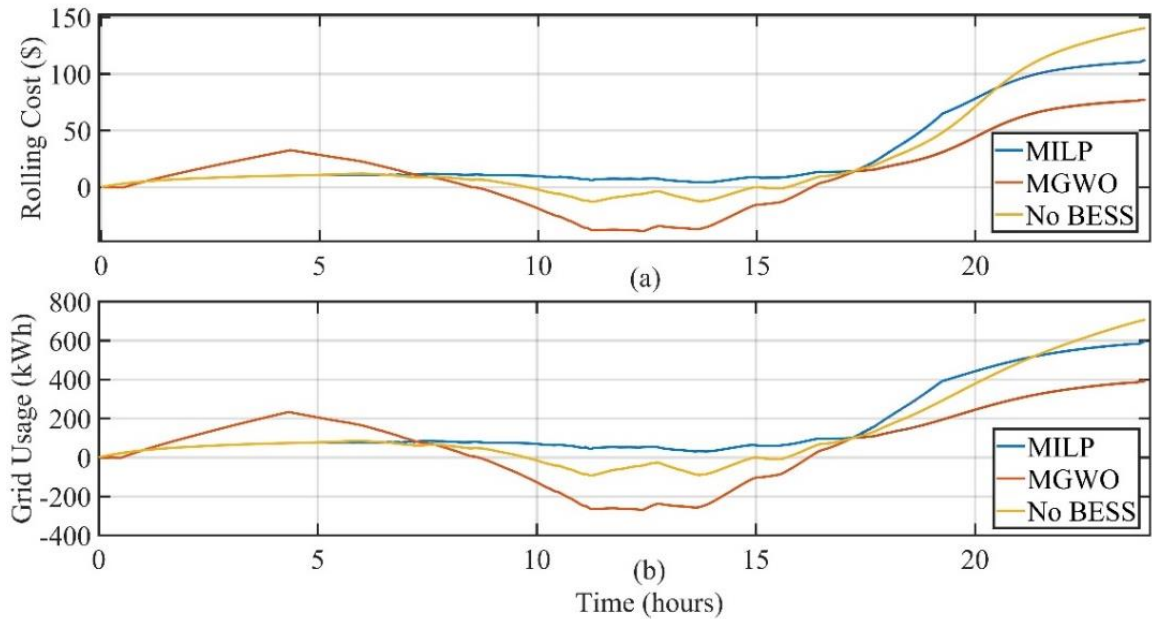


Fig. 6.22. Cloudy day performance (a) Rolling cost (b) Grid usage

From Figure 6.21 and Figure 6.22, it is seen that the performance of the MGWPSO-EMS is better and economically viable for both clear and cloudy conditions. The rolling cost is

much higher for the cloudy day when compared to the clear day, due to variability in the weather conditions.

Table 6.10. Comparative analysis of the developed EMS for MG

Condition	Parameters	MILP	MGWPSO
Clear	Rolling Cost (\$)	71.34	54.68
	Grid Usage (kWh)	327.81	188.23
Cloudy	Rolling Cost (\$)	112.43	77.24
	Grid Usage (kWh)	591.34	396.71

6.7 CONCLUSION

The optimal sizing and management of modern electrical system require geophysical conditions and parametric constraints. As the requirement of constant electrical energy in remote locations is of key importance off-grid SPV based MG system has been designed using TSLP method. TSLP approach is faster, reliable and suitable to minimize the size and cost (TCI) with different DERs and found better than the numerical methods. The major advantage of the developed technique is that it prevents the condition of oversizing or under-sizing. This method analyzes the solar irradiance, temperature and wind speed of the site for the prediction of power from these RES.

The optimal sizing of a hybrid microgrid and its management requires proper analysis of the demand response. So, an on-grid SPV system with grid exchanges has been designed using MGWPSO approach, In MGWPSO approach the effect of load flexibility on the size of components and ACI was observed and 21.24% of energy was sold to the grid. In addition, a seasonal comparative analysis for load management is also presented in the study.

Whenever an on-grid SPV based MG is being designed, the energy management system for controlling the demand and batteries is to be modeled effectively. The study further develops a hybrid energy management system using modified GWO. The economic analysis of the MGWPSO-EMS is tested at varying weather conditions and compared with MILP-EMS. The savings in operational/rolling cost is 23.34% and 45.55% than MILP-EMS in different scenarios.

CHAPTER 7

IMPROVING THE PERFORMANCE OF SPV SYSTEM USING ARRAY RECONFIGURATION AND MPPT CONTROLLER

7.1 INTRODUCTION

The performance of photovoltaics depends on numerous factors like irradiance, temperature, the material used for making panels, physical conditions, air mass, and some others. SPV power is generated by connecting the number of panels in series parallel combination to form a PV array. This type of configuration will result in reduced power output during partial shade (PS) and introduce large, multiple peaks in the P-V and I-V characteristics due to mismatching power losses between the modules. The movement of clouds is a key factor to introduce partial shading conditions (PSC). One of the key aspects to be considered by electrical engineers is the improvement of power efficiency of the SPV system. In this section use of array reconfiguration and maximum power point tracking algorithms is discussed in detailed. In addition to the array reconfiguration, different control algorithms are being used to search and track the MPP for maximizing the PV power output. The previous techniques for MPP tracking include P&O, INC (incremental conductance), current sweep, and fractional open circuit voltage etc. The control algorithm developed in this section is based on the adaptive neuro fuzzy inference system (ANFIS) approach. Solar cell efficiency refers to the amount of energy that is converted from sunlight in to electricity using photovoltaics, but here the efficiency improvement is referred to as the increase in the power extraction from the SPV system.

7.2 IMPACT OF PARTIAL SHADING

The shading of a group of cells results in reduction of output power. This condition is even more severe when the photodiodes are reversed biased due to partial shading. During this the diodes offer high resistance and reduce the load current. Furthermore, cells may be damaged due to heat produced as a result of high internal resistance. The output of the solar PV system in partial shaded conditions is different as the P-V characteristics have different MPP; global and local. The performance indicators considered for the developed shade dispersion method are mismatch power loss (MMPL), misleading power loss (MLPL), fill factor (FF) and performance ratio (PR). MMPL occurs because of reduced irradiance on various modules during partial shading conditions. Whereas, MLPL is the change in power between local MPP and GMPP. Fig. 7.1 represents the different types of the power losses namely mismatch power and misleading power in a PV array during PSC.

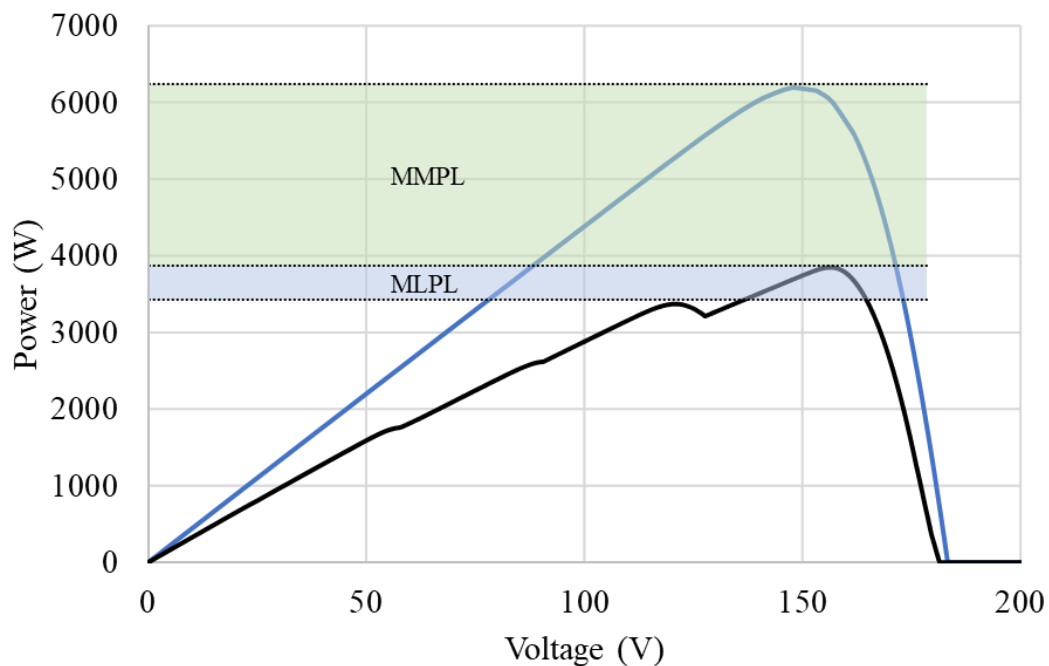


Fig. 7.1. Power loss in P-V curve during PSC

$$MMPL = MPP_{wopsc} - GMPP_{psc} \quad (7.1)$$

$$MLPL = (GMPP - MPP_{local}) \text{ during PSC} \quad (7.2)$$

Fill factor of a solar PV module is the squareness of I-V characteristics. In an ideal condition this represents a rectangle enclosed within the rectangle formed by open circuit voltage and short circuit current. In case of a PSC this shape deviates in a P-V characteristic and is measured in terms of FF.

$$FF = \frac{P_{psc}}{V_{oc}I_{sc}} \quad (7.3)$$

$$PR = \frac{P_{mx_{psc}}}{P_{mx_{stc}}} * 100 \quad (7.4)$$

7.3 CLOUD MOVEMENT AND MODELING OF SHADE

The shade will cause uneven and irregular irradiances on the modules. This reduced irradiance will further impact the current, open circuit voltage and short circuit voltage. In [157] authors have modeled the movement of cloud and explained that the irradiance on the panel is the function of the distance between the center of the module and shadow. In this work the movement of cloud is incorporated using acceleration, direction, and wind speed. This movement of cloud creates four different shading conditions, namely, short narrow (SN), long narrow (LN), short wide (SW) and long wide (LW). The authors of [123] have defined the above-mentioned shading conditions based on the width and length of the shading of the modules. The different shading conditions are represented in Fig. 7.2.

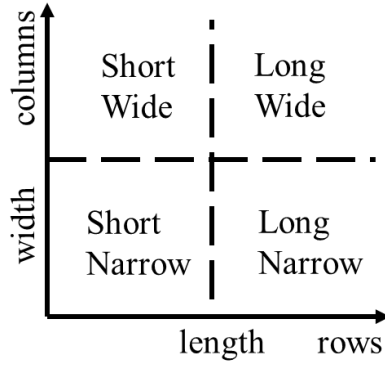


Fig. 7.2. Different shading conditions

The instantaneous velocity of the center of shadow is

$$v_{net} = u_{net} + a_{net}t \quad (7.5)$$

The movement of the clouds can be resolved into vertical (x) and horizontal (y) components, thus the equation (7.5) can be modified as

$$v_x = u_x + a_x t \quad (7.6)$$

$$v_y = u_y + a_y t \quad (7.7)$$

The vector representation of center of shadow and PV module at any given time is depicted in Fig. 7.2. Applying the vector addition using triangle law

$$\vec{P}_n = \vec{p}_1 + \vec{p}_2 \quad (7.8)$$

$$\vec{p}_1 = i \hat{i} + j \hat{j} \quad (7.9)$$

$$\vec{p}_2 = x_{current} \hat{i} + y_{current} \hat{j} \quad (7.10)$$

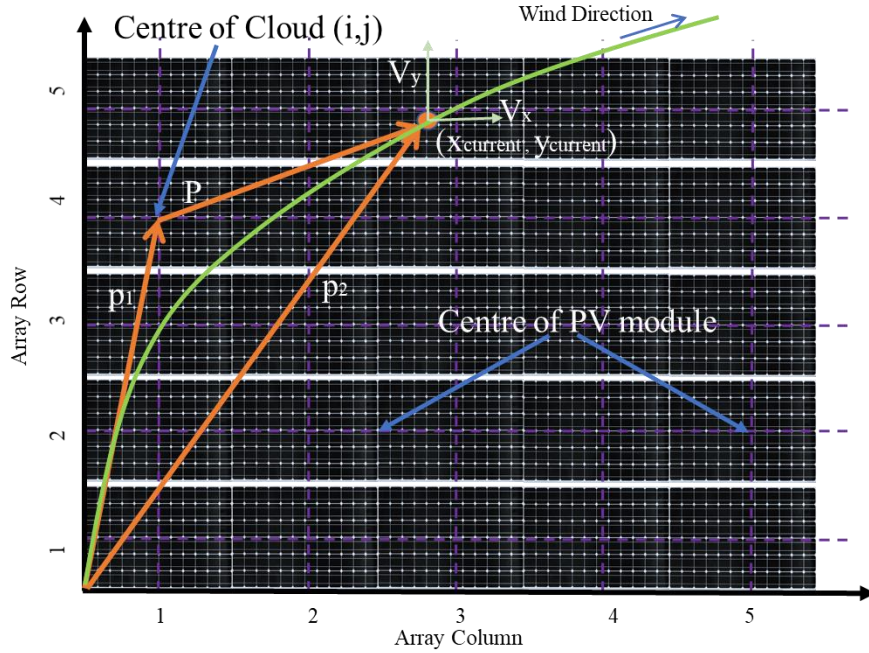


Fig. 7.3. Vector representation of shadow movement on 5x5 PV array

The position of shadow at instance t is

$$x_{current} = x + v_x t \quad (7.11)$$

$$y_{current} = y + v_y t \quad (7.12)$$

From equation (7.11) and (7.12), the magnitude of distance of shadow from the centre of the module is given below

$$\vec{P}_n = (x_{current} - i)\hat{i} + (y_{current} - j)\hat{j} \quad (7.13)$$

$$P_n = \sqrt{(x_{current} - i)^2 + (y_{current} - j)^2} \quad (7.14)$$

The effect of moving clouds on every module is modeled with respect to the change in short circuit current of that particular module [124]. The normalized values of irradiance is given by equation (7.11)

$$\frac{I_{sc}(i,j)}{I_{sc}} = 0.55 + \frac{\sin(P(i,j))}{1 + P(i,j)} \quad (7.15)$$

Fig. 7.3 represents the variation in cloud movement with time, resulting in non-uniform irradiance on the solar PV module. Moreover, this variation in movement of clouds presents four different types of shading conditions as elaborated in Fig. 7.4 (a) – (d).

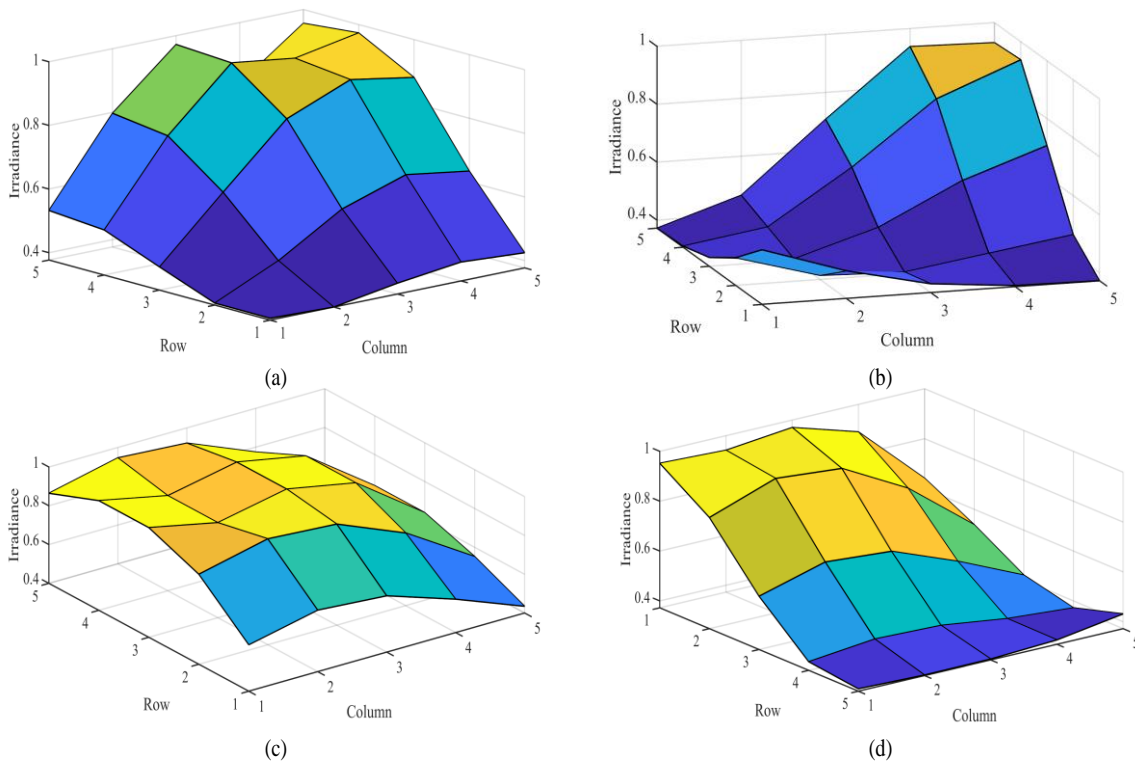


Fig. 7.4. Irregular irradiance at various instances representing different types of shade (a) short wide (b) long wide (c) short narrow (d) long narrow

7.4 GWO BASED ARRAY RECONFIGURATION METHOD

This section focuses on using grey wolf optimizer (GWO) to disperse the power losses incurred due to different PSC at different times. With the help of GWO technique a physical array reconfiguration method is implemented using row current minimization as the objective function, hence GWO based hybrid topology is proposed. The performance

of the proposed topology is compared with standard and hybrid topologies, namely, series-parallel (SP), total cross tied (TCT), BLTCT, and SuDoKu-BLTCT (SDK-BLTCT), on the basis of performance indicators, fill-factor (FF), performance ratio (PR), power enhancement (PE) and power loss. The performance indicators used for comparative analysis are power loss, FF, PR and PE.

7.4.1 Methodology

The application of intelligent meta-heuristic technique in array reconfiguration is vital because of numerous possibilities of shade dispersion. GWO is a modern nature inspired optimization technique, capable in solving complex, nonlinear stochastic problems. This algorithm uses the movement of grey wolf for encircling and targeting their prey [49] [150]. The algorithm uses randomly scattered particles in the search space known as wolves. These wolves are classified into four groups; alphas (α), betas (β), deltas (δ) and omegas (ω). Fig. 7.5 shows the movement of pack of wolves. This classification is performed on the basis of hierarchical order, where the alphas are the lead pack of wolves with least number. The betas follow the decision of the alphas, they are followed by the deltas and the remaining group of wolves are kept in omegas. The population of wolves increases from alphas to omegas. In optimization the best solution is given by the alphas (best position) and the entire pack is driven by them. The major benefit of implementing GWO based array reconfiguration are 1) method effectively converges to the best combination for varying conditions, 2) algorithm is robust and efficient, 3) probability of converging to local MPP is reduced, 4) speed of convergence is high.

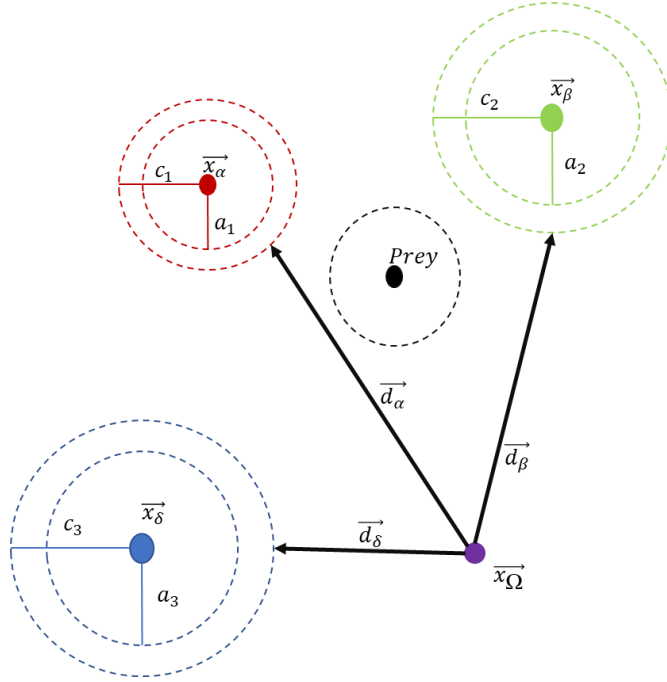


Fig. 7.5. Position update of wolves in GWO

The proposed GWO-AR method involves following steps as given in Fig. 7.6. This method consists of four different phases: a) initialization phase, b) evaluation phase, c) reconfiguration and d) termination phase.

- a. *Initialization phase*: In this phase initialization of the PV array size, coefficient vectors for GWO algorithm is done. Where, q are linearly decreased from 2 to 0 over the course of iterations and r_1, r_2 are random vectors in $[0,1]$.

$$a = 2q \cdot \vec{r}_1 - q \quad (7.16)$$

$$c = 2 \cdot \vec{r}_2 \quad (7.17)$$

The initial values of wolves are done using (7.18) - (7.19) function and moreover pack of them are formed.

$$\vec{D}_\alpha = |c \cdot \vec{X}_\alpha - \vec{X}(t)|; \quad \vec{D}_\beta = |c \cdot \vec{X}_\beta - \vec{X}(t)|; \quad \vec{D}_\delta = |c \cdot \vec{X}_\delta - \vec{X}(t)| \quad (7.18)$$

$$\vec{X}_1 = \vec{X}_\alpha - a \cdot \vec{D}_\alpha; \quad \vec{X}_2 = \vec{X}_\beta - a \cdot \vec{D}_\beta; \quad \vec{X}_3 = \vec{X}_\delta - a \cdot \vec{D}_\delta \quad (7.19)$$

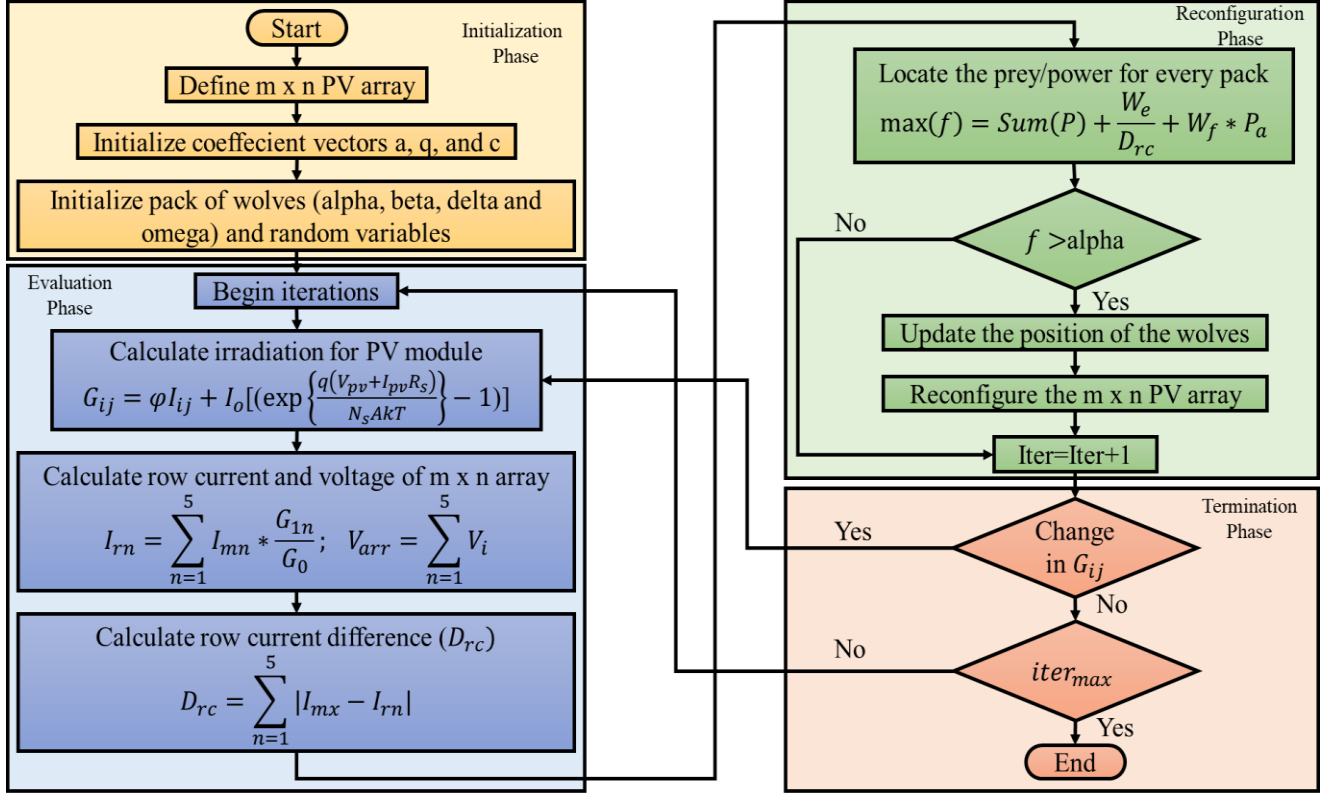


Fig. 7.6. Flowchart for grey wolf optimizer array reconfiguration (GWO-AR)

$\vec{X}_\alpha, \vec{X}_\beta, \vec{X}_\delta$ are the position vectors of alpha, beta and delta respectively. $\vec{D}_\alpha, \vec{D}_\beta, \vec{D}_\delta$ defines the encircling behavior of alpha, beta and delta respectively. The below equation defines the updated position vector of the wolf.

$$\vec{X}(t+1) = \frac{\vec{X}_1 + \vec{X}_2 + \vec{X}_3}{3} \quad (7.20)$$

- b. *Evaluation phase*: Irradiance (G_{ij}) for every module of the PV array is computed. Here i, j corresponds to row and column number. Then, row current (I_{rn}) and array voltage

(V_{arr}) is calculated. The objective function for the designed algorithm is row current difference (D_{rc}) as this should be minimum.

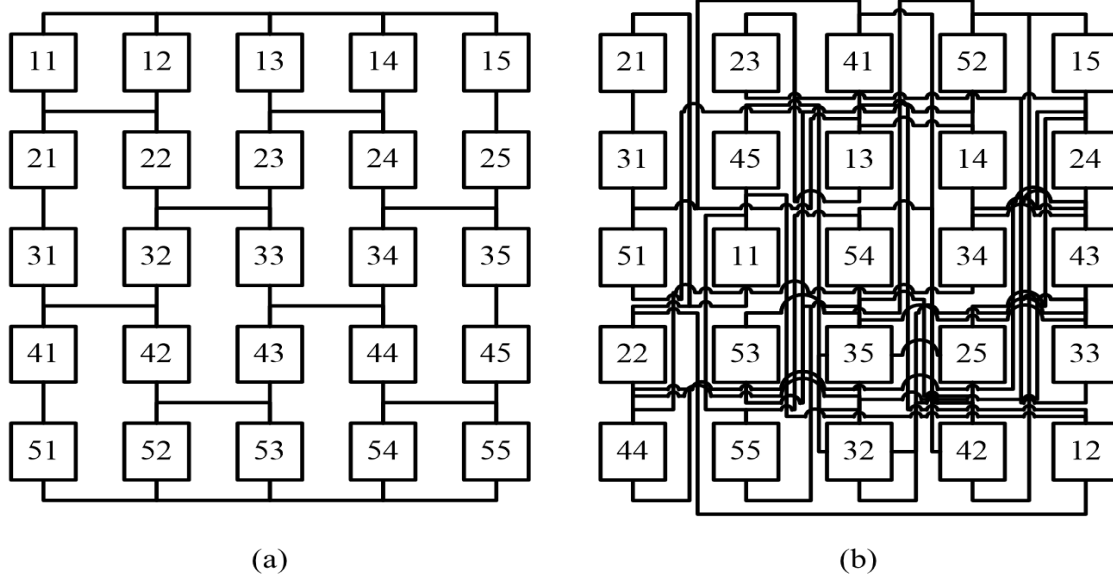


Fig. 7.7. (a) BL TCT configuration (b) Proposed BLTCT reconfiguration using GWO

- c. *Reconfiguration Phase:* Based on D_{rc} , I_{rn} and V_{arr} function f is computed [116]. Here, P_a is the panel output power. It is to be noted that as the objective function reduces the power output of the PV system increases. By trial-and-error method the value of W_e and W_f is observed to be 8 and 6 respectively. The updated position of the wolves is given by (7.22).

$$\vec{D}_i = |c \cdot \vec{X}_p(t) - \vec{X}(t)| \quad (7.21)$$

$$\vec{X}_i(t+1) = \vec{X}_p(t) - a \cdot \vec{D} \quad (7.22)$$

- d. *Termination Phase:* This stage checks for change in irradiance (presence of shade) and also evaluated the termination criteria i.e., the maximum iterations. If these conditions are not met then the whole process is reinitiated until the optimal results are obtained.

The GWO algorithm is implemented on the bridge linked total cross tied (BLTCT) configuration for the different shading conditions. This results in a physical relocation of modules in optimal pattern resulting in GWO-BLTCT configuration. Fig. 7.7(a) and 7.7(b) represents the BLTCT and optimal GWO-BLTCT configuration of 5x5 PV array for PSC. Table 7.1 represents the performance of designed configuration with the standard BLTCT configuration for current, voltage and power calculations.

Table 7.1. Current, voltage and power calculation of BLTCT and GWO-BLTCT for different shading patterns

Shading Condition	BLTCT			GWO BLTCT		
	I_{R}^{BL} (A)	V (V)	P (W)	I_{R}^{GWO} (A)	V (V)	P (W)
LN	I_{R5}^{BL} 2.5877 I_m	V_m	2.588 P_m	I_{R5}^{GWO} 2.9837 I_m	V_m	2.984 P_m
	I_{R4}^{BL} 4.1241 I_m	2 V_m	8.248 P_m	I_{R2}^{GWO} 3.0187 I_m	2 V_m	6.037 P_m
	I_{R2}^{BL} 2.7202 I_m	3 V_m	8.161 P_m	I_{R3}^{GWO} 3.1015 I_m	3 V_m	9.305 P_m
	I_{R3}^{BL} 3.4741 I_m	4 V_m	13.896 P_m	I_{R4}^{GWO} 3.1134 I_m	4 V_m	12.454 P_m
	I_{R1}^{BL} 3.0181 I_m	5 V_m	15.091 P_m	I_{R1}^{GWO} 3.2891 I_m	5 V_m	16.446 P_m
LW	I_{R4}^{BL} 2.1795 I_m	V_m	2.180 P_m	I_{R5}^{GWO} 3.2149 I_m	V_m	3.215 P_m
	I_{R5}^{BL} 2.1185 I_m	2 V_m	4.236 P_m	I_{R1}^{GWO} 3.4312 I_m	2 V_m	6.863 P_m
	I_{R2}^{BL} 3.9595 I_m	3 V_m	11.879 P_m	I_{R2}^{GWO} 3.5211 I_m	3 V_m	10.563 P_m
	I_{R1}^{BL} 3.1651 I_m	4 V_m	12.660 P_m	I_{R3}^{GWO} 3.6674 I_m	4 V_m	14.670 P_m
	I_{R3}^{BL} 3.4127 I_m	5 V_m	17.064 P_m	I_{R4}^{GWO} 3.7561 I_m	5 V_m	18.781 P_m
SW	I_{R5}^{BL} 2.5202 I_m	V_m	2.520 P_m	I_{R1}^{GWO} 4.2149 I_m	V_m	4.2149 P_m
	I_{R4}^{BL} 3.6292 I_m	2 V_m	7.258 P_m	I_{R3}^{GWO} 4.4123 I_m	2 V_m	4.4123 P_m
	I_{R3}^{BL} 4.4472 I_m	3 V_m	13.342 P_m	I_{R2}^{GWO} 4.7745 I_m	3 V_m	14.324 P_m
	I_{R2}^{BL} 4.9451 I_m	4 V_m	19.780 P_m	I_{R5}^{GWO} 4.7931 I_m	4 V_m	19.172 P_m
	I_{R1}^{BL} 4.4863 I_m	5 V_m	22.432 P_m	I_{R4}^{GWO} 4.8451 I_m	5 V_m	24.226 P_m
SN	I_{R5}^{BL} 3.0543 I_m	V_m	3.054 P_m	I_{R4}^{GWO} 4.1312 I_m	V_m	4.131 P_m
	I_{R4}^{BL} 4.8588 I_m	2 V_m	9.616 P_m	I_{R1}^{GWO} 4.3171 I_m	2 V_m	8.634 P_m
	I_{R2}^{BL} 4.3513 I_m	3 V_m	13.054 P_m	I_{R2}^{GWO} 4.5078 I_m	3 V_m	13.523 P_m
	I_{R3}^{BL} 4.3513 I_m	4 V_m	17.404 P_m	I_{R3}^{GWO} 4.6122 I_m	4 V_m	18.449 P_m
	I_{R1}^{BL} 4.0588 I_m	5 V_m	20.294 P_m	I_{R5}^{GWO} 4.7409 I_m	5 V_m	23.704 P_m

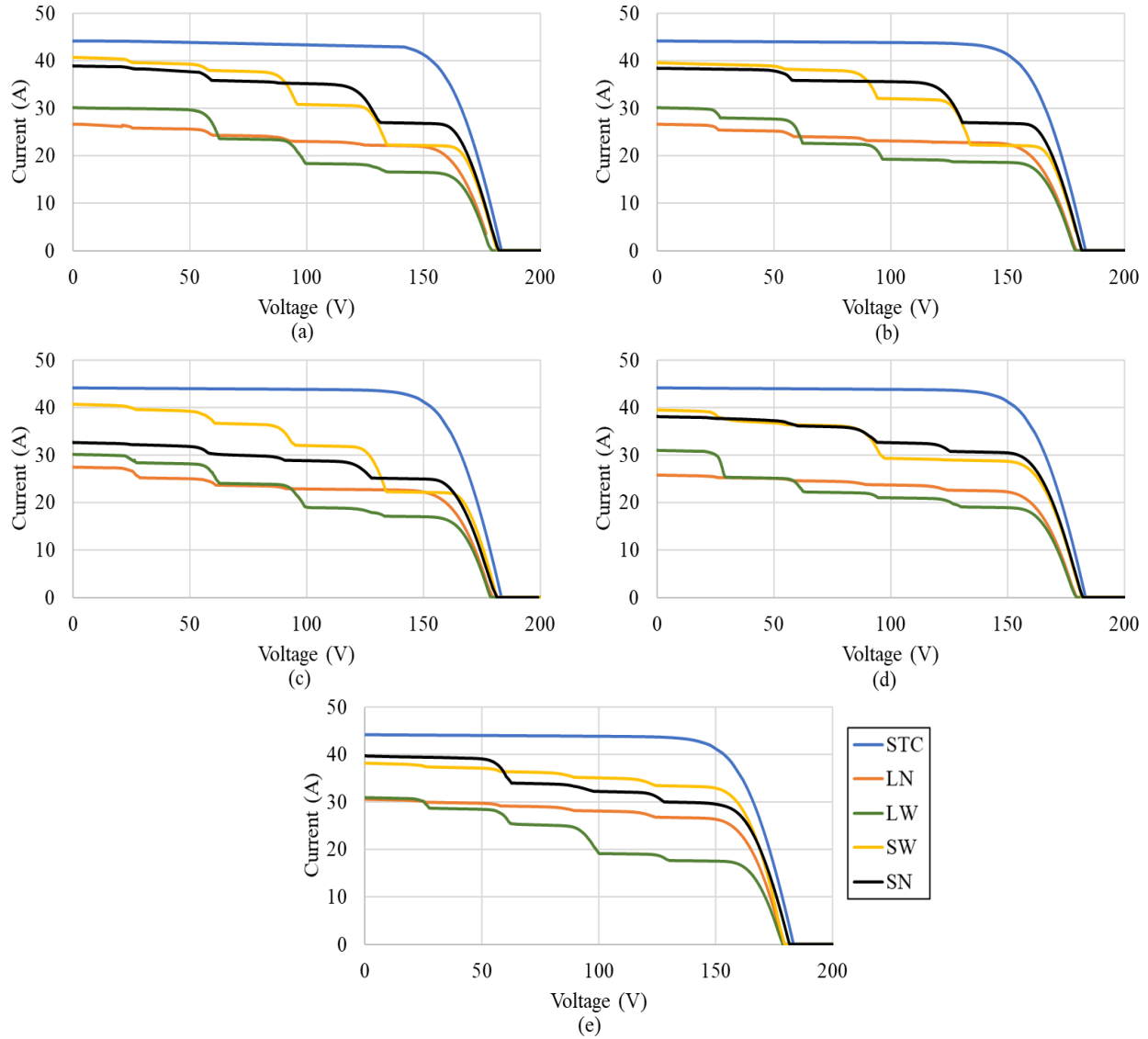


Fig. 7.8. I-V curves at different shading conditions for various configurations (a) SP (b) TCT (c) BL-TCT (d) SDK BL-TCT (e) GWO BL-TCT

7.4.2 Results and Discussions

The performance of the various configurations namely, Series-Parallel (SP), Total Cross Tied (TCT), Bridge Linked TCT (BLTCT), SuDoKu (SDK) BLTCT and GWO-BLTCT is evaluated at four different shading conditions. These shading conditions define the movement of clouds and different type of shadows LN, LW, SW and SN on the 5 x 5

PV array configuration. The I-V and P-V curves are given for each configuration in Fig. 7.8 and Fig. 7.9 respectively. In both Fig. 7.8 and Fig. 7.9, (a) represents SP, (b) represents TCT, (c), (d) and (e) depicts BLTCT, SDK BLTCT and GWO-BLTCT respectively. The focus of this paper is to increase the power of the PV array in partial shading conditions with incorporating the movement of clouds.

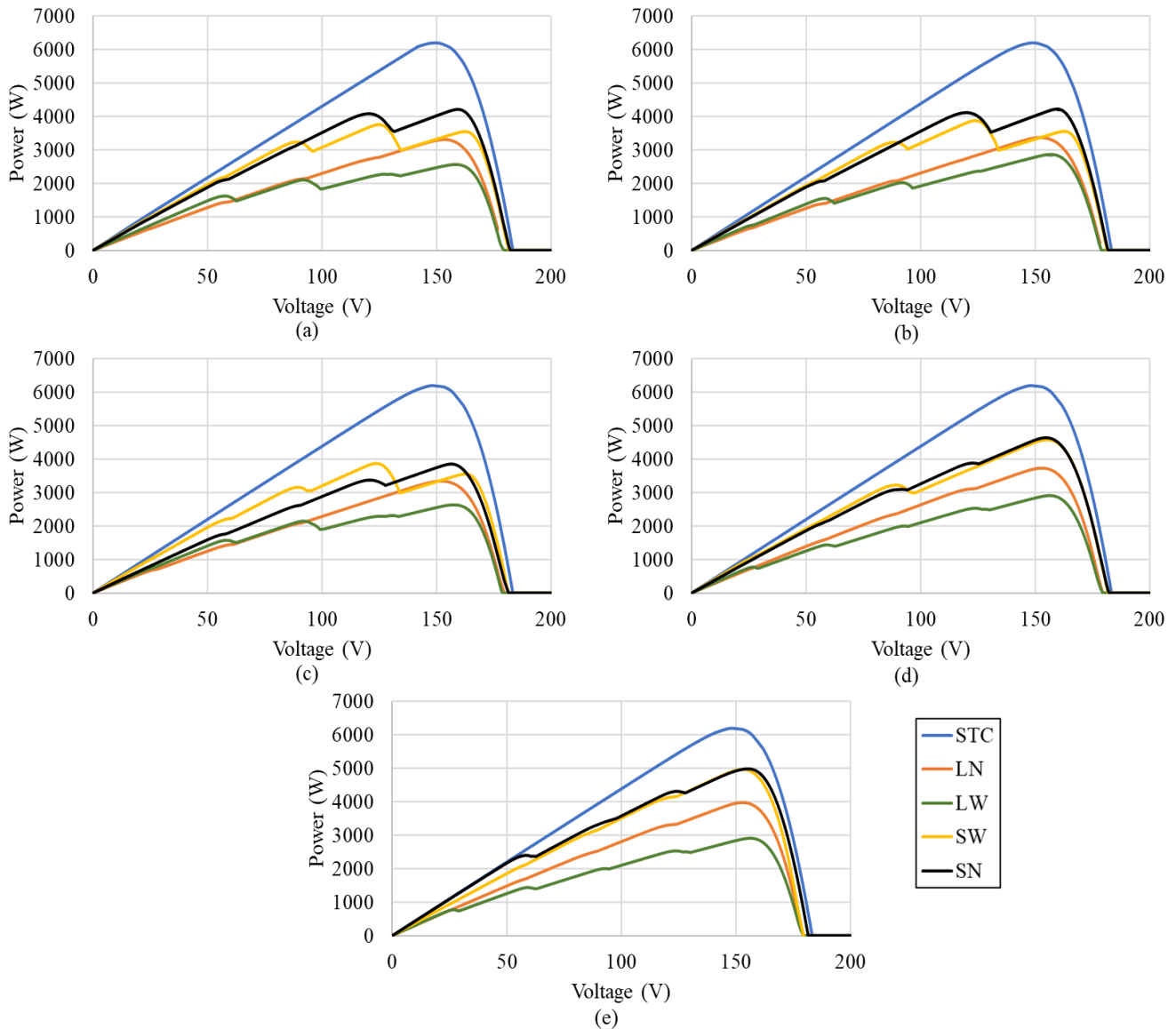


Fig. 7.9. P-V curves at different shading conditions for various configurations (a) SP (b) TCT (c) BL-TCT (d) SDK BL-TCT (e) GWO BL-TCT

The comparison of achieved global maximum power point by the different PV array configurations in the varying shading conditions is given by Fig. 7.10 (a), (b), (c) and (d). Table 7.2 shows the global maximum power point of different types of PV arrays in different shading conditions.

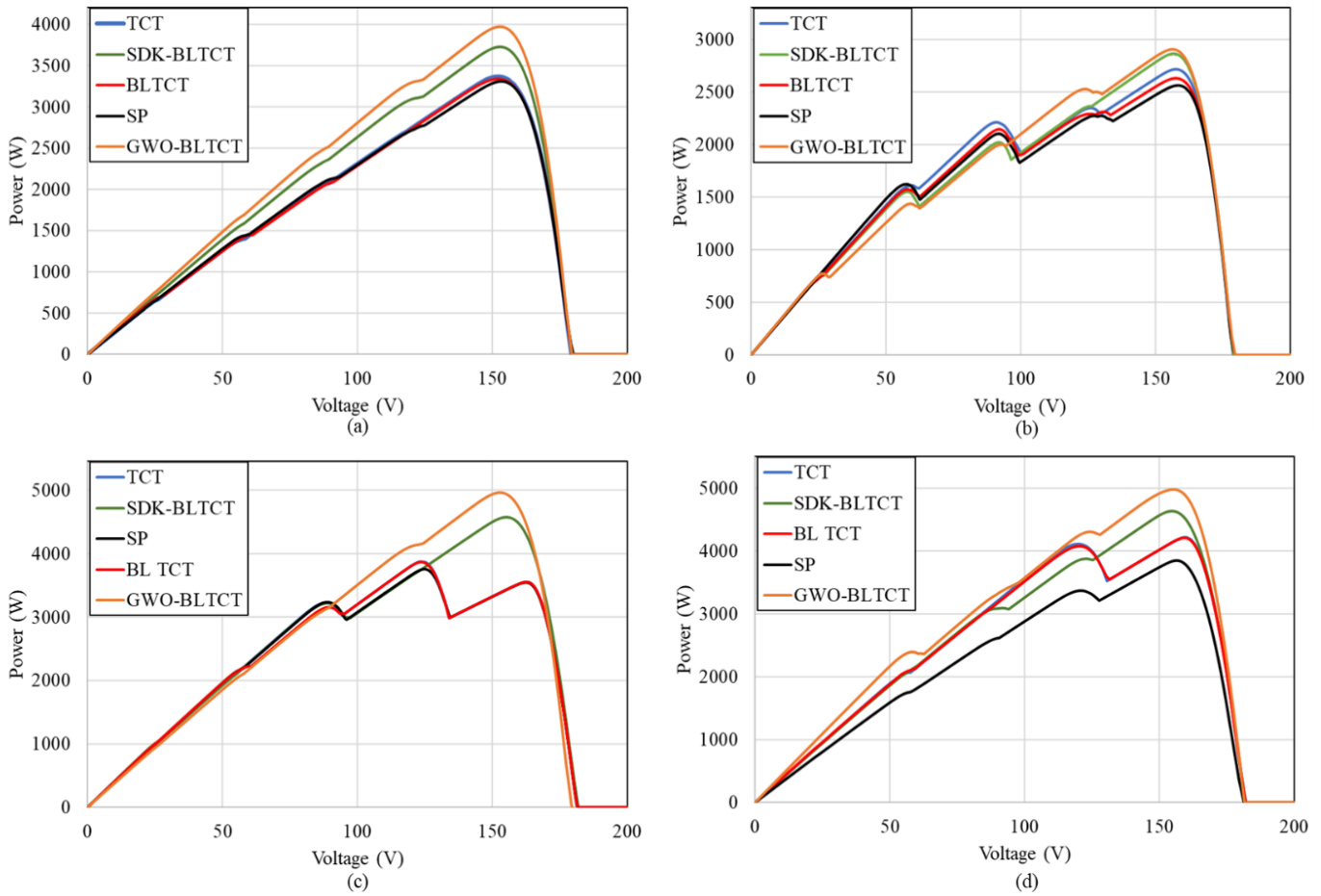


Fig. 7.10. Effect of different shade due to movement of cloud on the PV array (a) LN (b) LW (c) SW and (d) SN

Table 7.2. GMPP at different shading conditions at 25°C

Configurations	Global Maximum Power Point (W)			
	LN	LW	SW	SN
SP	3308.71	2563.16	3754.20	3848.51
TCT	3367.33	2864.67	3873.38	4208.90
BLTCT	3387.37	2629.98	3865.39	4219.19
SDK-BLTCT	3727.01	2895.45	4572.25	4634.51
GWO-BLTCT	3971.68	2905.87	4960.41	4977.97

Table 7.2 helps in identifying the topology in which maximum power can be extracted for the LN, LW, SW and SN shading pattern. In LN, SN and SW partial shade the proposed GWO-BLTCT topology produces the best global maximum power point. Furthermore, during LW shading GWO-BLTCT is better than SDK-BLTCT but the difference of 10.42 W is nominal and can be ignored when considering the significant advantage in GMPP in LN, SN, and SW shading pattern. From Table 7.2 and Fig. 7.10(c) and Fig. 7.10(d) it is evident that performance of TCT and BLTCT is closely matched in SW and SN types of shades.

Power enhancement (PE) is calculated for all the topologies with respect to the SP configuration, and is calculated using

$$PE = \frac{GMPP_{TCT|BLTCT|SDK|GWO} - GMPP_{SP}}{GMPP_{SP}} * 100 \quad (7.23)$$

Here, $GMPP_{SP}$ is the global maximum power point achieved by SP configuration, and $GMPP_{TCT|BLTCT|SDK|GWO}$ is the global maximum power point achieved by TCT, BLTCT, SDK-BLTCT or GWO-BLTCT configuration.

Table 7.3. Performance of the PV array in partial shading conditions due to cloud movement at different instances

Configuration	Performance Indicator	LN	LW	SW	SN
SP	MMPL (W)	2875.66	3621.21	2430.17	2343.43
	PR (%)	53.50	41.45	60.71	62.16
	FF	0.41	0.32	0.46	0.47
	PE (%)	Nil	Nil	Nil	Nil
TCT	MMPL (W)	2827.50	3561.96	2321.45	1975.64
	PR (%)	54.36	46.25	62.53	68.12
	FF	0.41	0.35	0.48	0.52
	PE (%)	1.80	11.77	3.18	9.65
BLTCT	MMPL (W)	2854.57	3330.16	2326.55	1975.47
	PR (%)	53.91	42.48	62.44	68.06
	FF	0.41	0.32	0.48	0.52
	PE (%)	2.41	2.61	2.97	9.38
SDK-BLTCT	MMPL (W)	2464.93	3286.07	1619.69	1557.43
	PR (%)	60.20	46.26	73.85	74.86
	FF	0.46	0.36	0.56	0.57
	PE (%)	12.70	12.91	21.80	20.44
GWO-BLTCT	MMPL (W)	2028.32	3104.55	1039.59	1022.03
	PR (%)	66.19	48.94	82.67	82.97
	FF	0.49	0.36	0.61	0.61
	PE (%)	20.11	13.27	32.14	29.37

From Table 7.3, it is observed that the LW type of shade due to wind speed and cloud movement is the most challenging type of shade as the performance of all the topology is most hampered during it. The best performing topologies during this instance is proposed GWO-BLTCT and is closely matched by SDK-BLTCT. The performance ratio is also least (<50%) for the LW shade for all the topologies, whereas for all the other type



Fig. 7.11. Performance indices (a) Power Loss (b) Fill-Factor (c) PR (d) PE

of shades LN, SW, and SN, performance ratio is high i.e., more than 50%. Among them SN type of shade is the least shaded. The developed GWO-BLTCT type of configuration is the best performing configuration for LN, SN and SW type of shade. Power enhancement of 20.11%, 32.14%, and 29.37% is achieved for LN, SN and SW respectively, being the highest among the rest of the topologies. Fig. 7.11 represents the performance indicators of all the above topologies for different type of shades. Fig. 7.11(a) shows the MMPL, Fig. 7.11(b) depicts the fill factor, Fig. 7.11(c) and Fig. 7.11(d) plots PR and PE respectively for the four shading conditions.

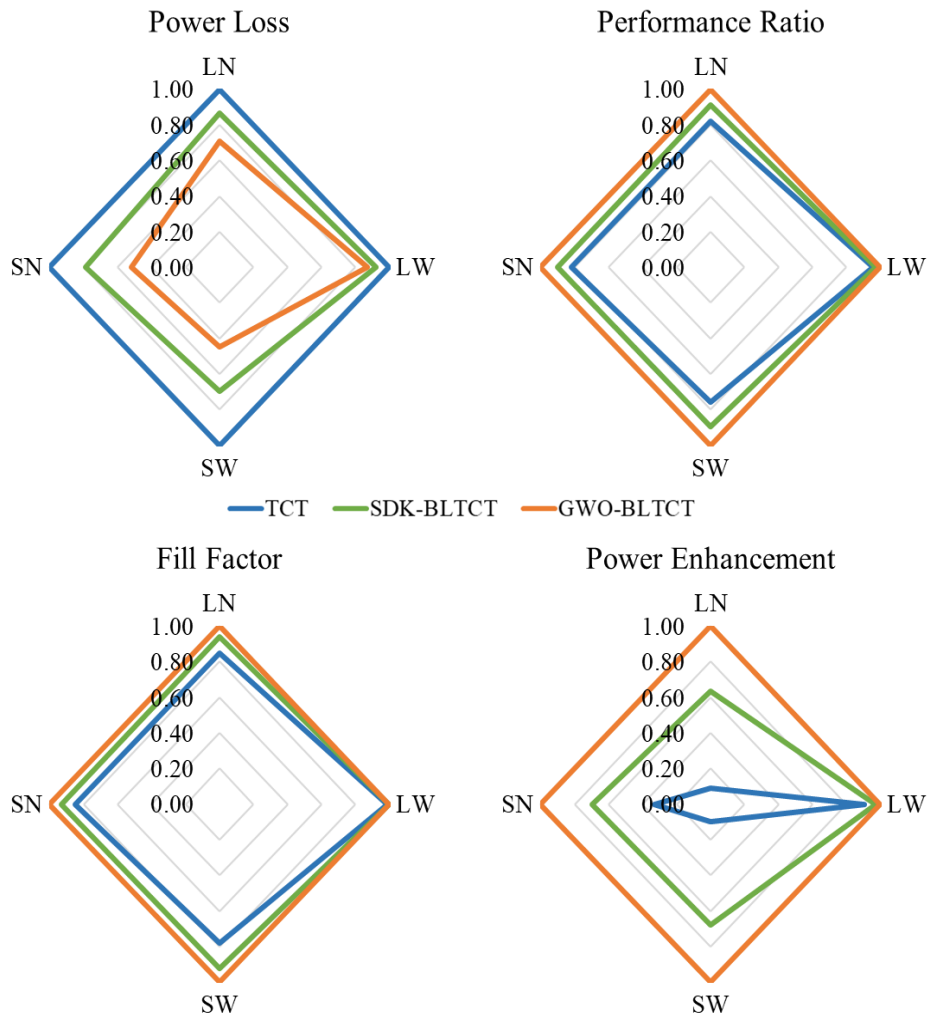


Fig. 7.12. Radar plot representing the performance indicators for different topologies

Fig. 7.12 represent a radar plot for TCT, SDK-BLTCT and GWO-BLTCT for different shading conditions i.e. SW, SN, LW and LN. From Fig. 7.12 it is observed that TCT and SDK-BLTCT are compared on the basis of different performance indicators with respect to that of the designed configuration GWO-BLTCT configurations. Power loss component is highest for TCT and least for GWO-BLTCT. Here, 1 represents the maximum value among the three and rest values have been calculated in accordance to that. GWO-BLTCT has highest FF, PE and PR for varying shading conditions.

7.5 ANFIS BASED MPPT CONTROLLER FOR SPV SYSTEM

The maximum power point tracking controller is an integral part for efficient implementation of PV system. In this paper, an adaptive neuro fuzzy inference system (ANFIS) based new algorithm for maximum power point tracking (MPPT) has been developed and implemented to track maximum power point in the standalone photovoltaic system (PV). In this section the developed work controls the switching of DC-DC boost converter using ANFIS approach and replace the conventional PI controller to detect the error signal. The results of the designed approach are compared with incremental conductance approach under constant and varying irradiance and temperature conditions. From the developed approach, the percentage error, rise time and voltage fluctuations have been improved as compared to the incremental conductance method. Further, the adaptive controller effectively tracks the MPP considering all the major non-linear variables and it improves the rise time and the steady state characteristics of the PV system. The block diagram of the PV system with MPPT is presented in Fig. 7.13.

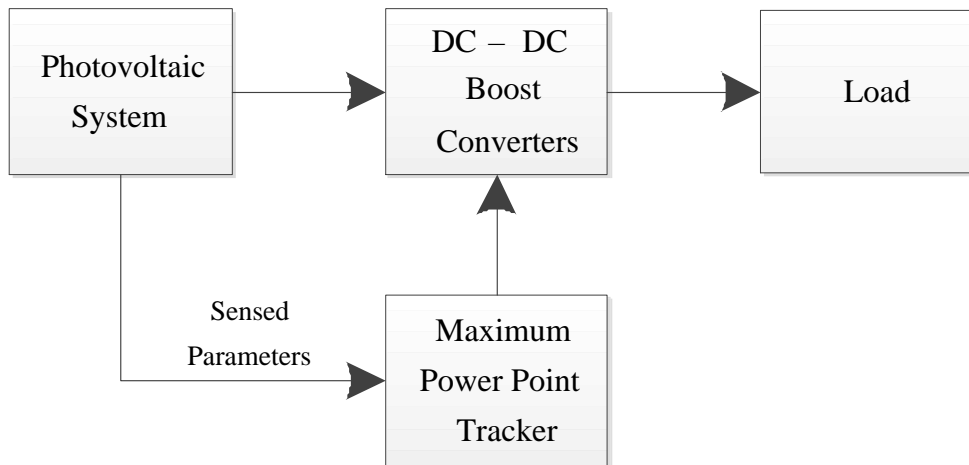


Fig. 7.13. Block diagram of SPV system with MPPT controller

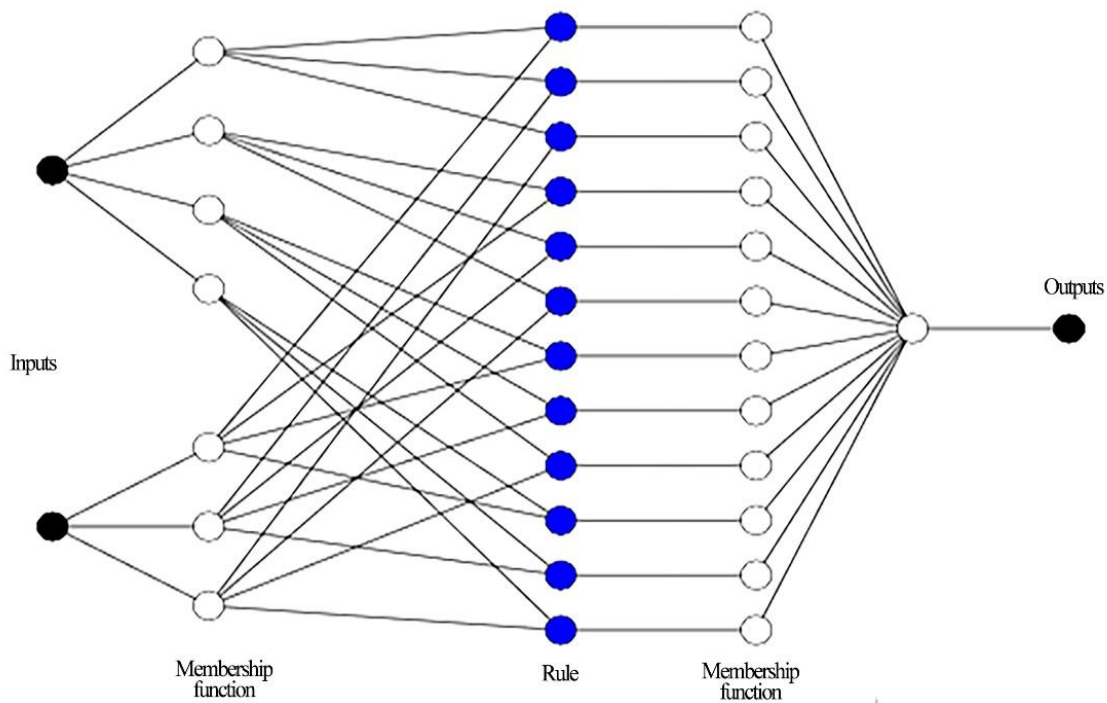


Fig. 7.14. Structure of the ANFIS based MPPT controller

7.5.1 ANFIS model

ANFIS is a hybrid intelligent system, which combines fuzzy systems with neural networks. To test the proposed control scheme, MATLAB simulink model of the solar photovoltaic standalone system was tested at STC conditions i.e., 25°C and 1000 W/m²

and at changing temperature and changing irradiance. By varying these variables, a large amount of data was generated which helped in training the ANFIS controller for tracking maximum power point. The ANFIS toolbox has been used to develop the controller. The developed ANFIS based MPPT controller comprises of a five-layer network as shown in the Fig. 7.14.

The ANFIS controller is trained using the data of INC controller. The developed MPPT algorithm was trained with 4500 pairs of data. It was observed that combination of Gaussian bell function along with triangular membership function was best suited for the controller. This generates membership functions for dI/dV and I/V which are shown in Fig. 3 and Fig. 4 respectively. The data collected for the training of the neurons in ANFIS was from the INC controller with integral regulator function. The two input variables considered for the designed controller are a) dI/dV (incremental conductance) and, b) I/V (conductance). The backpropagation algorithm for the learning of the neurons has been used. The Fig. 7.15 and Fig. 7.16 represent fuzzy subsets membership function generated after the training stage in MATLAB toolbox.

The four membership functions have been considered for incremental conductance. The membership functions include NH (negative high), NM (negative medium), PM (positive medium) and PH (positive high). In the same way, three membership functions for conductance are Z (zero), M (medium) and P (positive) are considered. To generate FIS for the above system, grid partitioning technique has been incorporated. Fig. 7.17 represents the surface plot of the designed controller. It shows the relationship between the inputs and the output of the developed system.

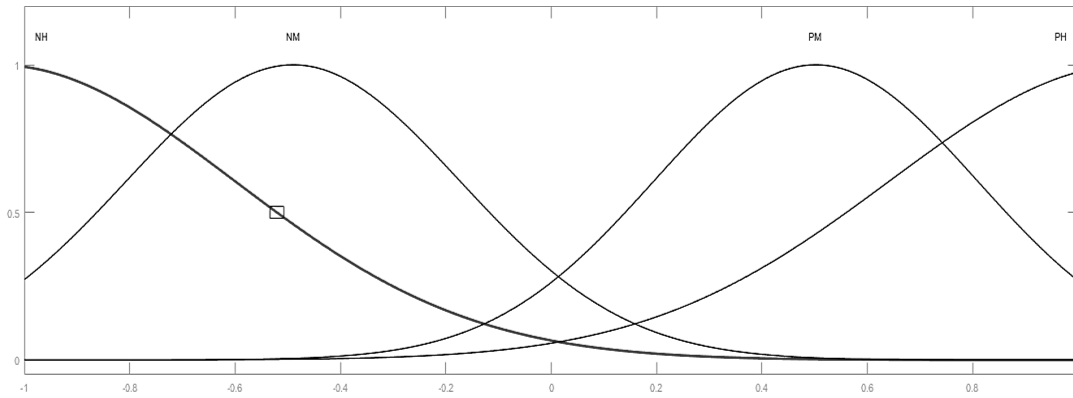


Fig. 7.15. Fuzzy subsets membership function for dI/dV

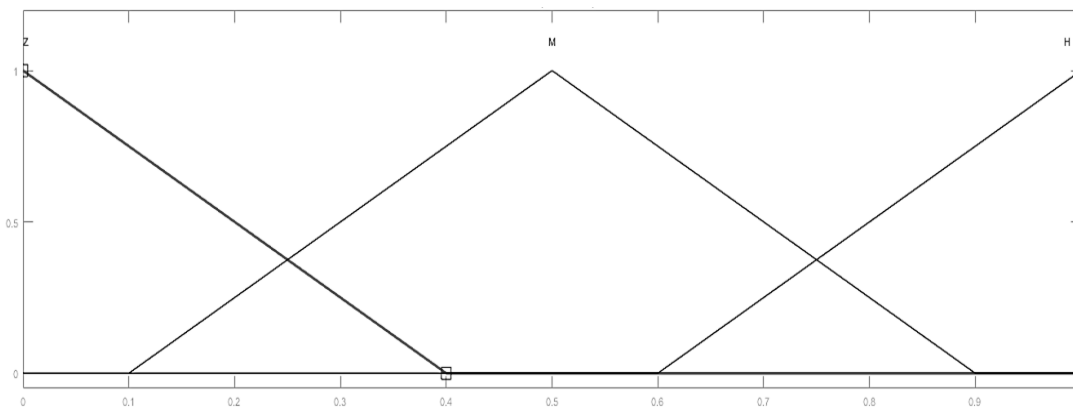


Fig. 7.16. Fuzzy subsets membership function for I/V

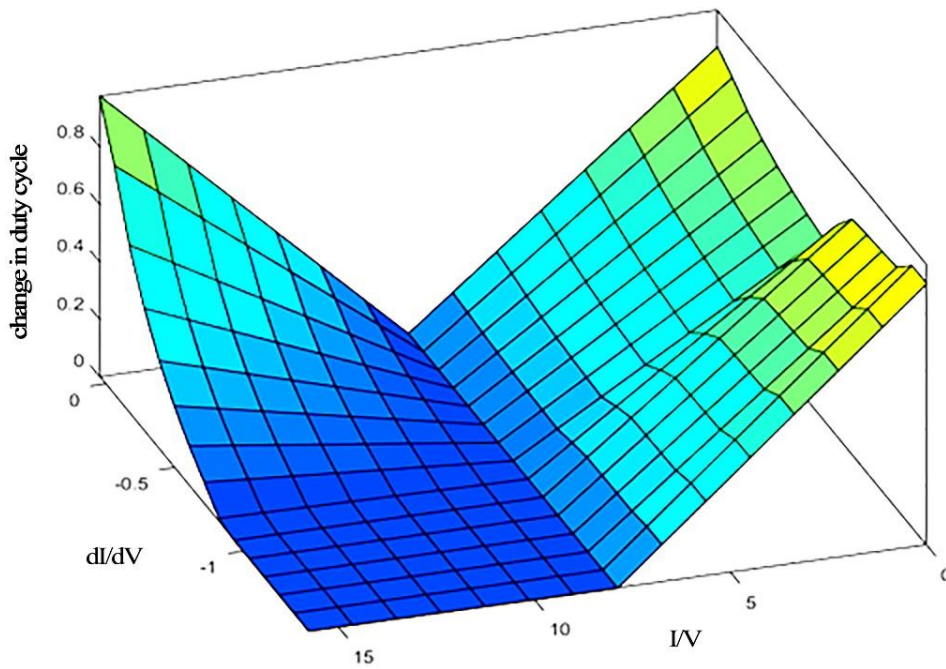


Fig. 7.17. Variation of duty cycle with respect to the inputs

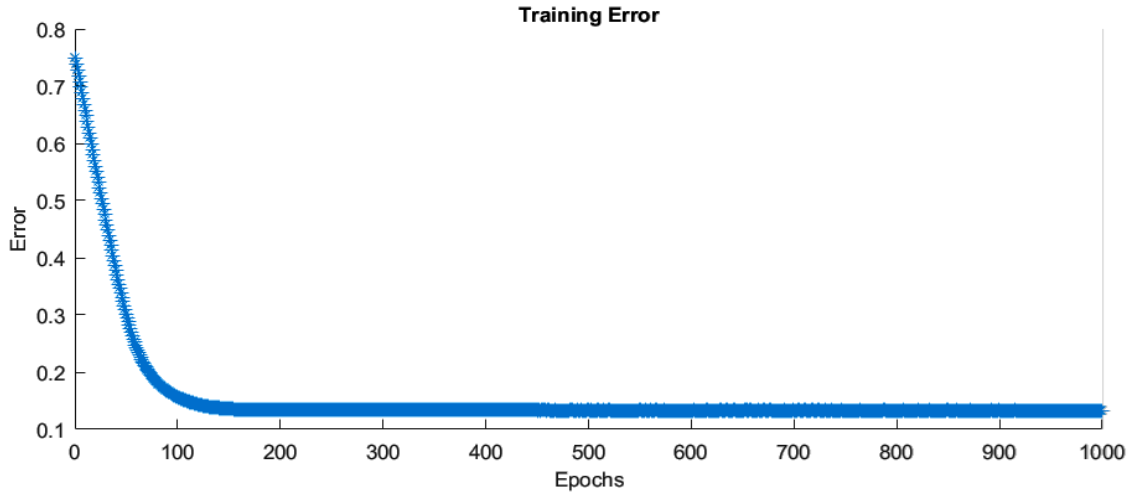


Fig. 7.18. Training performance of the designed controller

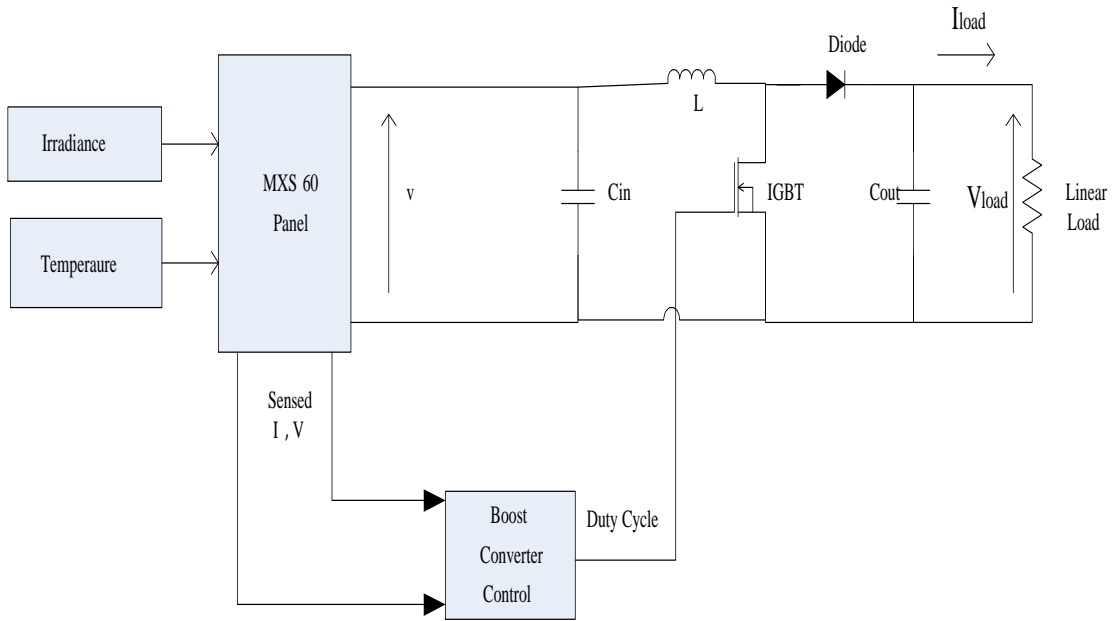


Fig. 7.19. ANFIS based MPPT controller for PV systems

In this work, the number of epochs was varied from 30 to 1000 for the training of ANFIS controller and training error was observed for all epochs. It was observed that the training error was decreased with increase in the number of epochs and was found to be constant at 0.13314 when epochs are varied from 200 to 1000. The variation of error vs epochs is projected in Fig. 7.18.

The proposed ANFIS controller comprises of 43 nodes with 12 linear parameters and 21 non-linear parameters defined by the 4500 datasets for training. The developed controller is formed using 12 fuzzy rules to track maximum power point for a standalone PV system. Further, the ANFIS based MPPT controller is presented in Fig. 7.19. The parameters for DC-DC boost converter are presented in Table 7.4.

Table 7.4. Parameter specification of DC-DC boost converter

Parameters	Variable	Value
Input Capacitance	C_{in}	10^{-6} F
Inductance	L	6.667×10^{-3} H
Output Capacitance	C_{out}	1100×10^{-6} F
Max. output ripple voltage	V_{mo}	50 V
Max. ripple current	I_{mo}	1.5 A
Switching Frequency	f_s	25kHz

7.5.2 Results and Discussion

The performance of the PV system was evaluated on Standard Testing Conditions (STC) and varying solar irradiance and temperature as these parameters affect the performance of the PV system significantly.

Fig. 7.20 shows the performance of the PV system using the designed controller at STC. This controller extracts 57.58 W of power from the 60 Wp photovoltaic module. The load current observed is 1.17 A with 48.6 V of potential developed across it. The rise time (t_r) is 0.085 s for ANFIS controller. Further, the performance of the system was compared with incremental conductance controller to validate the results. The power output and rise time using INC were found 52.2 W and 0.857 s respectively.

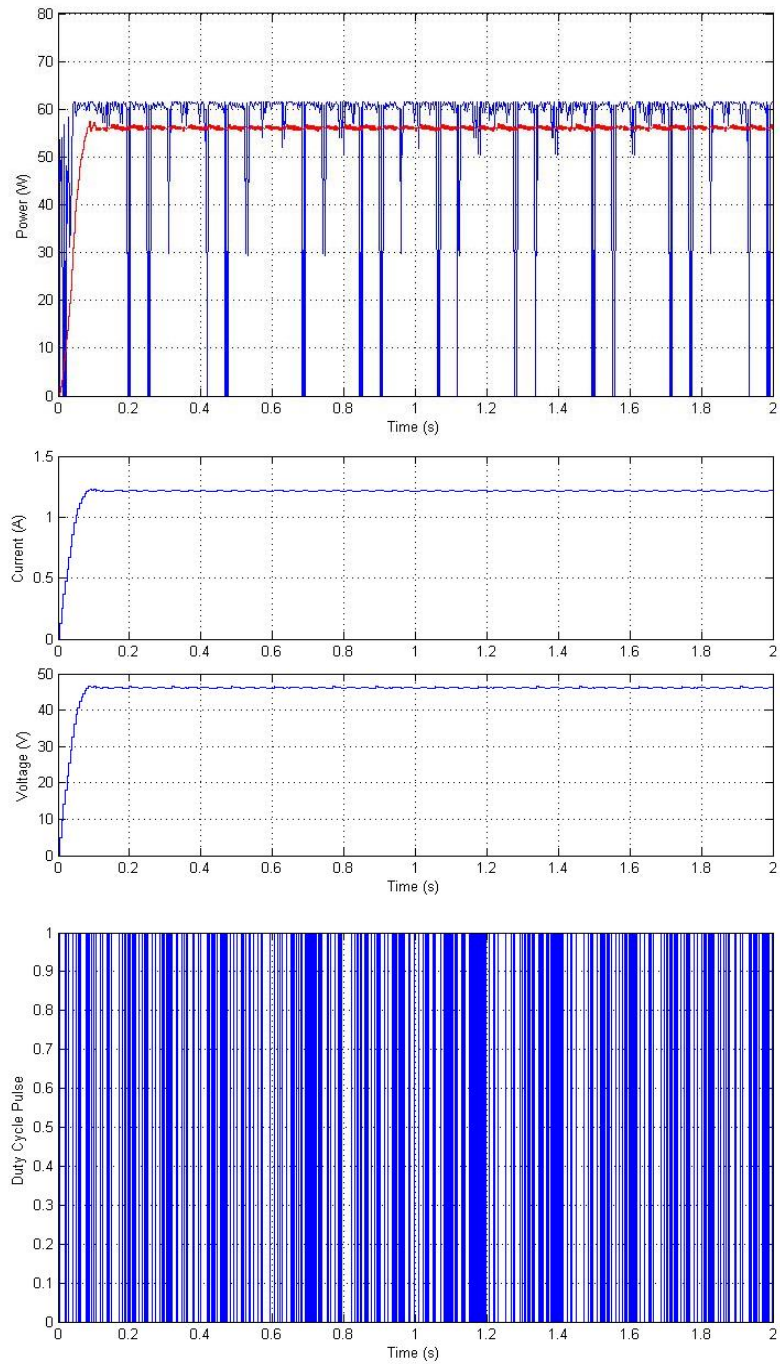


Fig. 7.20. Performance of the ANFIS controller at constant irradiance and temperature

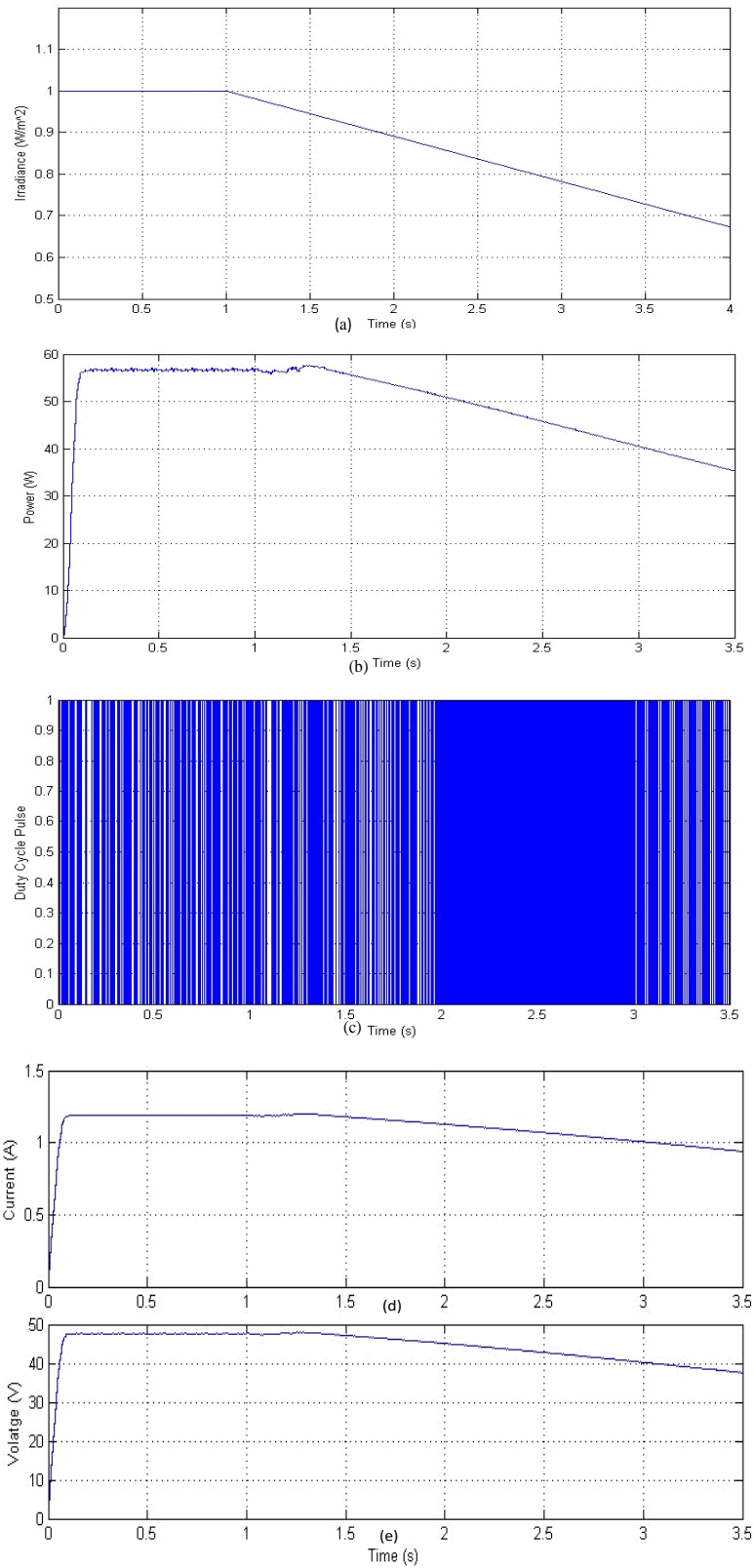


Fig. 7. 21. Performance of the ANFIS controller at varying irradiance and constant temperature

Fig. 7.21(a) shows the change in the irradiance level at various time intervals. Irradiance (G_{rr}) is 1000 W/m^2 till 1sec and then varies according to the eq. (7.24). Fig. 7.21 (b), 7.21(c), 7.21(d), and 7.21(e) depicts the maximum power output at changing irradiance, gating pulses, load current, voltage output respectively.

$$G_{rr} = 1000 - 9t \quad (7.24)$$

The gradual decrease in irradiance levels produces constantly decreasing power with no voltage and current ripples thus tracking the power effectively. The steady state output of the system is ripple free. The designed ANFIS MPPT is a better tracking algorithm, which can be observed from the above results in changing solar irradiance condition.

Fig. 7.22 shows the response of the developed adaptive controller for PV system when the two major environmental conditions change, simultaneously, the performance of the system at varying irradiance and temperature is presented in Fig. 7.22(a) and Fig. 7.22(b) respectively.

$$T_1 = 25; \text{ when } 0 \leq t \leq 1 \text{ s} \quad (7.25)$$

$$T_1 = 25 + 10t; \text{ when } 1 \leq t \leq 4 \text{ s} \quad (7.26)$$

Where, T_1 = Module Operating temperature in $^{\circ}\text{C}$ and t = time in seconds

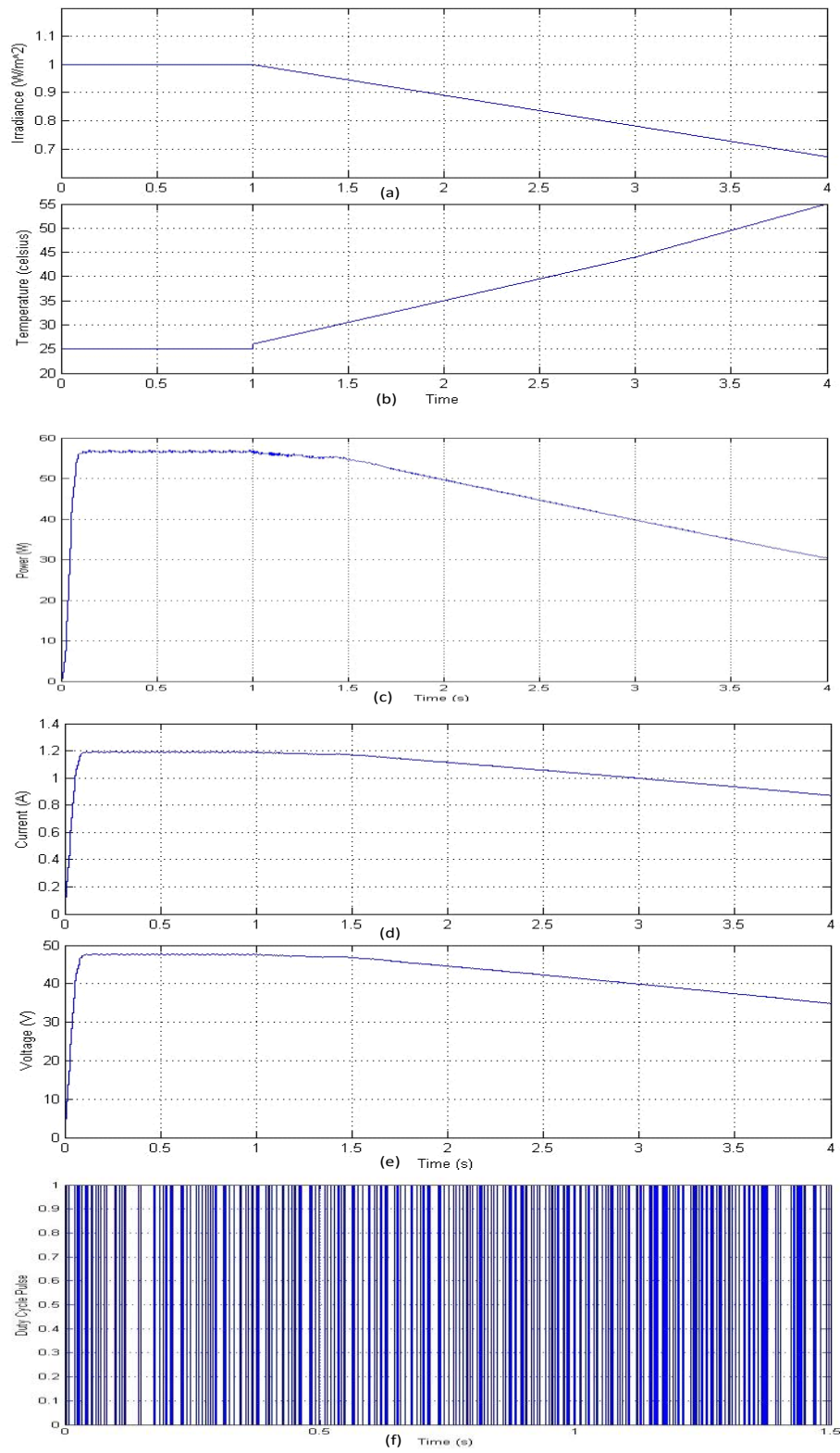


Fig. 7.22. Performance of the ANFIS controller at constant irradiance and varying temperature

In the above Fig. 7.22, the power tracked on the load side, load current and output voltage with gating pulses to the switching device i.e. MOSFET, are shown in Fig. 7.22(c), 7.22(d), 7.22(e) and 7.22(f) respectively.

From Fig. 7.22(c), it is observed that output power of the proposed controller is 30.6 W at the irradiance of 670 W/m² and temperature of 55°C. It is also observed that there are no voltage fluctuations i.e. the tracking characteristics are smooth. However, under same conditions, the power output using INC controller is 20.2 W and it results in a significant power loss. Also, the voltage fluctuations are observed to be 3.5 V to 6.5 V. Table 7.5 shows the comparison of the developed ANFIS MPPT controller against INC at STC and varying solar irradiance and temperature.

Table 7.5. Comparison of developed ANFIS with INC MPPT

Performance Parameter	Maximum Power Point Algorithm	
	<i>ANFIS</i>	<i>INC</i>
Error % (e_{ss})	4.03%	13%
Rise Time (t_r)	0.085 s	0.857 s
Voltage Fluctuations	Not present	3.5 V-6.5 V
Tracking characteristics at low irradiance	Smooth tracking curve for maximum power.	Oscillatory in nature
	Better performance under changing conditions.	Significant power loss at prolonged low irradiance.

The proposed adaptive controller for tracking maximum power has advantages over the traditional MPPT controllers. The response time of the PV system to track MPP reduces significantly by 0.765 s. The steady state performance of ANFIS MPPT is oscillation free

as no voltage and current ripples are present on the load side. The tracking performance of MPP also improves, especially during low irradiance and high cell temperature conditions. The steady state error for the developed ANFIS MPPT reduces to 4.03%. Hence, the designed controller performs efficiently to track the maximum power point and improves both steady state and transient characteristics of the PV system.

Further to this, steady state error can be further decreased by reducing the training error and increasing the size of the data set used for training of the fuzzy inference system. The proposed controller can be used to track the maximum power point in standalone PV systems.

7.6 CONCLUSION

In this chapter a physical array reconfiguration method based on GWO is developed for 5x5 PV array arrangement for different types of partial shading conditions due to varying cloud movement and wind speed. The GWO algorithm uses row current minimization for solving the objective function and designed a BLTCT type configuration. The performance of the developed GWO-BLTCT was analyzed using performance indicators, such as FF, Power loss, PR and PE. The developed GWO-BLTCT was compared with other topologies, SP, TCT, BLTCT and SDK-BLTCT for four different types of shades LN, LW, SW, and SN. For this array configuration GMPP, PR, PE and FF were the highest in comparison to other configurations, moreover, the loss component was minimum. Overall, for the proposed configuration the average PE and PR is observed to be 23.75% and 70.02% respectively. Thus, GWO-BLTCT PV array configuration is found to be superior when compared with SP, TCT, BLTCT and SDK-BLTCT.

Furthermore, an adaptive controller for tracking maximum power tracking has been developed under varying environmental conditions. This ANFIS based MPPT controller has advantages over the traditional MPPT controllers. The response time of the PV system to track MPP reduces significantly by 0.765 s. The steady state performance of ANFIS MPPT is oscillation free as no voltage and current ripples are present on the load side. The tracking performance of MPP also improves, especially during low irradiance and high cell temperature conditions. The steady state error for the developed ANFIS MPPT reduces to 4.03%. Hence, the designed controller performs efficiently to track the maximum power point and improves both steady state and transient characteristic of the PV system. The steady state error can be further decreased by reducing the training error and increasing the size of the data set used for training of the fuzzy inference system. The designed controller can be used to track the maximum power point in standalone PV systems.

CHAPTER 8

CONCLUSIONS AND FUTURE SCOPE OF WORK

8.1 CONCLUSIONS

PSO suffers from low convergence i.e. exploitation in large search spaces and GWO has low solving precision i.e. exploration. Thus, these swarm intelligence techniques i.e. PSO and GWO requires modifications for improvement in locating the optimum solution. A modified grey wolf particle swarm optimizer (MGWPSO) has been developed for sizing problem. A performance based comparative analysis of the GWO with MGWSPO using various benchmark functions is presented. The computational speed and convergence of the MGWPSO technique is found to be better and can tackle the nonlinearity and stochastic nature of the renewable energy sources when modelled mathematically.

A novel SPV power forecasting model based on GWO-ANN approach has been developed and presented for smart grid environment. This model along with irradiance, temperature, and wind speed also uses aerosol index to predict the performance of the SPV panels in a highly polluted city such as Delhi. The performance of the model is evaluated on the basis of statistical indicators and validated from the data set obtained from 5 kW_p PV system installed at the rooftop of the laboratory. The performance indicators such as TE, iterations and R were 3.23×10^{-4} , 148 and 0.99720 respectively, suggesting that the developed hybrid intelligent model is better. The GWO-ANN model offers relatively fast speed for training of the neurons and is comparatively less complex. The results of the

GWO-ANN model show the values of NMBE, NMAE and NRMSE are 2.267%, 4.681% and 6.67% respectively.

Further, a novel MGWPSO based approach for the sizing and management of hybrid MG in the modern power system, integrating the load management for controllable loads has been discussed. This framework was implemented for a retail outlet in Northern India to effectively and efficiently design a SPV based MG. The feasibility of the type of RE resource for the designed hybrid MG was found to be SPV due to high RE consumption of 52.33%, low payback period of 6.67 years, and highest AROI with 6.8%. The demand profile and the performance of the BESS were analyzed for four different seasons. The impact of load flexibility on the sizing components is also monitored by the sizing algorithm and ACI for different conditions was observed. An average of 39.04% energy is purchased and 21.24% energy is sold to the grid with help of the designed control technique. The savings in operational/rolling cost is 23.34% and 45.55% than MILP-EMS in different scenarios over a span of 24 hours.

Improvement of performance of SPV system under varying meteorological conditions are a challenge for researchers and electrical engineers. Thus, a physical array reconfiguration method based on GWO is developed for 5x5 PV array arrangement for different types of shading conditions. The partial shade is modelled considering cloud movement and wind speed and is categorized as SN, SW, LN and LW for a BLTCT type topology. The performance of the developed GWO-BLTCT was analyzed using performance indicators, such as FF, Power loss, PR and PE. GWO-BLTCT was compared with other topologies, SP, TCT, BLTCT and SDK-BLTCT. For, GWO-BLTCT configuration the average PE and PR is observed to be 23.75% and 70.02% respectively.

In addition to this an evolutionary MPPT algorithm i.e. ANFIS-MPPT is also designed for SPV standalone applications. It is compared with INC technique under varying irradiance and varying temperature conditions. Power improvement of 5.52% is observed along with faster response time of 0.765s when compared with incremental conductance (INC).

8.2 FUTURE SCOPE

The presented hybrid intelligent forecasting technique has been developed by recording the high-quality ground measurement data for Indian scenario. This approach can be further considered for predicting SPV power for other locations with higher impact of aerosol content.

The sky conditions considered for the SPV power forecasting were cloudy and clear, further the performance of the developed forecasting model can be evaluated for more sky conditions such as partly cloudy, partly clear, and rainy.

In the research work the optimal sizing and management of SPV based MG has been performed for a fuel outlet in Northern India. In addition, to the load demand considered the electric vehicle and its charging can be incorporated.

Due to unforeseen circumstances of COVID-19 the solar photovoltaic power enhancement techniques were simulated in MATLAB. In future, hardware development and testing of these methods can be performed.

LIST OF PUBLICATIONS

• List of papers (s) published in Peer Reviewed Referred International Journals

1. A. Kumar, M. Rizwan and U. Nangia, “A Hybrid Optimization Technique for Proficient Energy Management in Smart Grid Environment,” International Journal of Hydrogen Energy. (Accepted on 24.11.2021)
SCI-E Indexed, IF: 5.816
2. A. Kumar, M. Rizwan, U. Nangia and M. Alaraj, “Novel AI Based Energy Management System for Smart Grid with RES Integration”, IEEE Access. (Accepted on 24.11.2021)
SCI-E Indexed (IF:3.367)
3. A. Kumar, M. Rizwan and U. Nangia, “A New Approach to Design and Optimize Sizing of Hybrid Microgrid in Deregulated Electricity Environment,” IEEE-CSEE Journal of Power and Energy Systems, Early Access, pp. 1-10, 2020.
DOI: 10.17775/CSEEJPES.2020.03200
SCI Indexed, IF: 3.938
4. A. Kumar, M. Rizwan and U. Nangia, “A Hybrid Intelligent Approach for Solar Photovoltaic Power Forecasting: Impact of Aerosol Data,” Arabian Journal for Science and Engineering, vol. 45, pp. 1715-1732, 2020.
DOI: <https://doi.org/10.1007/s13369-019-04183-0>
SCI-E Indexed, IF: 2.334
5. A. Kumar, M. Rizwan and U. Nangia, “Development of ANFIS-Based Algorithm for MPPT Controller for Standalone Photovoltaic System,” International Journal of Advanced Intelligence Paradigms, vol. 18, pp. 247-264, 2021.
DOI: <https://doi.org/10.1504/IJAIP.2021.112906>
Scopus Indexed

• **List of Paper(s) Published in Peer Reviewed International Conference**

1. A. Kumar, M. Rizwan and U. Nangia, “Optimal Sizing of Renewable Energy Resources in a Microgrid for a Distributed Generation System,” IEEE International Symposium on Advanced Electrical and Communication Technologies (ISAECT), Rome, Italy, 27-29 Nov. 2019. [Scopus Indexed]
2. A. Kumar, M. Rizwan and U. Nangia, “Artificial Neural Network based Model for Short Term Solar Radiation Forecasting considering Aerosol Index,” IEEE International Conference on Power Electronics, Intelligent Control and Energy Systems (ICPEICES), Delhi, India, 22-24 Oct. 2018. [Scopus Indexed].

• **List of other publications**

1. A. Kumar, D. Karna, A. Vikram and M. Rizwan, “Extraction of Maximum Electrical Power from Solar Photovoltaic-Based Grid-Tied System”, Advances in Energy Technology. Lecture Notes in Electrical Engineering, vol. 766, pp. 1-10, 2022. DOI: https://doi.org/10.1007/978-981-16-1476-7_33 [Scopus Indexed]
2. A. Kumar, D. Karna, A. Vikram and M. Rizwan, “A Novel Fuzzy based Intelligent Demand Side Management for Automated Load Scheduling” IEEE International Conference on Green Energy and Applications (ICGEA), Singapore, 7-9 Mar. 2020. [Scopus Indexed]
3. A. Kumar, A. Vikram, D. Karna and M. Rizwan, “An Analytical Approach of Integrating Automated Load Scheduling to a Smart Energy Meter using Differential Evolution Algorithm” IOP Conference Series: Materials Science and Engineering (ICIPCE), Berkeley, USA, 27-29 Jun. 2020. [Scopus Indexed]

REFERENCES

- [1] IRENA, "Renewable capacity statistics 2021," International Renewable Energy Agency, Abu Dhabi, 2021.
- [2] U. Nations, "Paris Agreement," United Nations, Paris, 2016.
- [3] IBEF, "Renewable Energy Industry in India Report," India Brand Equity Foundation, 2021.
- [4] Ministry of Renewable Energy, "Development of Solar Parks and Ultra Mega Solar Power Projects," Government of India, New Delhi, 2017.
- [5] Ministry of Renewable Energy, "Scheme for setting up of over 5000 MW grid connected SPV power projects under IV of JNNSM PHASE II," Government of India, New Delhi, 2019.
- [6] Ministry of Renewable Energy, "Grid Connected Solar Rooftop Programme," Government of India, New Delhi, 2019.
- [7] S. Kumar, I. Hussain, B. Singh, A. Chandra and K. Al-Haddad, "An Adaptive Control Scheme of SPV System Integrated to AC Distribution System," *IEEE Transactions on Industry Applications*, vol. 53, no. 6, pp. 5173-5181, 2017.
- [8] J. Zhang, H. Cho and P. Mago, "Energy Conversion Systems And Energy Storage Systems," in *Energy Services Fundamentals and Financing*, Springer, 2021, pp. 155-179.
- [9] V. Chin, Z. Salam and K. Ishaque, "Cell Modelling And Model Parameters Estimation Techniques For Photovoltaic Simulator Application: A Review," *Applied Energy*, vol. 154, pp. 500-519, 2015.
- [10] B. Yang, W. Jingbo, Z. Xiaoshun, Y. Tao, Y. Wei, S. Hongchun, Z. Fang and S. Liming, "Comprehensive Overview Of Meta-Heuristic Algorithm Applications On PV Cell Parameter Identification," *Energy Conversion and Management*, vol. 208, pp. 112595-112605, 2020.
- [11] A. Jordehi, "Parameter Estimation Of Solar Photovoltaic (PV) Cells: A Review," *Renewable and Sustainable Energy Reviews*, vol. 61, pp. 354-371, 2016.
- [12] G. Ciulla, B. VL, V. Di Dio and G. Cipriani, "A Comparison Of Different One-Diode Models For The Representation Of I-V Characteristic Of A PV Cell," *Renewable and Sustainable Energy Reviews*, vol. 32, pp. 684-696, 2014.

- [13] M. Rasheed and S. Shihab, "Modelling And Parameter Extraction Of PV Cell Using Single-Diode Model," *Advanced Energy Conversion Materials*, vol. 1, pp. 70-104, 2020.
- [14] R. Kotla and S. Yarlagadda, "Mathematical Modelling Of SPV Array By Considering The Parasitic Effects," *Applied Sciences*, vol. 50, pp. 1-20, 2020.
- [15] C. Lupangu and R. Bansal, "A Review Of Technical Issues On The Development Of Solar Photovoltaic Systems," *Renewable and Sustainable Energy Reviews*, vol. 1, pp. 950-965, 2017.
- [16] A. Joyce, C. Rodrigues and R. Manso, "Modelling a PV system," *Renewable energy*, vol. 22, pp. 275-280, 2001.
- [17] A. Chouder, S. Silvestre, B. Taghezouit and E. Karatepe, "Monitoring, Modelling And Simulation Of PV Systems Using LabVIEW," *Solar Energy*, vol. 91, pp. 337-349, 2013.
- [18] A. Banik, A. Shrivastava, R. Potdar, S. Jain, S. Nagpure and M. Soni, "Design, Modelling, and Analysis of Novel Solar PV System using MATLAB," *Materials Today: Proceedings*, 2021.
- [19] A. Merabet, H. Eshaft and A. Tanvir, "Power-Current Controller Based Sliding Mode Control For DFIG-Wind Energy Conversion System," *IET Renewable Power Generation*, vol. 12, pp. 1155-1163, 2018.
- [20] R. Badwawi, M. Abusara and T. Mallick, "A Review Of Hybrid Solar PV And Wind Energy System," *Smart Science*, vol. 3, pp. 127-138, 2015.
- [21] L. Al-Ghussain, O. Taylan and D. Baker, "An Investigation Of Optimum PV And Wind Energy System Capacities For Alternate Short And Long-Term Energy Storage Sizing Methodologies," *International Journal of Energy Research*, vol. 43, pp. 204-218, 2019.
- [22] Y. Liu, X. Wu, J. Du, Z. Song and G. Wu, "Optimal Sizing Of A Wind-Energy Storage System Considering Battery Life," *Renewable Energy*, vol. 47, pp. 2470-2483, 2020.
- [23] M. Jayachandran and G. Ravi, "Design And Optimization Of Hybrid Micro-Grid System," *Energy Procedia*, vol. 117, pp. 95-103, 2017.
- [24] S. Nojavan, M. Majidi and N. Esfetanaj, "An Efficient Cost-Reliability Optimization Model For Optimal Siting And Sizing Of Energy Storage System In A Microgrid In The Presence Of Responsible Load Management," *Energy*, vol. 139, pp. 89-97, 2017.

- [25] Y. Kumar and R. Bhimasingu, "Renewable Energy Based Microgrid System Sizing And Energy Management For Green Buildings," *Journal of Modern Power Systems and Clean Energy*, vol. 3, pp. 1-13, 2015.
- [26] B. Somaiah, V. Agarwal, S. Choudhury, S. Duttagupta and K. Govindan, "Analysis And Comparative Study Of Pulsating Current Of Fuel Cells By Inverter Load With Different Power Converter Topologies," *International journal of hydrogen energy*, vol. 36, pp. 15018-15028, 2011.
- [27] R. Siddaiah and R. Saini, "A Review On Planning, Configurations, Modeling And Optimization Techniques Of Hybrid Renewable Energy Systems For Off Grid Applications," *Renewable and Sustainable Energy Reviews*, vol. 58, pp. 376-396, 2016.
- [28] P. Goud and R. Gupta, "Dual-Mode Control Of Multi-Functional Converter In Solar PV System For Small Off-Grid Applications," *IET Power Electronics*, vol. 12, pp. 2851-2857, 2019.
- [29] M. Kumar, M. Anwar and A. Kumar, "Comparative Analysis Of Dc-Dc Converter Topologies And MPPT Techniques Used In SPV Based Water Pumping System Using Bldc Motor," *2nd International Conference on Power, Energy and Environment: Towards Smart Technology (ICEPE)*, Shillong, India, 2018.
- [30] A. El Khateb, N. Abd Rahim, J. Selvaraj and B. Williams, "DC-To-DC Converter With Low Input Current Ripple For Maximum Photovoltaic Power Extraction," *IEEE Transactions on Industrial Electronics*, vol. 62, pp. 2246-2256, 2014.
- [31] G. Venter, "Review Of Optimization Techniques," *Encyclopedia of Aerospace Engineering*, New Jersey, USA, Wiley and Sons., 2010, pp. 1-12.
- [32] D. Weile and E. Michielssen, "Genetic algorithm optimization applied to electromagnetics: A review," *IEEE Transactions on Antennas and Propagation*, vol. 45, pp. 343-353, 1997.
- [33] N. Jain, U. Nangia and J. Jain, "A Review Of Particle Swarm Optimization," *Journal of The Institution of Engineers (India): Series B*, vol. 99, pp. 407-411, 2018.
- [34] A. Mohamad, A. Zain and N. Nazira Bazin, "Cuckoo Search Algorithm For Optimization Problems—A Literature Review And Its Applications," *Applied Artificial Intelligence*, vol. 28, pp. 419-448, 2014.
- [35] F. Gharehchopogh and H. Gholizadeh, "A Comprehensive Survey: Whale Optimization Algorithm And Its Applications," *Swarm and Evolutionary Computation*, vol. 48, pp. 1-24, 2019.

- [36] I. Trelea, "The Particle Swarm Optimization Algorithm: Convergence Analysis And Parameter Selection," *Information processing letters*, vol. 85, pp. 317-325, 2003.
- [37] A. Nickabadi, M. Ebadzadeh and R. Safabakhsh, "A Novel Particle Swarm Optimization Algorithm With Adaptive Inertia Weight," *Applied soft computing*, vol. 11, pp. 3658-3670, 2011.
- [38] M. Tanweer, S. Suresh and N. Sundararajan, "Self regulating particle swarm optimization algorithm," *Information Sciences*, vol. 294, pp. 182-202, 2015.
- [39] B. Jiao, Z. Lian and X. Gu, "A Dynamic Inertia Weight Particle Swarm Optimization Algorithm," *Chaos, Solitons & Fractals*, vol. 37, pp. 698-705, 2008.
- [40] R. Cheng and Y. Jin, "A Social Learning Particle Swarm Optimization Algorithm For Scalable Optimization," *Information Sciences*, vol. 291, pp. 43-60, 2015.
- [41] H. Haklı and H. Uğuz, "A Novel Particle Swarm Optimization Algorithm With Levy Flight," *Applied Soft Computing*, vol. 23, pp. 333-345, 2014.
- [42] H. Fakhouri, A. Hudaib and A. Sleit, "Multivector Particle Swarm Optimization Algorithm," *Soft Computing*, vol. 23, pp. 1-9, 2019.
- [43] D. Simon, *Evolutionary optimization algorithms*, New Jersey, USA: John Wiley & Sons, 2013.
- [44] T. Niknam, B. Amiri, J. Olamaei and A. Arefi, "An Efficient Hybrid Evolutionary Optimization Algorithm Based On PSO And SA For Clustering," *Journal of Zhejiang University-SCIENCE A*, vol. 10, pp. 512-519, 2010.
- [45] P. Jamwal, B. Abdikenov and S. Hussain, "Evolutionary Optimization Using Equitable Fuzzy Sorting Genetic Algorithm (EFSGA)," *IEEE Access*, vol. 7, pp. 8111-8126, 2019.
- [46] A. Deb, J. Roy and B. Gupta, "Performance Comparison Of Differential Evolution, Particle Swarm Optimization And Genetic Algorithm In The Design Of Circularly Polarized Microstrip Antennas," *IEEE transactions on antennas and propagation*, vol. 62, pp. 3920-3928, 2014.
- [47] W. Song, L. Choi, S. Park and X. Ding, "Fuzzy Evolutionary Optimization Modeling And Its Applications To Unsupervised Categorization And Extractive Summarization," *Expert Systems with Applications*, vol. 38, pp. 9112-9121, 2011.
- [48] S. Mirjalili and A. Lewis, "The Whale Optimization Algorithm," *Advances in engineering software*, vol. 95, pp. 51-67, 2016.

- [49] S. Mirjalili, S. Mirjalili and L. A. , "Grey Wolf Optimizer," *Advances in Engineering Software*, vol. 69, pp. 46-61, 2014.
- [50] M. Marzband, F. Azarnejadian, M. Savaghebi, E. Pouresmaeil, J. Guerrero and G. Lightbody, "Smart Transactive Energy Framework In Grid-Connected Multiple Home Microgrids Under Independent And Coalition Operations," *Renewable Energy*, vol. 126, pp. 96-106, 2018.
- [51] H. Monfared, A. Ghasemi, A. Loni and M. Marzband, "A Hybrid Price-Based Demand Response Program For The Residential Micro-Grid," *Energy*, vol. 185, pp. 274-285, 2019.
- [52] A. Al-Sumaiti, M. Salama, M. El-Moursi, T. Alsumaiti and M. Marzband, "Enabling Electricity Access: Revisiting Load Models For AC-Grid Operation - Part I," *IET Generation, Transmission & Distribution*, vol. 12, pp. 2563-2571, 2019.
- [53] V. Aryanpur, M. Atabaki, M. Marzband, P. Siano and K. Ghayoumi, "An Overview Of Energy Planning In Iran And Transition Pathways Towards Sustainable Electricity Supply Sector," *Renewable and Sustainable Energy Reviews*, vol. 112, pp. 58-74, 2019.
- [54] C. Voyant, G. Notton, G. Kalogirou, M. Nivet, C. Paoli, F. Motte and A. Fouilloy, "Machine Learning Methods For Solar Radiation Forecasting: A Review.," *Renewable Energy*, vol. 107, pp. 569-582, 2017.
- [55] C. Wan, J. Zhao, Y. Song, Z. Xu, J. Lin and Z. Hu, "Photovoltaic and Solar Power Forecasting for Smart Grid Energy Management," *CSEE Journal Of Power and Energy Systems*, vol. 1, pp. 38-47, 2015.
- [56] M. Diagne, M. David, P. Lauret, J. Boland and n. Schmutz, "Review Of Solar Irradiance Forecasting Methods And A Proposition For Small-Scale Insular Grids," *Renewable and Sustainable Energy Reviews*, vol. 27, pp. 67-76, 2013.
- [57] M. De Giorgi, P. Congedo and M. Malvoni, "Photovoltaic Power Forecasting Using Statistical Methods: Impact Of Weather Data," *IET Science, Measurement and Technology*, vol. 8, pp. 90-97, 2013.
- [58] J. Antonanzas, N. Osorio, R. Escobar, R. Urraca, F. Martinez-de-Pison and F. Antonanzas-Torres, "Review of Photovoltaic Power Forecasting," *Solar Energy*, vol. 136, pp. 78-111, 2016.
- [59] D. Chaturvedi and Isha, "Solar Forecasting: A Review," *International Journal of Computer Applications*, vol. 145, pp. 28-50, 2016.

- [60] C. Martinez-Anido, B. Botor, A. Florita, C. Draxl, S. Lu, H. Hamann and B. Hodge, "The Value Of Day-Ahead Solar Power Forecasting Improvement.," *Solar Energy*, vol. 129, pp. 192-203 , 2016.
- [61] Y. Sanusi and M. Ojo, "Evaluation of Clearness Index and Diffuse Ratio of Some Locations in South Western, Nigeria using Solar Radiation Data," *Journal of Applied Physics*, vol. 5, pp. 45-51, 2015.
- [62] Y. Chu, B. Urquhart, S. Gohari, H. Pedro, J. Kleissl and C. Coimbra, "Short-Term Reforecasting Of Power Output From A 48 Mwe Solar PV Plant," *Solar Energy*, vol. 112, pp. 68-77, 2015.
- [63] X. Lia, F. Wagner, W. Peng, J. Yang and D. Mauzeralla, "Reduction Of Solar Photovoltaic Resources Due To Air Pollution In China," *Proceedings of the National Academy of Science, China*, 2017.
- [64] M. Garba, A. Muhammad, M. Musa and A. Mohammed, "Assessing The Performance Of Global Solar Radiation Empirical Equations In Sokoto, Nigeria Using Meteorological Parameters," *Nigeria Journal of Technology*, vol. 37, pp. 358-364, 2018.
- [65] B. Amrouche and X. Pivert, "Artificial Neural Network Based Daily Local Forecasting For Global Solar Radiation," *Applied Energy*, vol. 130, pp. 333-341, 2015.
- [66] A. Mellit and A. Pavan, "A 24-H Forecast Of Solar Irradiance Using Artificial Neural Network: Application For Performance Prediction Of A Grid-Connected PV Plant At Trieste, Italy," *Solar Energy*, vol. 84, pp. 807-821, 2010.
- [67] R. Ehsan, S. Simon and P. Venkateswaran, "Day-Ahead Forecasting Of Solar Photovoltaic Output Power Using Multilayer Perceptron," *Neural Computing and Applications*, vol. 28, pp. 3981-3992, 2017.
- [68] S. Chen, H. Gooi and M. Wang, "Solar Radiation Forecast Based On Fuzzy Logic And Neural Networks," *Renewable Energy*, vol. 60, pp. 195-201, 2013.
- [69] S. Safi, A. Zeroual and M. Hassani, "Prediction Of Global Daily Solar Radiation Using Higher Order Statistics," *Renewable Energy*, vol. 27, pp. 647-660, 2002.
- [70] C. Chupong and B. Plangklang, "Forecasting Power Output Of PV Grid Connected System In Thailand Without Using Solar Radiation Measurement," *Energy Procedia*, vol. 9, p. 230–237, 2011.

- [71] M. De Giorgi, A. Ficarella and M. Tarantino, "Assessment Of The Benefits Of Numerical Weather Predictions In Wind Power Forecasting Based On Statistical Methods," *Energy*, vol. 36, pp. 3968-3978, 2011.
- [72] H. Yang, C. Huang, Y. Huang and Y. Pa, "A Weather-Based Hybrid Method for 1-Day Ahead Hourly Forecasting of PV Power Output," *IEEE Transaction on Sustainable Energy*, vol. 5, pp. 917-925, 2014.
- [73] K. Basaran, A. Özçift and D. Kılınc, "A New Approach for Prediction of Solar Radiation with Using Ensemble Learning Algorithm," *Arabian Journal of Science and Engineering*, vol. 4, pp. 1-13, 2019.
- [74] M. Douiri, "A Predictive Model for Solar Photovoltaic Power based on Computational Intelligence Technique," *Arabian Journal of Science and Engineering*, vol. 2, pp. 1-18, 2019.
- [75] P. Prakash and D. Khatod, "Optimal Sizing And Siting Techniques For Distributed Generation In Distribution Systems: A Review," *Renewable and Sustainable Energy Reviews*, vol. 57, pp. 111-130, 2016.
- [76] A. Hirsch, Y. Parag and J. Guerrero, "Microgrids: A Review Of Technologies, Key Drivers, And Outstanding Issues," *Renewable Sustainable Energy Reviews*, vol. 90, pp. 402-411, 2018.
- [77] S. Sinha and S. S. Chandel, "Review Of Recent Trends In Optimization Techniques For Solar Photovoltaic–Wind Based Hybrid Energy Systems," *Renewable Sustainable Energy Reviews*, vol. 50, pp. 755-769, 2015.
- [78] N. Singh and S. B. Singh, "Hybrid Algorithm of Particle Swarm Optimization and Grey Wolf Optimizer for Improving Convergence Performance," *Journal of Applied Mathematics*, vol. 2017, pp. 1-16, 2017.
- [79] A. A. Hafez , A. Y. Hatata and M. Aldl, "Optimal Sizing Of Hybrid Renewable Energy System Via Artificial Immune System Under Frequency Stability Constraints," *Journal of Renewable and Sustainable Energy*, vol. 11, no. 1, pp. 1-12, 2019.
- [80] M. Shaneh, H. Shahinzadeh, M. Moazzami and G. B. Gharehpetian, "Optimal Sizing And Management Of Hybrid Renewable Energy System For Highways Lighting," *International Journal of Renewable Energy Research*, vol. 8, no. 4, pp. 2336-2349, 2018.
- [81] M. Yousif, Q. Ai, Y. Gao, W. Wattoo, Z. Jiang and R. Hao, "An Optimal Dispatch Strategy For Distributed Microgrids Using PSO," *CSEE Journal of Power and Energy Systems*, vol. 6, pp. 724-734, 2020..

- [82] B. Zhao, X. Zhang, P. Li, K. Wang, M. Xue and C. Wang, "Optimal Sizing, Operating Strategy And Operational Experience Of A Stand-Alone Microgrid On Dongfushan Island," *Applied Energy*, vol. 113, pp. 1656-1666, 2014.
- [83] K. Lai, Y. Wang, D. Shi, M. Illindala, Y. Jin and Z. Wang, "Sizing Battery Storage For Islanded Microgrid Systems To Enhance Robustness Against Attacks On Energy Sources," *Journal of Modern Power Systems and Clean Energy*, vol. 7, pp. 1177-1188, 2019.
- [84] K. Kusakana, H. Vermaak and B. Numbi, "Optimal Sizing Of A Hybrid Renewable Energy Plant Using Linear Programming," *IEEE Power and Energy Society Conference and Exposition in Africa: Intelligent Grid Integration of Renewable Energy Resources (Power Africa)*, Johannesburg, 2012.
- [85] A. Eltamaly and A. Mohamed, "Optimal Sizing and Designing of Hybrid Renewable Energy Systems in Smart Grid Applications," *Advances in Renewable Energies and Power Technologies*, Amsterdam: Elsevier, pp. 231-313., 2018.
- [86] U. Akram, M. Khalid and S. Shafiq, "Optimal Sizing Of A Wind/Solar/Battery Hybrid Grid-Connected Microgrid System," *IET Renewable Power Generation*, vol. 12, pp. 72-80, 2018.
- [87] J. A. Aguado, S. Torre and A. Trivino, "Battery Energy Storage Systems In Transmission Network Expansion Planning," *Electric Power Systems Research*, vol. 145, pp. 63-72, 2017.
- [88] R. Fernandez-Blanco, Y. Dvorkin, B. Xu, Y. Wang and D. S. Kirschen, "Optimal Energy Storage Siting and Sizing: A WECC Case Study," *IEEE Transactions on Sustainable Energy*, vol. 8, pp. 733 - 743, 2016.
- [89] M. Korpaas, A. Holen and R. Hildrum, "Operation And Sizing Of Energy Storage For Wind Power Plants In A Market System," *International Journal of Electrical Power & Energy Systems*, vol. 25, pp. 599-606, 2003.
- [90] L. Xu, X. Ruan, C. Mao, B. Zhang and L. Luo, "An Improved Optimal Sizing Method For Wind-Solar-Battery Hybrid Power System," *IEEE Transaction on Sustainable Energy*, vol. 4, pp. 774-785, 2013.
- [91] M. Sharafi and T. Y. El-Mekkawy, "Multi-Objective Optimal Design Of Hybrid Renewable Energy Systems Using PSO-Simulation Based Approach," *Renewable Energy*, vol. 68, pp. 67-79, 2014.
- [92] V. M. Vallem and A. Kumar, "Optimal Energy Dispatch In Microgrids With Renewable Energy Sources And Demand Response," *International Transactions on Electrical Energy Systems*, vol. 30, pp. 1-27, 2020.

- [93] A. Scalfati, D. Iannuzzi, M. Fantauzzi and M. Roscia, "Optimal Sizing Of Distributed Energy Resources In Smart Microgrids: A Mixed Integer Linear Programming Formulation," *IEEE 6th International Conference on Renewable Energy Research and Applications*, San Diego, pp. 568-573, 2017.
- [94] X. Li, D. Hui and X. Lai, "Battery Energy Storage Station (BESS)-Based Smoothing Control of Photovoltaic (PV) and Wind Power Generation Fluctuations," *IEEE Transactions on Sustainable Energy*, vol. 4, pp. 464-473, 2013.
- [95] E. Matallanas, M. Castillo-Cagigal, A. Gutierrez, F. Monasterio-Huelin, E. Martin, D. Masa and J. Jimenez-Leube, "Neural network controller for Active Demand-Side Management with PV energy in the residential sector," *Applied Energy*, vol. 91, pp. 90-97, 2012.
- [96] Z. Yi, Y. Xu, W. Gu and W. Wu, "A Multi-time-scale Economic Scheduling Strategy for Virtual Power Plant Based on Deferrable Loads Aggregation and Disaggregation," *IEEE Transactions on Sustainable Energy*, pp. 1-13, 2019.
- [97] R. Atia and N. Yamada, "Sizing and Analysis of Renewable Energy and Battery Systems in Residential Microgrids," *IEEE Transactions on Smart Grid*, vol. 7, pp. 1204-1213, 2016.
- [98] S. Ong, C. Campbell, P. Denholm, R. Margolis and G. Heath, "Land-Use Requirements for Solar Power Plants in the United States," National Renewable Energy, Colorado, 2013.
- [99] M. Green, K. Emery, Y. Hishikawa, W. Warta, E. Dunlop, D. Levi and A. Ho-Baillie, "Solar Cell Efficiency Tables," *Progress in Photovoltaics: Research and Applications*, vol. 25, no. 4, pp. 333-334, 2017.
- [100] B. I. Rani, G. S. Ilango and C. Nagamani, "Enhanced Power Generation From PV Array Under Partial Shading Conditions By Shade Dispersion Using Su Do Ku Configuration," *IEEE Transactions on Sustainable Energy*, vol. 4, pp. 594-601, 2013.
- [101] P. d. S. Vicente, T. C. Pimenta, and E. R. Ribeiro, "Photovoltaic Array Reconfiguration Strategy for Maximization of Energy Production," *International Journal of Photoenergy*, vol. 2015, 2015.
- [102] S. N. Deshkar, S. B. Dhale, J. S. Mukherjee, T. S. Babu and N. Rajasekar, "Solar PV Array Reconfiguration Under Partial Shading Conditions For Maximum Power Extraction Using Genetic Algorithm," *Renewable and Sustainable Energy Reviews*, vol. 43, pp. 102-110, 2015.

- [103] R. Pachauri, R. Singh, A. Gehlot, R. Samakaria and S. Chudhary, "Experimental Analysis To Extract Maximum Power From PV Array Reconfiguration Under Partial Shading Conditions," *Engineering Science and Technology, an International Journal*, vol. 22, pp. 109-130, 2019.
- [104] S. R. Potnuru, D. Pattabiraman, S. I. Ganesan and N. Chilakapati, "Positioning Of PV Panels For Reduction In Line Losses And Mismatch Losses In PV Array," *Renewable Energy*, vol. 78, pp. 264-275, 2015.
- [105] A. Eltamaly and H. Farh, "Dynamic Global Maximum Power Point Tracking Of The PV Systems Under Variant Partial Shading Using Hybrid GWO-FLC," *Solar Energy*, vol. 177, pp. 306-316, 2018.
- [106] J. Camilo, T. Guedes, D. Fernandes, J. Melo, F. Costa and A. Filho, "A Maximum Power Point Tracking For Photovoltaic Systems Based On Monod Equation.," *Renewable Energy*, vol. 130, pp. 428-438, 2019.
- [107] A. Fathy, "Recent Meta-Heuristic Grasshopper Optimization Algorithm For Optimal Reconfiguration Of Partially Shaded PV Array," *Solar Energy*, vol. 171, pp. 638-651, 2018.
- [108] D. Yousri, T. Babu, E. Beshr, M. Eteiba and D. Allam, "A Robust Strategy Based on Marine Predators Algorithm for Large Scale Photovoltaic Array Reconfiguration to Mitigate the Partial Shading Effect on the Performance of PV System," *IEEE Access*, vol. 8, pp. 112407-112426, 2020.
- [109] S. R. Pendem and S. Mikkili, "Modelling And Performance Assessment Of PV Array Topologies Under Partial Shading Conditions To Mitigate The Mismatching Power Losses," *Solar Energy*, vol. 160, pp. 303-321, 2018.
- [110] A. Yadav, R. Pachauri and Y. Chauhan, "Comprehensive Investigation Of PV Arrays Under Different Shading Patterns By Shade Dispersion Using Puzzled Pattern Based Su-Do-Ku Puzzle Configuration," *IEEE Conference on Next Generation Computing Technologies*, Dehradun, 2015.
- [111] A. Yadav, R. Pachauri and Y. Chauhan, "Comprehensive Investigation Of PV Arrays With Puzzle Shade Dispersion For Improved Performance," *Solar Energy*, vol. 129, pp. 256-285, 2016.
- [112] S. Vijayalekshmy, G. Bindu and S. Iyer, "A Novel Zig-Zag Scheme For Power Enhancement Of Partially Shaded Solar Arrays," *Solar Energy*, vol. 135, pp. 92-102, 2016.

- [113] G. Sagar, D. Pathak, P. Gaur and V. Jain, "A Su Do Ku Puzzle Based Shade Dispersion For Maximum Power Enhancement Of Partially Shaded Hybrid Bridge-Link-Total-Cross-Tied PV Array," *Solar Energy*, vol. 204, pp. 161-180, 2020.
- [114] R. Venkateswari and N. Rajasekar, "Power enhancement of PV system via physical array reconfiguration based Lo Shu technique," *Energy Conversion and Management*, vol. 215, pp. 1-22, 2020.
- [115] X. Liu and Y. Wang, "Reconfiguration Method to Extract more Power from Partially Shaded Photovoltaic Arrays with Series-Parallel Topology," *Energies*, vol. 12, pp. 1-16, 2019.
- [116] T. S. Babu, J. P. Ram, T. Dragicevic, M. Miyatake, F. Blaabjerg and N. Rajasekar, "Particle Swarm Optimization based Solar PV Array Reconfiguration of the Maximum Power Extraction under Partial Shading Conditions," *IEEE PES Transactions on Sustainable Energy*, vol. 9, pp. 74-85, 2017.
- [117] M. Alkahtani, Z. Wu, C. Kuka, M. Alahammad and K. Ni, "A Novel PV Array Reconfiguration Algorithm Approach to Optimising Power Generation across Non-Uniformly Aged PV Arrays by Merely Repositioning," *J*, vol. 3, pp. 32-53, 2020.
- [118] D. Pillai, N. Rajasekar, J. Ram and V. Chinnaiyan, "Design And Testing Of Two Phase Array Reconfiguration Procedure For Maximizing Power In Solar PV Systems Under Partial Shade Conditions (PSC)," *Energy Conversion Management*, vol. 178, pp. 92-110, 2018.
- [119] D. Nguyen and B. Lehman, "Modeling And Simulation Of Solar PV Arrays Under Changing Illumination Conditions.," *Proceedings of the IEEE Workshop on Computers in Power Electronics, COMPEL*, 295–299., 2006.
- [120] J. Storey, P. Wilson and D. Bagnall, "Improved Optimization Strategy for Irradiance Equalization in Dynamic Photovoltaic Arrays," *IEEE Transactions on Power Electronics*, vol. 28, no. 6, pp. 2946 - 2956, 2013.
- [121] A. Tabanjat, M. Becherif and D. Hissel, "Reconfiguration Solution For Shaded PV Panels Using Switching Control," *Renewable Energy*, vol. 82, no. 10, pp. 4-13, 2015.
- [122] K. S. Parlak, "PV Array Reconfiguration Method Under Partial Shading Conditions," *International Journal of Electrical Power & Energy Systems*, vol. 63, no. 12, pp. 713-721, 2014.
- [123] F. Villa, D. Picault, B. Raison, S. Bacha and A. Labonne, "Maximizing The Power Output Of Partially Shaded Photovoltaic Plants Through Optimization Of The

- Interconnections Among Its Modules," *IEEE Journal of Photovoltaic*, vol. 2, pp. 154-163, 2012.
- [124] S. Vijayalekshmy, G. Bindu and S. Iyer, "Performance of Partially Shaded Photovoltaic Array Configurations under Shade Dispersion.," *IEEE International Conference on Advances in Green Energy*, Thiruvananthapuram, India, 2014.
- [125] B. Dhanalakshmi and N. Rajasekar, "Dominance Square Based Array Reconfiguration Scheme For Power Loss Reduction In Solar Photovoltaic (PV) Systems," *Energy Conversion and Management*, vol. 156, no. 1, pp. 84-102, 2018.
- [126] A. S. Yadav, R. K. Pachauri, Y. K. Chauhan, S. Choudhury and R. Singh, "Performance Enhancement Of Partially Shaded PV Array Using Novel Shade Dispersion Effect On Magic-Square Puzzle Configuration," *Solar Energy*, vol. 144, no. 3, pp. 780-797, 2017.
- [127] H. Sahu, S. Nayak and S. Mishra, "Maximizing the Power Generation of a Partially Shaded PV Array," *IEEE Journal of Emerging and Selected Topics in Power Electronics*, vol. 4, no. 2, pp. 626-637, 2016.
- [128] G. Yu, Y. Jung, J. Choi and G. Kim, "A Novel Two-Mode MPPT Control Algorithm Based on Comparative Study of Existing Algorithms," *Solar Energy*, vol. 76, pp. 455-463, 2004.
- [129] A. Podder, N. Roy and H. Pota, "MPPT Methods For Solar PV Systems: A Critical Review Based On Tracking Nature," *IET Renewable Power Generation*, vol. 13, pp. 1615-1632, 2019.
- [130] D. Wonohadidjojo, "Performance Comparison of Intelligent Control of Maximum Power Point Tracking in Photovoltaic System," *International Conference on Electrical Systems, Technology and Information*, vol. 2, pp. 203-213, 2015.
- [131] B. Pakkiri and G. Sukumar, "Research Survey on Various MPPT Performance Issues to Improve the Solar PV System Efficiency," *Journal of Solar Energy*, vol. 2, pp. 1-20, 2016.
- [132] N. Karami, N. Moubayed and R. Outib, "General Review And Classification Of Different MPPT Techniques," *Renewable and Sustainable Energy Reviews*, vol. 68, pp. 1-18, 2017.
- [133] A. Reisi, M. Moradi and S. Jamsab, "Classification And Comparison Of Maximum Power Point Tracking Techniques For Photovoltaic System: A Review," *Renewable and Sustainable Energy Reviews*, vol. 19, pp. 433-443, 2013.

- [134] I. Houssamo, F. Locment and M. Sechilariu, "Development and experimental comparison of two maximum power point tracking algorithms for photovoltaic power system," *Renewable Energy*, vol. 35, pp. 2381-2387, 2010.
- [135] T. Sruthy and F. Mohan, "Fast-Converging MPPT Technique For Photovoltaic System Using dsPic Controller," *International Conference on Intelligent Systems and Control*, Chennai, 2017.
- [136] R. Faranda, S. Leva and V. Maugeri, "MPPT Techniques For PV Systems: Energetic And Cost Comparison," *IEEE Conference on Power and Energy Society General Meeting: Conversion and Delivery of Electrical Energy in the 21st Century*, Pittsburgh, 2008.
- [137] T. Eswam and P. Chapman, "Comparison Of Photovoltaic Array Maximum Power Point Tracking Techniques," *IEEE Transaction on Energy Conversion*, vol. 22, pp. 439-449, 2007.
- [138] A. Anurag, S. Bal, S. Sourav and M. Nanda, "A Review Of Maximum Power-Point Tracking Techniques For Photovoltaic Systems," *International Journal of Sustainable Energy*, vol. 35, pp. 478-501, 2016.
- [139] O. Ezinwanne, F. Zhongwen and L. Zhijun, "Energy Performance and Cost Comparison of MPPT Techniques for Photovoltaics and other Applications', , Vol. 107 No. 3, pp.,," *Energy Procedia: International Conference on Energy and Environment Research*, vol. 107, pp. 297-303, 2017.
- [140] A. Kumar, P. Chaudhary and M. Rizwan, "Development of Fuzzy Logic based MPPT Controller for PV System at varying Meteorological parameters," *IEEE Annaul INDICON Conference*, Delhi, 2016.
- [141] S. D. Al-Majidi, M. Abbod and H. Al-Raweshidy, "A Novel Maximum Power Point Tracking Technique Based On Fuzzy Logic For Photovoltaic Systems," *International Journal of Hydrogen Energy*, vol. 31, pp. 14158-14171, 2018.
- [142] F. Kazan, S. Karaki, R. Jabr and M. and Mansour, "Maximum Power Point Tracking Using Ripple Correlation And Incremental Conductance," *47th IEEE Universities Power Engineering Conference*, Middlesex, UK, 2012.
- [143] K. Kanimozhi and B. Rabi, "Development of Hybrid MPPT Algorithm for Maximum Power Harvesting under Partial Shading Conditions," *Circuits and Systems*, vol. 7, pp. 1611-1622, 2016.
- [144] J. Jung and S. Ahmed, "Model Construction Of Single Crystalline Photovoltaic Panels For Real-Time Simulation," *IEEE Conference on Energy Conversion Congress and Exposition*, 342-349, 2010.

- [145] K. Ishaque, Z. Salam and H. Tahri, "Accurate MATLAB Simulink PV Systems Simulator Based On A Two-Diode Model," *Journal of power electronics*, vol. 11, pp. 179-187, 2011.
- [146] M. Abdulkadir, A. Samosir and A. Yatim, "Modelling and Simulation of Maximum Power Point Tracking of Photovoltaic System in Simulink model," *IEEE International Conference on Power and Energy*, 325-330, 2012.
- [147] H. Bellia, R. Youcef and M. Fatima, "A Detailed Modeling of Photovoltaic Module Using MATLAB," *NRIAG Journal of Astronomy and Geophysics*, vol. 3, no. 1, pp. 53-61, 2014.
- [148] Y. Riffonneau, S. Bacha, F. Barruel and S. Ploix, "Optimal Power Flow Management For Grid Connected PV Systems With Batteries," *IEEE Transactions on Sustainable Energy*, vol. 2, pp. 309-320, 2011.
- [149] J. Kennedy and R. Eberhart, "Particle Swam Optimization," *IEEE International Conference on Neural Networks*, 1942-1948, 1995.
- [150] A. Kumar, M. Rizwan and U. Nangia, "A Hybrid Intelligent Approach for Solar Photovoltaic Power Forecasting: Impact of Aerosol Data," *Arabian Journal for Science and Engineering*, vol. 45, pp. 1715-1732, 2020.
- [151] M. Hosenuzzaman, N. Rahima, J. Selvaraj, M. Hasanuzzaman, A. Maleka and A. Nahar, "Global prospects, progress, policies, and environmental impact of solar photovoltaic power generation," *Renewable and Sustainable Energy Reviews*, vol. 41, p. 284–297, 2015.
- [152] H. Long, Z. Zhang and Y. Su, "Analysis of daily solar power prediction with data-driven approaches," *Application Energy*, vol. 126, p. 29–37, 2014.
- [153] M. Rizwan, M. Jamil, S. Kirmani and D. Kothari, "Fuzzy logic based modeling and estimation of global solar energy using meteorological parameters," *Energy*, vol. 70, pp. 685-691, 2014.
- [154] Y. Gala, A. Fernandez, J. Díaz and J. Dorronsoro, "Hybrid machine learning forecasting of solar radiation values," *Neurocomputing*, vol. 176, pp. 48-59, 2016.
- [155] E. Kuznetsova, C. Ruiz and C. Li, "Analysis of robust optimization for decentralized microgrid energy management under uncertainty," *International Journal of Electronics and Power Energy Systems*, vol. 64, pp. 815-832, 2015.
- [156] Z. Zhu, J. Tang, S. Lambotharan and W. Chin, "An integer linear programming based optimization for home demand-side management in smart grid," in, " *IEEE PES Innovative Smart Grid Technologies*, Washington, DC, USA, 2012.

- [157] D. Nguyen and B. Lehman, "Modeling and simulation of solar PV arrays under changing illumination conditions," *IEEE Workshop on Computers in Power Electronics*, New York, USA, 2006.
- [158] M. Diagne, M. David, P. Lauret, J. Boland and N. Schmutz, "Review of solar irradiance forecasting methods and a proposition for small-scale insular grids," *Renewable and Sustainable Energy Reviews*, vol. 27, pp. 67-76, 2013.
- [159] D. Meer, G. C. Mouli, and P. Bauer. "Energy management system with PV power forecast to optimally charge EVs at the workplace." *IEEE Transactions On Industrial Informatics* vol. 14, 311-320, 2016.
- [160] M. Guo, H. Zang, S. Gao, T. Chen and G. Sun. "Optimal tilt angle and orientation of photovoltaic modules using HS algorithm in different climates of China." *Applied Sciences*, vol 7, pp. 1028, 2017.
- [161] H. Braun, T. Buddha, V. Krishnan, C. Tepedelenlioglu, M. Banavar and D. Srinivasan, "Topology reconfiguration for optimization of photovoltaic array output." *Sustainable Energy, Grids and Networks*, vol. 6, pp. 58-69, 2016.
- [162] S. Arefifar, F. Paz and M. Ordonez. "Improving solar power PV plants using multivariate design optimization." *IEEE Journal of Emerging and Selected Topics in Power Electronics*, vol. 5, pp. 638-650, 2017.